

BIOGEOCHEMICAL DYNAMICS IN COASTAL SEDIMENTS AND SHALLOW
AQUIFERS

by

WILLIAM P. PORUBSKY

(Under the Direction of Samantha B. Joye)

ABSTRACT

Patterns of benthic metabolism and the relative importance of assimilatory and dissimilatory processes as sinks for nitrate (NO_3^-) in intertidal sediments were examined. Under illuminated, nitrogen (N)-replete conditions, sequential nutrient limitation of benthic microalgae (BMA) was observed, with N limitation preceding silicate limitation; and biological assimilation dominated nitrate uptake. Conversely, under dark hypoxic and anoxic conditions, water column NO_3^- uptake was dominated largely by three competing dissimilatory reductive processes; denitrification (DNF), dissimilatory nitrate reduction to ammonium (DNRA), and, on one occasion, anaerobic ammonium oxidation (anammox). High sulfide concentrations negatively impacted DNF and DNRA rates, while high dissolved organic carbon (DOC): NO_3^- ratios favored DNRA over DNF. Under baseline conditions sediments exhibited tight coupling between photosynthesis and respiration. Nitrogen addition shifted the metabolic status of the sediments from a balance between autotrophy and heterotrophy to net autotrophy, and the sediments became a source of DOC.

The role of groundwater as a source of nutrients and organics to the coastal ocean was evaluated using a combination of radium isotopes and geochemical characterization.

Geochemical data indicated significant spatial variations in groundwater chemical composition and radium activity ratios indicated geographically distinct hydrological regimes. Spatial variations in microbially mediated processes, DOC distribution, and/or groundwater residence time contributed to this pattern. Radium based geochemical loading rates illustrated a substantial groundwater contribution of organics, DIC, nutrients, methane and nitrous oxide to the Okatee estuary.

The groundwater biogeochemical dynamics along a shallow monitoring well transect on a coastal hammock were evaluated by density-dependent reaction transport model. A switch in the redox status of the DIN pool occurred during the spring-neap tidal transition (spring high NO_3^- low NH_4^+ ; neap low NO_3^- high NH_4^+). The observed N redox-switch was evaluated with regard to the relative roles of nitrification, DNF, DNRA, ammonium adsorption, and variations in inflowing water geochemistry between spring and neap tides. The latter was found to most significantly affect the observed pattern in DIN dynamics. Additionally, the fate of DOC and DIN originating from a septic system was studied. Simulation results indicated that while DNF increased ~15 fold, higher N removal rates could not keep pace with the increase in DIN loading, resulting in higher export of DIN to coastal waters.

INDEX WORDS: Biogeochemistry, Intertidal sediments, Sediment-water column exchange, Benthic fluxes, Benthic microalgae, Nitrogen, Denitrification, Dissimilatory nitrate reduction to ammonium, Anaerobic ammonium oxidation, Nutrients, Dissolved organic carbon, Groundwater, Hydrology, Sulfate reduction, Radium tracers, Reaction-transport modeling, Septic systems

BIOGEOCHEMICAL DYNAMICS IN COASTAL SEDIMENTS AND SHALLOW
AQUIFERS

by

WILLIAM P. PORUBSKY

B.A., University of North Carolina at Chapel Hill, 1998

A Dissertation Submitted to the Graduate Faculty of The University of Georgia in Partial
Fulfillment of the Requirements for the Degree

DOCTOR OF PHILOSOPHY

ATHENS, GEORGIA

2008

© 2008

William P. Porubsky

All Rights Reserved

BIOGEOCHEMICAL DYNAMICS IN COASTAL SEDIMENTS AND SHALLOW
AQUIFERS

by

WILLIAM P. PORUBSKY

Major Professor: Samantha B. Joye
Committee: Christof Meile
James T. Hollibaugh
Wei-Jun Cai
Iris C. Anderson

Electronic Version Approved:

Maureen Grasso
Dean of the Graduate School
The University of Georgia
December 2008

DEDICATION

I would like to dedicate this work to my parents, Edward and Noreen Porubsky. I could never repay the kindness, generosity, and faith that you have both given me. I am truly grateful.

Thank you.

ACKNOWLEDGMENTS

I would like to thank the various sources of funding that have made this work possible; the National Science Foundation Georgia Coastal Ecosystem Long Term Ecological Research project (OCE 99-82133 and OCE 06-20959), the National Oceanic and Atmospheric Administration's Georgia Sea Grant Program (NA06RG0029-R/WQ11, R/WQ12A, and NA04OAR4170033), and South Carolina Sea Grant Program (award number: NA960PO113).

There are many people I would like to thank who have helped in the field, in the laboratory, and with manuscripts, including, Peter Baas, Steven Bell, Marshall Bowles, Steve Carini, Sarah Fisher, Jon Garbisch, Erinn Howard, Kim Hunter, Rosalynn Lee, Anika Mahoney, Steve MacAvoy, Megan Machmuller, Beth! Orcutt, Paula Olecki, Mary Price, Vladimir Samarkin, Kate Segarra, Wade Sheldon, and Liliana Velasquez. I would like to say a special thanks to Matthew Erickson and Nathaniel Weston, who have been extremely helpful and without whom this dissertation would not exist. I would like to thank the staff at the University of Georgia Instrument Shop and especially Lewis Fortner, for making so many wonderful toys for us to use in the field. I would also like to thank everyone in the Marine Science Department at the University of Georgia; you have all been great friends and colleagues through the years. And a special thanks to all of the administrative staff in the Marine Science Department.

My dissertation committee, Mandy Joye, Christof Meile, Tim Hollibaugh, Wei-Jun Cai, and Iris Anderson, have been supportive and I am grateful for their encouragement and input. I would also like to acknowledge the support of Richard Jahnke as my committee member in absentia. Christof Meile's support and encouragement to expand my research into the field of

computer modeling has been invaluable, as has the competition with him on the soccer field. I owe a great deal of gratitude to my advisor, Mandy Joye. Her continued support and enthusiasm has been instrumental in the completion of my degree. It has been an amazing experience to work in such an environment with so many great collaborators.

I would be remiss to not thank my sisters Amy and Julie and my brother Eddie for their support, and the support of their wonderful families. You have all been there for me at any cost and I truly appreciate it. And finally, I would like to thank my dogs Duke and Zoe for always being happy to see me.

TABLE OF CONTENTS

	Page
ACKNOWLEDGMENTS	v
CHAPTER	
1 INTRODUCTION	1
2 BENTHIC METABOLISM AND THE FATE OF DISSOLVED INORGANIC NITROGEN IN INTERTIDAL SEDIMENTS	14
3 NUTRIENT REPLETE BENTHIC MICROALGAE AS A SOURCE OF DISSOLVED ORGANIC CARBON TO COASTAL WATERS.....	59
4 GROUNDWATER AS A POTENTIAL SOURCE OF NUTRIENTS AND DISSOLVED ORGANIC MATTER TO THE OKATEE RIVER ESTUARY, SOUTH CAROLINA.....	112
5 HAMMOCK GROUNDWATER FLOW AND BIOGEOCHEMISTRY: FIELD MEASUREMENTS, LABORATORY ASSAYS, AND PREDICTIVE MODELING.....	159
6 CONCLUSIONS	211

CHAPTER 1

INTRODUCTION

Coastal areas are dynamic regions where the interaction of fresh and salt water significantly impacts near-shore and adjacent terrestrial habitats. These regions represent a rich ecotone of high productivity and diversity. They are also desirable locations for human residence with approximately 60% of the human population living within 100km of the coast globally (Vitousek et al. 1997). The high density of humans living in such proximity to the coast, and the associated changes in land and water use, leads to anthropogenic pressure on coastal environments (Vitousek et al. 1997; Paerl et al. 1998). One of the consequences is increased nutrient supply to coastal waters (Valiela et al. 1990; Rabalais et al. 1996; Howarth et al. 2002; Seitzinger et al. 2002).

The role of nitrogen (N) supply is given special attention in marine systems as coastal waters are often nitrogen limited (Ryther and Dunstan 1971; Nixon et al. 1996; Paerl et al. 1997). The relationship between N inputs and riverine export has been used as an indicator of anthropogenic impacts at large scales (Howarth et al. 1996). Between 1961 and 1997, anthropogenic N loads have doubled across the United States, with N fertilizers being the largest source of the increase (Howarth et al. 2002). An increase in the frequency of estuarine hypoxia/anoxia has been linked to higher nitrogen and organic matter delivery from developed watersheds (De Jonge et al. 1994, Paerl et al. 1998, Persky 1986). Approximately 20% of

anthropogenic N inputs are exported in rivers (Howarth et al. 1998), indicating that terrestrial inputs of N often undergo significant processing before reaching rivers and coastal waters.

One active site of N processing is the sediment water interface in coastal sediments. Nutrient regeneration in sediments and subsequent release to the overlying water column, commonly referred to as benthic-pelagic coupling, fuels a significant portion of water column production in shallow estuarine systems (Nixon et al. 1976). Factors such as water depth, turbidity, sedimentation rates, organic matter remineralization rates, bioturbation, and diffusive or advective transport (Aller 1994; Jahnke et al. 2000; Huettel et al. 2003) influence the magnitude and efficiency of benthic-pelagic coupling. The presence and activity of a benthic microalgal (BMA) community also strongly affects benthic-pelagic coupling (Joye et al. 1996; Jahnke et al. 2000). By modulating O₂ dynamics, BMA alter the sediment redox status and influence rates and pathways of nutrient cycling. BMA also consume nutrients from both the water column and underlying sediments. Under oxic conditions, BMA-dominated sediments act as a nutrient sink while under hypoxic or anoxic conditions, the same sediments serve as a nutrient source to the water column (Joye et al. 1996; Eyre and Ferguson 2002).

In **CHAPTER 2**, we examine patterns of benthic metabolism and the relative importance of denitrification (DNF) and dissimilatory nitrate reduction to ammonium (DNRA) as sinks for nitrate (NO₃⁻) in intertidal sediments in the presence and absence of benthic microalgal activity. The processes of DNF and DNRA can compete for nitrogen oxides (NO₃⁻ or NO₂⁻) in sediments in the absence of oxygen (O₂), and these processes influence the dissolved inorganic nitrogen (DIN) available for flux to the overlying water column. Oxygen production by BMA can stimulate nitrification, which in turn may enhance dissimilatory nitrate sinks, e.g. DNF or DNRA (Joye and Hollibaugh 1995). DNF and DNRA represent two different fates for available NO₃⁻:

DNF produces dinitrogen (N_2) gas that is not readily bioavailable (Howarth et al. 1988) and can diffuse out of the system representing a loss of total N while DNRA produces NH_4^+ that remains in the system and can be recycled (Koike and Hattori 1978; An and Gardner 2002). The relative importance of DNRA versus DNF as NO_3^- sinks in coastal systems is unclear; however, DNRA rates rival DNF rates in some environments (Koike and Hattori 1978; Jørgensen and Sørensen 1985; An and Gardner 2002).

In **CHAPTER 2** we used sediment flux core incubations and ^{15}N amendments to examine interactions between BMA activity and dissimilatory NO_3^- sinks in intertidal coastal sediments from Georgia and South Carolina, USA. Given that the relative magnitude of the dissimilatory processes has implications for the nitrogen budget of the system, it is important to understand their regulation individually and collectively. Slurry experiments were used to investigate the impact of two potential controlling factors of the DNF/DNRA relationship; sulfide (H_2S) concentration and the dissolved organic carbon (DOC): NO_3^- ratio. The results provide insight into the interactions between benthic photosynthesis, DNF and DNRA.

CHAPTER 3 further examines the fate of DIN in sediments by exploring the role of BMA in DIN assimilation and in DOC dynamics in intertidal sediments. Rates of benthic microalgal production rival macrophytic and planktonic production (Pinckney and Zingmark 1993b) and may account for up to one-third of gross primary production in estuarine systems (Pinckney and Zingmark 1993a). Epipellic diatoms often dominate the BMA community (Williams 1962) because their tidally-induced migratory behavior affords an advantage under dynamic conditions where variable light intensity, potentially high salinities, exposure, desiccation and scouring tides could limit, suspend, and export less well adapted BMA (Aleem 1949; Pomeroy 1959; Sundbäck and Granéli 1988; Cabrita and Brotas 2000). As shown in

CHAPTER 2, the assimilatory demands of BMA can regulate fluxes of inorganic nitrogen (NO_3^- and NH_4^+) as well as dissolved silicate ($\text{H}_2\text{SiO}_4^{2-}$) (Sigmon and Cahoon 1997). Additionally, BMA serve as a source of DOC in intertidal sediments. Direct release of DOC by epipelagic diatoms to support motility is accomplished by secretion of extracellular polymeric substances (EPS; Edgar and Pickett-Heaps 1984; Perkins et al. 2001); this DOC represents a source of labile organic matter for heterotrophic consumption or efflux from the sediment to the water column (Middelburg et al. 2000). To examine the role of BMA in the cycling of carbon we used benthic flux core incubations to quantify flux rates of inorganic nutrients, DIC and DOC under natural and NO_3^- amended conditions. The ^{15}N -labeled NO_3^- addition helped distinguish assimilatory (biological uptake, including BMA and bacterial assimilation) and dissimilatory (DNF and DNRA) pathways of nitrate reduction. Under diel (light-dark) light conditions, BMA were hypothesized to be the dominant sink for water column and sediment derived DIN, out-competing dissimilatory nitrate reduction processes. Under dark conditions, dissimilatory nitrate reduction processes (DNF and DNRA) were hypothesized to be the dominant sink for the added NO_3^- , as documented in **CHAPTER 2**.

Shallow groundwater has long been recognized as a dynamic and potentially important source of nutrients and dissolved organics to coastal waters (Giblin and Gaines 1990; Li et al. 1999; Kroeger and Charette 2008). **CHAPTER 4** examines the role of groundwater as a source of chemical constituents to coastal systems. Though groundwater only accounts for ~6-10% of surface water inputs to coastal waters globally (Burnett et al. 2003; Moore et al. 2008), the nutrient load associated with groundwater inputs may rival riverine inputs of nutrients because nutrient concentrations in groundwater often exceed those in surface waters (Moore et al. 2006; Swarzenski et al. 2007; Kroeger et al. 2007). Groundwater originating from developed

watersheds often contains even higher concentration of nutrients and organic matter (LaPointe et al. 1990; Cole et al. 2006). Inputs of nutrient enriched groundwater to coastal receiving waters can alter the rates and types of primary producers (e.g. phytoplankton, seagrass versus macroalgae) that are active in the system (Valiela et al. 1990; Gobler and Sañudo-Wilhemly 2001; Gobler and Boneillo 2003). Quantification of groundwater inputs is necessary for developing comprehensive nutrient budgets for coastal ecosystems.

Despite significant methodological advances in recent years (summarized in Burnett et al. 2003), quantifying groundwater inputs to coastal waters remains a challenge and, as a result, groundwater inputs are often the least constrained component of coastal nutrient and carbon budgets (Moore 1996; Burnett et al. 2003). The four isotopes of radium (^{223}Ra , ^{224}Ra , ^{226}Ra and ^{228}Ra) offer an extremely effective means to track groundwater input (Moore 1996; Rama and Moore 1996; Krest et al. 2000). Measuring the Ra isotopic composition and activity in groundwater reveals the volume of groundwater required to support the inferred groundwater-derived Ra flux. Contemporaneous measurement of groundwater nutrient concentrations permits estimation of groundwater-derived nutrient fluxes.

In **CHAPTER 4** we document the importance of groundwater-derived inputs to the Okatee River estuary, a coastal ecosystem in South Carolina. We quantified the relationship between the concentrations of DOC, nutrients, redox metabolites, trace gases (methane (CH_4) and nitrous oxide (N_2O)) and dissolved radium isotopes in shallow groundwater and used these data to develop radium vs. constituent regressions. Using the data from these regressions in conjunction with system-scale radium concentration data, we estimated groundwater derived loading rates of these components for the Okatee. Additionally, we quantified potential denitrification (pDNF) rates in sediment slurries and diffusive benthic fluxes of nutrients, redox

metabolites and organic carbon to evaluate the ability of Okatee sediments to remove nitrate.

Together, the data show that groundwater is an important source of nutrients and organic matter to the Okatee estuary.

The microbially-mediated processes that cycle N in intertidal sediments also influence N dynamics in shallow coastal aquifers. In **CHAPTER 5** we use a combination of field measurements, laboratory experiments and numerical model simulations to characterize the groundwater biogeochemical dynamics along a shallow monitoring well transect on Moses Hammock, a coastal hammock off of Sapelo Island, GA. This study was motivated by an observed switch in the redox status of the DIN pool in the well at the upland/saltmarsh interface that occurred during the spring-neap tidal transition: the DIN pool was dominated by NO_x ($\text{NO}_2^- + \text{NO}_3^-$) during spring tide and by NH_4^+ during neap tide.

The speciation of DIN has important consequences for DIN transport and the N mitigation potential of the subsurface DIN pools. The two main forms of DIN in groundwater are NO_3^- and NH_4^+ . Groundwater flow exposes DIN to different physico-chemical environments that impact the chemical composition of the fluid. In particular, the transition from fresh to saline groundwater in the so-called subterranean estuary constitutes a favorable setting for chemical and microbially-mediated processes that alter the form, bioavailability, and concentration of nutrients (e.g. Moore 1999). Ammonium can be converted to NO_3^- under oxic conditions (nitrification), combined with NO_2^- to produce N_2 (anaerobic ammonium oxidation, anammox) or taken up or released in the creation/breakdown of organic matter; NH_4^+ is also subject to cation exchange. In addition to being biologically assimilated, NO_3^- can serve as a terminal electron acceptor leading to N_2 (DNF or anammox via NO_2^-) or NH_4^+ (DNRA). Thus, the speciation of the groundwater-associated inorganic nitrogen both impacts and results from the

microbial processes occurring along the transport route. Because DNF and anammox constitute nitrogen sinks by converting bioavailable N into dinitrogen gas, these processes can mitigate inputs of NO_3^- and reduce eutrophication of receiving waters.

In **CHAPTER 5**, we attempted to identify the factors driving the recurring change in the $\text{NO}_x/\text{NH}_4^+$ ratio of groundwater near the upland-marsh transition zone. We used laboratory experiments to quantify the role of NH_4^+ adsorption and DNF/DNRA relationships that reflected the impact of H_2S concentration and $\text{DOC}:\text{NO}_3^-$ ratios (**CHAPTER 2**). Field and laboratory findings were integrated into a variable density reactive transport model representing a vertical 2D cross section of the upland. Model simulations were carried out for both spring and neap tide conditions to identify the processes responsible for the observed variation in DIN speciation. Finally, building on the calibrated model and expanding beyond the relatively pristine conditions of Moses Hammock, simulations were performed to assess the potential impact of discharge from a septic tank on groundwater biogeochemistry and to quantify the N removal potential in the aquifer.

LITERATURE CITED

- Aleem, A. 1950. The diatom community inhabiting the mud-flats at Whitstable. *New Phytologist* 49: 174-187.
- Aller, R. 1994. Bioturbation and remineralization of sedimentary organic matter: Effects of redox oscillation. *Chemical Geology* 114: 331-345.
- An, S., and W. Gardner. 2002. Dissimilatory nitrate reduction to ammonium (DNRA) as a nitrogen link, versus denitrification as a sink in a shallow estuary (Laguna Madre/Baffin Bay, Texas). *Marine Ecology Progress Series* 237: 41-50.

- Burnett, W., H. Bokuniewicz, M. Huettel, W. Moore, and M. Taniguchi. 2003. Groundwater and pore water inputs to the coastal zone. *Biogeochemistry* 66: 3-33.
- Cabrita, M., and V. Brotas. 2000. Seasonal variation in denitrification and dissolved nitrogen fluxes in intertidal sediments of the Tagus estuary, Portugal. *Marine Ecology Progress Series* 202: 51-65.
- Cole, M., K. Kroeger, J. McClelland, and I. Valiela. 2006. Effects of watershed land use on nitrogen concentrations and δ^{15} nitrogen in groundwater. *Biogeochemistry* 77: 199-215.
- De Jonge, V., W. Boynton, C. D'Elia, R. Elmgren, and B. Welsh. 1994. Responses to developments in eutrophication in four different North Atlantic estuarine systems, p. 179-196. In K. Dyer and R. Orth [eds.] *Changes in fluxes in estuaries: Implications from science to management*. Olsen & Olsen.
- Edgar, L., and J. Pickett-Heaps. 1984. Diatom locomotion, p. 48-88. In D. Chapman and F. Round [eds.] *Progress in Phycological Research, Volume 3*. Biopress, Bristol.
- Eyre, B., and A. Ferguson. 2002. Comparison of carbon production and decomposition, benthic nutrient fluxes and denitrification in seagrass, phytoplankton, benthic microalgae- and macroalgae-dominated warm-temperate Australian lagoons. *Marine Ecology Progress Series* 229: 43-59.
- Giblin, A., and A. Gaines. 1990. Nitrogen inputs to a marine embayment - the importance of groundwater. *Biogeochemistry* 10: 309-328.
- Gobler, C., and G. Boneillo. 2003. Impacts of anthropogenically influenced groundwater seepage on water chemistry and phytoplankton dynamics within a coastal marine system. *Marine Ecology Progress Series* 255: 101-114.

- Gobler, C., and S. Sañudo-Wilhemy. 2001. Temporal variability of groundwater seepage and brown tide blooms in a Long Island embayment. *Marine Ecology Progress Series* 217: 299-309.
- Howarth, R., R. Marino, J. Lane, and J. Cole. 1988. Nitrogen fixation in freshwater, estuarine and marine ecosystems: 1. Rates and importance. *Limnology and Oceanography* 33:669-687.
- Howarth, R., G. Billen, D. Swaney, A. Townsend, N. Jaworski, K. Lajtha, J. Downing, R. Elmgren, N. Caraco, T. Jordan, F. Berendse, J. Freney, V. Kudeyarov, P. Murdoch, and Zhu Zhao-Liang. 1996. Regional nitrogen budgets and riverine N & P fluxes for the drainages to the North Atlantic Ocean: Natural and human influences. *Biogeochemistry* 35: 75-139.
- Howarth, R., E. Boyer, W. Pabich, and J. Galloway. 2002. Nitrogen use in the United States from 1961-2000 and potential future trends. *Ambio* 31: 88-96.
- Huettel, M., H. Roy, E. Precht, and S. Ehrenhauss. 2003. Hydrodynamical impact on biogeochemical processes in aquatic sediments. *Hydrobiologia* 494:231-236.
- Jahnke, R., J. Nelson, R. Marinelli, and J. Eckman. 2000. Benthic flux of biogenic elements on the Southeastern US continental shelf: influence of pore water advective transport and benthic microalgae. *Continental Shelf Research* 20:109-127.
- Joye, S., and J. Hollibaugh. 1995. Sulfide inhibition of nitrification influences nitrogen regeneration in sediments. *Science* 270: 623-625.
- Joye, S., M. Mazzotta, and J. Hollibaugh. 1996. Community metabolism in microbial mats: The occurrence of biologically-mediated iron and manganese reduction. *Estuarine, Coastal and Shelf Science* 43: 747-766.

- Jørgensen, B., and J. Sørensen. 1985. Seasonal cycles of O₂, NO₃⁻, and SO₄²⁻ reduction in estuarine sediments: The significance of a NO₃⁻ reduction maximum in spring. *Marine Ecology Progress Series* 24: 65-74.
- Koike, I., and A. Hattori. 1978. Simultaneous determinations of nitrification and nitrate reduction in coastal sediments by a ¹⁵N dilution technique. *Applied and Environmental Microbiology* 25: 853-857.
- Krest, J., W. Moore, L. Gardner, and J. Morris. 2000. Marsh nutrient export supplied by groundwater discharge: Evidence from Ra measurements. *Global Biogeochemical Cycles* 14: 167-176.
- Kroeger, K., and M. Charette. 2008. Nitrogen biogeochemistry of submarine groundwater discharge. *Limnology and Oceanography* 53: 1025-1039.
- Kroeger, K., P. Swarzenski, Wm. Greenwood, and C. Reich. 2007. Submarine groundwater discharge to Tampa Bay: Nutrient fluxes and biogeochemistry of the coastal aquifer. *Marine Chemistry* 104: 85-97.
- LaPointe, B., J. O'Connell, and G. Garrett, 1990. Nutrient couplings between on-site sewage disposal systems, groundwaters, and nearshore waters of the Florida Keys. *Biogeochemistry* 10: 289-307.
- Li, L., D. Barry, F. Stagnitti, and J. Parlange. 1999. Submarine groundwater discharge and associated chemical input to a coastal sea. *Water Resources Research* 35: 3253-3259.
- Middelburg, J., C. Barranguet, H. Boschker, P. Herman, T. Moens, and C. Heip. 2000. The fate of intertidal microphytobenthos carbon: An in situ ¹³C-labeling study. *Limnology and Oceanography* 45: 1224-1234.

- Moore, W. 1996. Large groundwater inputs to coastal waters revealed by ^{226}Ra enrichments. *Nature* 380: 612-614.
- Moore, W. 1999. The subterranean estuary: A reaction zone of ground water and sea water. *Marine Chemistry* 65: 111-125.
- Moore, W., J. Blanton, and S. Joye. 2006. Estimates of flushing times, submarine groundwater discharge, and nutrient fluxes to Okatee Estuary, South Carolina. *Journal of Geophysical Research* 111, C09006, doi: 10.1029/2005JC003041.
- Moore, W., J. Sarmiento, and R. Key. 2008. Submarine groundwater discharge revealed by ^{228}Ra distribution in the upper Atlantic Ocean. *Nature Geoscience* doi: 10.1038/geo183.
- Nixon, S., C. Oviatt, and S. Hale. 1976. Nitrogen regeneration and the metabolism of coastal marine bottom communities, p. 269-283. In J. Anderson and A. Macfadyen. [eds.] The role of terrestrial and aquatic organisms in decomposition processes. Blackwell.
- Nixon, W., J. Ammermann, L. Atkinson, V. Berounsky, G. Billen, W. Boicourt, W. Boynton, T. Church, D. Ditoro, R. Elmgren, J. Garber, A. Giblin, R. Jahnke, N. Owens, M. Pilson, S. Seitzinger. 1996. The fate of nitrogen and phosphorous at the land-sea margin of the North Atlantic Ocean. *Biogeochemistry* 35: 141-180.
- Paerl, H. 1997. Coastal eutrophication and harmful algal blooms: Importance of atmospheric deposition and groundwater as “new” nitrogen and other nutrient sources. *Limnology and Oceanography* 42: 1154-1165.
- Paerl, H., J. Pinckney, J. Fear, and B. Peierls. 1998. Ecosystem responses to internal and watershed organic matter loading: Consequences for hypoxia in the eutrophying Neuse River Estuary, North Carolina, USA. *Marine Ecology Progress Series* 166: 17-25.

- Perkins, R., G. Underwood, V. Brotas, G. Snow, B. Jesus, and L. Ribeiro. 2001. Responses of microphytobenthos to light: Primary production and carbohydrate allocation over an emersion period. *Marine Ecology Progress Series* 223: 101-112.
- Persky, J. 1986. The relations of ground-water quality to housing density, Cape Cod, Massachusetts. USGS Water-Resources Investigations Report 86-4093.
- Pinckney, J., and R. Zingmark. 1993a. Biomass and production of benthic microalgal communities in estuarine habitats. *Estuaries* 16: 887-897.
- Pinckney, J., and R. Zingmark. 1993b. Modeling the annual production of intertidal benthic microalgae in estuarine ecosystems. *Journal of Phycology* 29: 396-407.
- Pomeroy, L. 1959. Algal productivity in salt marshes of Georgia. *Limnology and Oceanography* 4: 386-397.
- Rabalais, N., R. Turner, D. Justić, Q. Dortch, W. Wiseman Jr., and B. Gupta. 1996. Nutrient changes in the Mississippi River and system responses on the adjacent continental shelf. *Estuaries* 19: 386-407.
- Rama, and W. Moore. 1996. Using the radium quartet to estimate water exchange and groundwater input in salt marshes. *Geochimica et Cosmochimica Acta* 60: 4645-4652.
- Ryther, J. and W. Dunstan. 1971. Nitrogen, phosphorous and eutrophication in the coastal marine environment. *Science* 171: 1008-1112.
- Seitzinger, S., C. Kroeze, A. Bouwman, N. Caraco, F. Dentener, and R. Styles. 2002. Global patterns of dissolved inorganic and particulate nitrogen inputs to coastal systems: Recent conditions and future projections. *Estuaries* 25: 640-655.
- Sigmon, D., and L. Cahoon. 1997. Comparative effects of benthic microalgae and phytoplankton on dissolved silica fluxes. *Aquatic Microbial Ecology* 13: 275-284.

- Sundbäck, K., and W. Granéli. 1988. Influence of microphytobenthos on nutrient fluxes between sediment and water: A laboratory continuous flow study. *Marine Ecology Progress Series* 43: 63-69.
- Swarzenski, P., C. Reich, K. Kroeger, and M. Baskaran. 2007. Ra and Rn isotopes as natural tracers of submarine groundwater discharge in Tampa Bay, Florida. *Marine Chemistry* 104: 69-84.
- Valiela, I., J. Costa, K. Foreman, J. Teal, B. Howes, and D. Aubrey. 1990. Transport of groundwater-borne nutrients from watersheds and their effects on coastal water. *Biogeochemistry* 10: 177-197.
- Vitousek, P., H. Mooney, J. Lubchenco, and J. Melillo. 1997. Human domination of Earth's ecosystems. *Science* 277: 494-499.
- Williams, R. 1962. The ecology of diatom populations in a Georgia salt marsh. Ph. D. thesis. Harvard Univ.

CHAPTER 2

BENTHIC METABOLISM AND THE FATE OF DISSOLVED INORGANIC NITROGEN IN INTERTIDAL SEDIMENTS¹

¹Porubsky, W., N. Weston, and S. Joye. Re-submitted to *Estuarine, Coastal and Shelf Science*, 09/15/2008.

ABSTRACT

We determined patterns of benthic metabolism and examined the relative importance of denitrification (DNF) and dissimilatory nitrate reduction to ammonium (DNRA) as sinks for nitrate (NO_3^-) in intertidal sediments in the presence and absence of benthic microalgal (BMA) activity. By influencing the activity of BMA, light regulated the metabolic status of the sediments, and, in turn, exerted strong control on sediment nitrogen dynamics and the fate of inorganic nitrogen. A pulsed addition of ^{15}N labeled NO_3^- tracked the effect and fate of dissolved inorganic nitrogen (DIN) in the system. Under illuminated conditions, BMA communities influenced benthic fluxes directly, via DIN uptake, and indirectly, by altering the oxygen penetration depth. Under dark hypoxic and anoxic conditions, the fate of water column NO_3^- was determined largely by three competing dissimilatory reductive processes; DNF, DNRA, and, on one occasion, anaerobic ammonium oxidation (anammox). Mass balance of the added ^{15}N tracer illustrated that DNF accounted for a maximum of 48.2% of the $^{15}\text{NO}_3^-$ reduced while DNRA (a minimum of 11.4%) and anammox (a minimum of 2.2%) accounted for much less. A slurry experiment was employed to further examine the partitioning between the main dissimilatory NO_3^- sinks, DNF and DNRA. High sulfide concentrations negatively impacted rates of both processes, while high DOC: NO_3^- ratios favored DNRA over DNF.

INTRODUCTION

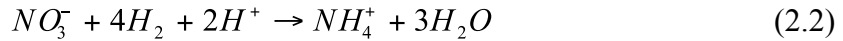
Nutrient regeneration in sediments and subsequent release to the overlying water column, commonly referred to as benthic-pelagic coupling, fuels a significant portion of water column production in shallow estuarine systems (Nixon et al. 1976). Factors such as water depth,

turbidity, sedimentation rates, organic matter remineralization rates, bioturbation, and diffusive or advective transport (Aller 1994; Jahnke et al. 2000; Huettel et al. 2003) influence the magnitude and efficiency of benthic-pelagic coupling. The presence and activity of a benthic microalgal community also strongly affects benthic-pelagic coupling (Joye et al. 1996; Jahnke et al. 2000). Benthic microalgae (BMA) occupy a μm to mm thick layer at the surface of intertidal and shallow subtidal sediments and their activity affects both the oxygen (O_2) flux and the O_2 penetration depth in the sediment. By modulating O_2 dynamics, BMA alter the sediment redox status and influence rates and pathways of nutrient cycling. BMA also consume nutrients from both the water column and underlying sediments. Under oxic conditions, BMA-dominated sediments act as a nutrient sink while under hypoxic or anoxic conditions, the same sediments serve as a nutrient source of to the water column (Joye et al. 1996; Eyre and Ferguson 2002).

Oxygen production by BMA can stimulate nitrification, which in turn may enhance dissimilatory nitrate (NO_3^-) sinks, e.g., denitrification (DNF) or dissimilatory nitrate reduction to ammonium (DNRA). Complete DNF is the reduction of NO_3^- to N_2 as described by (Zumft 1992; Eq. 2.1):



The reduction of NO_3^- to N_2 via DNF involves a $5 e^-$ transfer and has a free energy yield of $-560 \text{ kJ mole}^{-1} \text{ NO}_3^-$ at steady state (Zumft 1992). DNF produces mainly gaseous end products (N_2O and N_2) that readily diffuse from the system and N_2 is generally not bioavailable (Howarth et al. 1988); thus, DNF represents a net loss of fixed nitrogen from a system. Conversely, the end product of DNRA is NH_4^+ , which is readily assimilable and can support additional production. The DNRA reaction includes NO_3^- reduction to NO_2^- and then to NH_4^+ (Tiedje 1994; Thauer et al. 1977; Eq. 2.2):



DNRA involves 8 e⁻ per NO₃⁻ reduced and has a free energy yield of -600 kJ mole⁻¹ NO₃⁻ (Thauer et al. 1977). The interplay between DNF and DNRA is further complicated by recent evidence for a third pathway of NO₃⁻ reduction: anaerobic ammonium oxidation (hereafter anammox). Anammox involves the production of N₂ via the reduction of NO₂⁻ coupled to the oxidation of NH₄⁺ (van de Graaf et al. 1995; Eq. 2.3):



Anammox has a free energy yield of -358 kJ mole⁻¹ NO₂⁻ (van de Graaf et al. 1995). Like DNF, anammox generates N₂ and thus represents a net loss of nitrogen from the system.

The processes of DNF, DNRA, and anammox may compete for nitrogen oxides (NO₃⁻ or NO₂⁻) in sediments in the absence of O₂, and influence the DIN available for flux to the overlying water column. The relative importance of DNRA versus DNF as NO₃⁻ sinks in coastal systems is unclear; however, DNRA rates rival DNF rates in some environments (Koike and Hattori 1978; Jørgensen and Sørensen 1985; An and Gardner 2002). While no previous studies have examined the interplay between these three processes, a number of studies have examined the relative importance of DNF versus DNRA. The environmental controls on these two processes include the ratio of dissolved organic carbon (DOC) to NO₃⁻ (Tiedje et al. 1982), temperature (King and Nedwell 1984; Ogilvie et al. 1997b; Kelly-Gerreyn et al. 2001), NO₃⁻ concentration (Fazzolari et al. 1998), and hydrogen sulfide (H₂S) concentration (Brunet and Garcia-Gil 1996; An and Gardner 2002). The controls on anammox are uncertain and how anammox interacts with DNF and DNRA is not known at present. Available evidence suggests that anammox and DNF can occur simultaneously (Thamdrup and Dalsgaard 2002; Risgaard-Petersen et al. 2003) and anammox bacteria may be capable of DNRA (Kartal et al. 2007).

We used sediment flux core incubations and ^{15}N amendments to examine interactions between BMA activity and dissimilatory NO_3^- sinks in intertidal coastal sediments in Georgia and South Carolina, USA. We hypothesized that under diel, illuminated conditions, a pulse of DIN supplied to the water column would be assimilated by BMA. In contrast, under dark-induced anoxic conditions, DIN would be reduced by one of three competing dissimilatory pathways. The relative importance of the dissimilatory processes has implications for the nitrogen budget of the system; thus, it is important to understand their regulation individually and collectively. Slurry experiments were used to investigate the impact of H_2S concentration and the $\text{DOC}:\text{NO}_3^-$ ratio on the partitioning of dissimilatory NO_3^- reduction between DNF and DNRA. The results provide insight into the interactions between benthic photosynthesis, DNF, DNRA and anammox.

METHODS

Study sites

Two intertidal creek bank sites in Georgia and South Carolina, USA (Fig. 2.1) were sampled on four occasions between 2002 and 2004, and in 2005. At both sites, the adjacent saltmarsh was dominated by *Spartina alterniflora*. Creek bank sediments were macrophyte free but were overlain by dense accumulations of benthic microalgae, mainly diatoms (Velasquez 2005).

The Dover Bluff (DB) site, located on Umbrella Creek along the Satilla River (Georgia), has annual salinity and temperature ranges of approximately 12 to 30 and 15.5 to 25.6°C respectively. The site lies adjacent to a residential community and receives septic inputs from the developed upland (Weston et al. 2006). The Grave's Dock (GD) site, located within the Okatee

River estuary (South Carolina), was characterized by near seawater salinity (Weston et al. 2006) and annual temperatures ranging from 15.5 to 26.8°C. The Okatee watershed is heavily developed and nutrient inputs to the system are expected to increase in the coming years (Windom et al. 1998). To contrast the two study sites, we include limited data from a previously published biogeochemistry study of these sediments (Table 2.1; see Weston et al. 2006 for detailed methods of pore water collection and analytical methods).

Benthic flux experimental design

Benthic fluxes were determined in flow-through incubations of sediment cores ($n = 2-3$ cores per treatment per site). Clear acrylic core tubes with a diameter of 12 cm contained the top 20 cm of sediment above which a water column of 20 cm (approximately 2.25-2.5 liters) was circulated. Creek water and intact sediment cores were collected at the same time and returned to the lab for incubation. The creek water was filtered (0.7 μm GF/F filter) and flow through the cores was maintained via a peristaltic pump during the 2002 incubations; the flow speed was approximately 30 ml min^{-1} . During the 2004 incubations, the overlying water column was mixed by magnetically-driven stir bars. Both methods served to limit the development of a diffusive boundary layer (adequate mixing was confirmed by dye tests).

Two incubation treatments were included for each study site and date. Dark treatments were incubated by wrapping each core in 3 layers of aluminum foil. Diel treatments were maintained at light levels representative of those at the sediment water interface at high tide ($2 - 4 \times 10^{-4}$ mol photons $\text{m}^{-2} \text{s}^{-1}$; as estimated from turbidity, PAR, and water column depth; data not shown) over a simulated natural diel cycle (winter: 10.5 hours light, 13.5 hours dark; summer: 13.5 hours light, 10.5 hours dark). Three different light exposure regimes were achieved using

this design: “dark” (continuous darkness), “diel-day” (diel treatment during illumination), and “diel-night” (diel treatment during darkness). Flux experiments were conducted in an incubator to maintain temperatures at field levels. Cores were sampled every 6 to 12 hours for 6 to 14 days.

Flux experiments occurred in two phases. The first phase of the incubation determined “baseline” fluxes in diel and dark treatments. The second phase consisted of a $\text{K}^{15}\text{NO}_3^-$ amendment, which was made to all cores after the dark treatments became hypoxic ($[\text{O}_2] < 50 \mu\text{mol L}^{-1}$). Hereafter, the first phase is referred to as “baseline” and the second phase is referred to as “amended”. Fluxes were calculated from the linear change in water column species concentration over time. Fluxes into the sediment (uptake) are reported as negative numbers while fluxes out of the sediment (release) are reported as positive numbers. Statistical comparisons of concentrations and rates between treatments were obtained by analysis of variance (ANOVA).

Sample collection

At each time point a water sample was collected via in-line syringe, and aliquots were dispensed into different vials for a variety of analyses. The volume removed, approximately 100 ml or 4% of the total volume per time point, was replaced with time zero, filtered creek water from a reservoir. Dissolved O_2 concentration and pH were determined immediately by a galvanic dissolved O_2 probe and a combination pH/reference electrode respectively. H_2S samples were fixed immediately with 500 μL of 20% zinc acetate and concentrations were determined colorimetrically (Cline 1969).

Dissolved inorganic carbon (DIC) concentration was determined using a Shimadzu GC-14A gas chromatograph equipped with a methanizer and a flame ionization detector in

January/February 2002. For the August 2002 and the January 2004 experiments, DIC concentrations were determined on a Shimadzu (TOC-5000) infrared carbon analyzer.

A 30 mL sub-sample was filtered (0.2 μm) into a high density polyethylene bottle and stored at 4°C for subsequent determination of ammonium, nitrate + nitrite (NO_x), nitrite, and total dissolved nitrogen (TDN). A 5ml subsample was preserved with 200 μL of phenol and NH_4^+ concentration was quantified using the phenol-hypochlorite method (Solorzano 1969). Concentrations of NO_x and NO_2^- were determined by vanadium reduction and NO detection (Antek 745 $\text{NO}_3^-/\text{NO}_2^-$ reduction assembly and 7050 NO detector). TDN was determined using a Shimadzu TOC-5000 coupled to an Antek 7050 NO detector (Álvarez-Salgado and Miller 1998). Dissolved organic nitrogen (DON) was determined by difference ($\text{DON} = \text{TDN} - (\text{NO}_x + \text{NH}_4^+)$). DOC was measured on an acidified subsample (stored at 4°C) using a Shimadzu TOC-5000 analyzer. After the experiment, triplicate samples were collected from each core for chlorophyll *a* quantification via 24 hour extraction in 100% acetone and subsequent spectrophotometric analysis (Strickland and Parsons 1972).

¹⁵N addition experiments

¹⁵N amendments were used to determine the fate of NO_3^- in the sediment via both dissimilatory and assimilatory pathways. The water column of all cores was amended with 99 atom % $\text{K}^{15}\text{NO}_3^-$ to a final concentration of $\sim 100 \mu\text{mol L}^{-1}$ and the $^{15}\text{NO}_3^-$ was tracked into the N_2 pool by measuring the $^{29}\text{N}_2$ and $^{30}\text{N}_2$ masses using a membrane inlet mass spectrometer (MIMS, Kana et al. 1998; Eyre et al. 2002). The isotope pairing technique (IPT; Nielsen 1992) was used to estimate the amount of DNF that occurred without NO_3^- amendment (D_{14}) and denitrification of the added $^{15}\text{NO}_3^-$ (D_{15}) was estimated from the amount of ^{15}N in the N_2 pool.

The contribution of anammox to NO_3^- consumption in the dark treatment for August 2002 was inferred from $^{29}\text{N}_2$ production under anoxic conditions. In order for DNF to produce $^{29}\text{N}_2$, one $^{15}\text{NO}_3^-$ and one $^{14}\text{NO}_3^-$ would be consumed. The amount of $^{14}\text{NO}_x$ available was calculated from the mean concentration of NO_x in the overlying water of the sediment cores for each site during the sampling that preceded the amendment ($0.23 \mu\text{mol L}^{-1} \text{NO}_x$ for DB and $0.24 \mu\text{mol L}^{-1} \text{NO}_x$ for GD) and the amount of $^{14}\text{NO}_3^-$ in the tracer amendment (99% $^{15}\text{NO}_3^-$ and 1% $^{14}\text{NO}_3^-$ giving $0.74 \mu\text{mol L}^{-1} \text{NO}_3^-$ in the addition for DB and $1.02 \mu\text{mol L}^{-1} \text{NO}_3^-$ for GD). Given the low pore water NO_3^- concentration observed in the surface sediments under in situ conditions ($0.7 - 2.4 \mu\text{mol L}^{-1}$), that the sediments were anoxic, and that DNF, as well as microbial NO_3^- assimilation, were active during the previous 4 days of incubation, it is extremely unlikely that any pore water $^{14}\text{NO}_3^-$ remained during the amended portion of the incubation. The total amount of $^{14}\text{NO}_x$ following the amendment could account for no more than 0.97 (DB) to 1.26 (GD) $\mu\text{mol L}^{-1} \text{NO}_x$. Excess $^{29}\text{N}_2$ above that amount thus serves as a minimum estimate of anammox activity, reflecting the conversion of $^{15}\text{NO}_2^-$ and $^{14}\text{NH}_4^+$ to $^{29}\text{N}_2$.

For the August 2002 and January 2004 experiments, the amount of $^{15}\text{NH}_4^+$ produced during the incubation was quantified at the termination of the experiment using the ammonium diffusion method (Holmes et al. 1998). Potential DNRA rates were determined by calculating the amount of NH_4^+ produced following the $^{15}\text{NO}_3^-$ amendment and multiplying that by the ^{15}N -labeled fraction of NH_4^+ (determined from the atom % ^{15}N of the final NH_4^+ pool), which corrected for any production of $^{14}\text{NH}_4^+$ from organic matter remineralization. The resulting $^{15}\text{NH}_4^+$ concentration was compared to the $^{15}\text{NH}_4^+$ concentration prior to the ^{15}N amendment, which was calculated from the NH_4^+ concentration and ^{15}N natural abundance, to determine a potential DNRA rate of $^{15}\text{NO}_3^-$.

Slurry experiment

Intact sediment cores (30 cm in depth) collected from each site ($n = 10$ per site) in December 2005 were sectioned in an anaerobic chamber under an N_2 (~97%) and H_2 (~3%) atmosphere. A 2 ml sample of wet sediment was collected for characterization of physical properties. Sediment from two depth intervals, 0-3 and 8-13 cm, was used in laboratory experiments. Artificial salt water (ASW) was used for all incubations with a salinity of 19.4 (equivalent to field salinities) and was free of NH_4^+ and SO_4^{2-} , which allowed us to detect low levels of NH_4^+ production and to eliminate H_2S produced by sulfate reduction. Slurry incubations were performed at 23°C.

Sediments were washed five times in the anaerobic chamber in a 4:1 (ASW:sediment) ratio prior to the onset of each experiment (Weston and Joye 2005). Five wash cycles lowered the dissolved NH_4^+ , SO_4^{2-} and H_2S concentrations to below $10 \mu\text{mol L}^{-1}$ and NO_x to below $0.5 \mu\text{mol L}^{-1}$ (data not shown). Washed sediment was combined with ASW in a 1:4 ratio and purged with a 0.9% Ar in a balance of N_2 for 30 minutes. After purging, 16 mL aliquots of the slurry were placed into glass tubes that were sealed without a headspace. Samples were then amended with the appropriate substrate additions and the incubation began.

Time series incubations were conducted to determine the optimum incubation time to ensure linear rates and no substrate limitation (data not shown). The influence of H_2S on NO_3^- reduction was examined by the addition of a range of H_2S concentrations ($0 - 5000 \mu\text{mol L}^{-1}$) in combination with $^{15}NO_3^-$ (as a substrate for DNF and DNRA) and acetate (to prevent carbon limitation); the H_2S treatments were pH adjusted to approximately 7.25 (typical pH value for porewater in the top 20 cm, data not shown) following H_2S addition. The influence of the DOC to electron acceptor (i.e. NO_3^-) ratio was examined by addition of $^{15}NO_3^-$ and various

concentrations of acetate. Time zero incubations were killed immediately by injection of ZnCl_2 ; all other samples were gently shaken for 6 hours, prior to centrifugation at 400 rpm for 10 minutes and subsequent sampling.

Species quantification for the incubation experiments used the same analytical methods as described above for the benthic flux samples except where noted below. Following the initial sub-sampling, the three isotopic species of N_2 and the N_2/Ar ratio were quantified on the MIMS by inserting the inlet tube of the MIMS directly into the incubation tube taking care to prevent sediment from being drawn into the inlet. A 1 mL sub-sample of sediment was collected for determination of exchangeable NH_4^+ (modified from Mackin and Aller 1984; Morin and Morse 1999). Rates were calculated as the change in concentration over time.

RESULTS

Sediment Biogeochemistry

Benthic chl *a* concentrations were similar at both sites on all sampling dates (range 45 to 56 mg chlorophyll *a* m^{-2} ; Table 2.1); pore water salinities were not significantly different between the sampling dates. Integrated pore water inventories (upper 10 cm) for NO_3^- , NH_4^+ , DOC, and salt (Cl^-), for DB and GD sites in January 2002 and August 2002 are shown in Table 2.1 (Weston et al. 2006). Inventories of NO_3^- were similar for both sites while NH_4^+ inventories were always higher at DB (Weston et al. 2006). Concentrations of H_2S and DOC were higher at DB than GD, especially during summer (Weston et al. 2006).

Oxic benthic fluxes: Baseline conditions

Baseline (prior to $^{15}\text{NO}_3^-$ addition) O_2 concentrations showed a strong diel cycle, with O_2 production during the day and O_2 consumption at night (Fig. 2.2A and 2.3A; Table 2). The O_2 concentration remained above $150 \mu\text{mol L}^{-1}$ under baseline conditions in the diel treatments. Oxygen fluxes in diel treatments indicated net autotrophy, while O_2 fluxes observed in dark treatments indicated net heterotrophy (Table 2.2). Baseline NO_3^- fluxes were low at both sites on all dates (Figs. 2.2C and 2.3C; Table 2.2). Sediments were a NO_3^- sink under diel-day and diel-night conditions, with the exception of diel-day fluxes at DB in January 2004 and diel-night fluxes at GD in February 2002 (Table 2.2). Concentrations of NH_4^+ decreased quickly in baseline diel treatments, usually under both diel-day and diel-night conditions (Table 2.2). Dissolved organic N was released under baseline diel-day conditions and taken up under diel-night conditions (Table 2.2). Fluxes of DOC were higher at DB than GD (Table 2.2), but were not significantly different.

Oxic benthic fluxes: Amended conditions

Following the $^{15}\text{NO}_3^-$ amendment, the absolute magnitude of O_2 fluxes increased. Amended O_2 production for August 2002 was approximately 1.5 times higher than the corresponding baseline rates under diel-day conditions (Table 2.2). Under diel-night conditions, amended O_2 uptake rates were approximately 3.5 times higher than baseline rates (Table 2.2). During the August experiment, both O_2 production (diel-day) and consumption (diel-night) were stimulated to comparable levels. Fluxes of DIC showed a similar increase under diel-night conditions with release increasing approximately 3.5 times over baseline rates (Table 2.2). A different response to the $^{15}\text{NO}_3^-$ amendment was observed at DB in January 2004. Amended O_2

release rates under diel-day conditions were approximately 2.3 fold higher than baseline rates while diel-night O₂ consumption rates increased 1.5 times (Table 2.2). The uptake of DIC under amended diel-day conditions exceeded DIC release rates under diel-night conditions for January 2004.

Following the ¹⁵NO₃⁻ amendment, NO₃⁻ concentrations decreased quickly, with highest NO₃⁻ uptake rates usually observed under diel-day conditions, followed usually by dark conditions, and finally diel-night conditions (Figs. 2.2C and 2.3C; Table 2.2). Following the ¹⁵NO₃⁻ amendment, fluxes of NH₄⁺ remained low in diel treatments (Figs. 2.2E and 2.3E; Table 2.2). The DON release observed under baseline conditions continued after N amendment for the diel-day treatments (Table 2.2). Fluxes of DOC increased following ¹⁵NO₃⁻ addition at both sites, but DOC fluxes were higher (by about 3.5 times) at the DB site (Table 2.2). At both sites, DOC release (net production) was observed during diel-day incubations while DOC uptake (net consumption) was observed during diel-night incubations.

Oxic benthic fluxes: DNF rates

Rates of D₁₄ under diel conditions were generally low for both sites on all dates, with rates ranging from 0 to 5 μmol N m⁻² h⁻¹ (Table 2.3). Lower D₁₄ rates correlated with lower temperatures (February 2002 GD; and January 2004 both sites). In incubations with warmer temperatures, D₁₄ rates in diel incubations were lower than the corresponding rates in dark incubations. Rates of D₁₅ increased by an order of magnitude in diel treatments following the ¹⁵NO₃⁻ amendment (Table 2.3); D₁₅ rates were ~4 to 13 times higher than the corresponding D₁₄ rates (Table 2.3).

Hypoxic / anoxic benthic fluxes: Baseline conditions

Under dark conditions, O₂ concentrations decreased from 200 μmol L⁻¹ to < 50 μmol L⁻¹ within about two days at both sites in August 2002 (Figs. 2.2B and 2.3B) and at DB in January 2002 (data not shown). Though baseline dark NO₃⁻ fluxes were low (Figs. 2.2D and 2.3D; Table 2.2), sediments were a consistent sink for NO₃⁻. Concentrations of NH₄⁺ decreased initially under baseline dark conditions but then increased under hypoxic conditions (Figs. 2.2F and 2.3F; Table 2.2).

Hypoxic / anoxic benthic fluxes: Amended conditions

Nitrate uptake rates in dark incubations increased following the ¹⁵NO₃⁻ amendment (Figs. 2.2D and 2.3D; Table 2.2) with dark uptake rates usually being lower than diel-day uptake rates, but higher than diel-night rates (Table 2.2). Ammonium release rates under amended dark conditions increased up to 14 times in the August 2002 DB experiments (Fig. 2.2F).

Hypoxic / anoxic benthic fluxes: DNF rates

Rates of D₁₄ under dark conditions were low for all sampling dates, with rates ranging from ~0 to 15 μmol N m⁻² h⁻¹ (Table 2.3). D₁₄ rates were significantly higher under dark conditions ($p < 0.01$) except at GD in January 2002. Following the ¹⁵NO₃⁻ amendment, D₁₅ rates were ~15 to 45 times higher than the D₁₄ rates (Table 2.3). Dark D₁₅ rates were significantly higher than diel D₁₅ rates at DB in January 2002 ($p < 0.01$) and at both sites in August 2002 ($p < 0.05$; Table 2.3).

Dissimilatory NO₃⁻ sinks

Results from the DB dark experiment in August 2002 illustrated the complex interactions that can result from a sudden increase in water column NO₃⁻ concentration. Prior to the ¹⁵NO₃⁻ amendment, the concentration of NH₄⁺ had increased by an order of magnitude (Fig. 2.2F). The amendment increased the NO₃⁻ concentration from 0.23 to 73.6 μmol L⁻¹. Afterwards, NO₂⁻ concentration increased from 0.56 to 21.7 μmol L⁻¹. Then, NO₂⁻ concentration decreased to 1.2 μmol L⁻¹ and the NH₄⁺ concentration decreased to 74.4 μmol L⁻¹ (Fig. 2.2D). The stoichiometry of NH₄⁺ and NO₂⁻ uptake was approximately 1:1. Concentrations of ²⁹N₂ increased concomitantly with the decrease in NO₂⁻ and NH₄⁺ concentrations. ³⁰N₂ concentrations increased from baseline levels to approximately 22 μmol L⁻¹ following the ¹⁵NO₃⁻ amendment (Fig. 2.2F).

After the NO₂⁻ concentration declined to zero, the NH₄⁺ concentration increased to 123 μmol L⁻¹ (Fig. 2.2F). The atom % ¹⁵N of the NH₄⁺ pool (6.9 atom % ¹⁵N at DB) indicated a minimum production of 8.4 μmol L⁻¹ ¹⁵NH₄⁺ via DNRA, which amounted to 11.4% of the ¹⁵NO₃⁻ amendment. This value may be an underestimate as it does not include ¹⁵NH₄⁺ that may have been produced and subsequently utilized via anammox (¹⁵NO₂⁻ + ¹⁵NH₄⁺ = ³⁰N₂) or ¹⁵NH₄⁺ that may have sorbed onto the sediment or been immobilized by bacteria. The rate of DNRA at DB in August 2002 was 38 μmol N m⁻² h⁻¹, which amounts to 13.5% of the D₁₅ rate (~280 μmol N m⁻² h⁻¹) for the dark treatment (Table 2.3).

Slurry experiments

The influence of H₂S concentration on NO₃⁻ reduction was investigated by addition of ¹⁵NO₃⁻ and one of four H₂S concentrations (0, 20, 500, or 5000 μmol H₂S L⁻¹; Fig. 2.4A-D). Higher H₂S concentrations correlated with lower NO₃⁻ consumption rates and less NO₂⁻

accumulation (Fig. 2.4A and B). There was no correlation between NH_4^+ concentration and H_2S concentration. Even at a low ($20 \mu\text{mol L}^{-1}$) H_2S concentration, the percentage of N_2O relative to N_2 production increased (Fig. 2.4C and D) from 22 to 83% at DB and from 9 to 36% at GD (Fig. 2.4C and D). The total products of DNF from the $^{15}\text{NO}_3^-$ addition ($2 \times ([\text{N}_2\text{O}] + [^{30}\text{N}_2]) + 1 \times [^{29}\text{N}_2]$) decreased as H_2S concentration increased in the 0-3 cm depth at both sites (Fig. 2.4C and D).

The influence of the DOC/NO_3^- ratio on NO_3^- reduction rates and pathways was examined by the addition of $50 \mu\text{mol } ^{15}\text{NO}_3^- \text{ L}^{-1}$ and various concentrations of acetate ($0 - 10000 \mu\text{mol C L}^{-1}$; Fig. 2.5A-D) to DB surface (0-3 cm) sediments. The NO_3^- concentration decreased similarly and significantly ($p < 0.05$) in all treatments (data not shown). Significant ($p < 0.05$) increases in NH_4^+ concentration occurred only at DOC concentrations $\geq 7500 \mu\text{mol L}^{-1}$ (data not shown). Rates of N_2O production showed little variation with increasing DOC concentration (Fig. 2.5A). The production of $^{30}\text{N}_2$ increased up to a $\text{DOC}:\text{NO}_3^-$ ratio of 20, and then decreased significantly ($p < 0.05$) with increasing DOC/NO_3^- ratio between 20 and 200 (Fig. 2.5A).

The DOC/NO_3^- ratio did not significantly affect the consumption of NO_3^- (data not shown) but led to differences in the end products of DNF, with N_2O comprising a larger fraction of the DNF rate with increasing DOC/NO_3^- ratio (Fig. 2.5A). The total rate of DNF ($\text{N}_2\text{O} + ^{15}\text{N}-\text{N}_2$) decreased as the DOC/NO_3^- ratio increased (Fig. 2.5B). The DNRA rate increased as the DOC/NO_3^- ratio increased (Fig. 2.5C). The ratio of the rates of DNRA to DNF was influenced by the DOC/NO_3^- ratio (Fig. 2.5D).

DISCUSSION

Light level, the balance of autotrophy and heterotrophy, and influence of BMA on biogeochemical cycling

Light levels are correlated with the net metabolic state of shallow sediments (Cabrita and Brotas 2000). In diel-day treatments, baseline primary production rates (Table 2.2) were consistent with the findings of others (-5000 to $6000 \mu\text{mol O}_2 \text{ m}^{-2} \text{ h}^{-1}$; Cabrita and Brotas 2000; Sundbäck et al. 2000). Net O_2 production rates in the diel-day treatment were ~ 2 times higher than O_2 uptake at night, indicating net autotrophy. Dark treatments became hypoxic within 24 to 48 hours and ultimately became anoxic (Figs. 2.2B and 2.3B). Anoxic conditions resulted in significant changes in the fluxes of nutrients and dissolved gases across the sediment water interface. Though the metabolic rates presented here could have been impacted by the incubation duration, the N amendment likely had a larger impact.

Extended periods of decreased light availability in the benthos can result from storm runoff, which leads to higher turbidity. In addition to storm-induced turbidity, coastal eutrophication, driven by anthropogenic nutrient loading (Nixon 1995), has increased the frequency and spatial coverage of water column algal blooms (Paerl et al. 2003). Increased turbidity resulting from algal blooms leads to light limitation of the benthos, which generates hypoxic/anoxic conditions and affects benthic fluxes. Furthermore, as algal blooms decline bottom water and sediment metabolism are stimulated (Paerl et al. 2003). Such events lead to dramatic changes to the already fragile balance of heterotrophy and autotrophy in coastal ecosystems (Steward et al. 2006).

Inorganic nutrient availability also impacted the flux of dissolved organics. DOC release increased during the diel-day period following the N amendment. Though DOC uptake in the

diel-night increased as well, daytime release of DOC outpaced nighttime uptake. Some diatom species release between ~5 and 20% of the total C fixed as DOC (Wetz and Wheeler 2007). BMA-derived DOC efflux can occur as simple exudation of excess production as DOC during times of nutrient limitation when cellular C/N ratios are unfavorable (Cook et al. 2004). Bacteria have been shown to rapidly assimilate DOC released by BMA (Jensen 1984) and microalgal and heterotrophic processes are often tightly coupled (Joye et al. 1996). Here, DOC production by BMA exceeded the bacterial consumption typically observed in benthic systems. This nutrient stimulated decoupling of organic matter (OM) production and consumption in the benthos could be intensified by short-term nutrient inputs that satiate BMA with DIN (Porubsky et al. 2008, Chapter 3).

In addition to DIN delivery by surface runoff and riverine inputs, coastal areas are also subject to groundwater DIN inputs (Moore 1996). Groundwater DIN inputs are unique in that they are not accompanied by turbidity and the relative abundance of different N species, as well as the loci of inputs, may vary. Surface runoff is typically higher in oxidized N species and turbidity, and delivers nutrients in a top-down way so that nutrients are transported into the sediments by diffusion and/or advection. Groundwater is often lower in O₂ and thus is higher in reduced N species and DON; and delivers nutrients from below by passing upward through the sediment.

The N amendment performed in these experiments mimics surface water inputs by the method of its delivery and the N speciation. N transported to intertidal creek bank sediments by surface water will diffuse into the sediments but must first pass through the BMA filter (Porubsky et al. 2008, Chapter 3). DIN delivered by groundwater may diffuse up through the

lower depths of the sediment and is therefore vulnerable to microbial consumption prior to contact with BMA (Veuger et al. 2007). This contrast could drive different responses to N inputs.

Denitrification

NO_3^- availability can regulate rates and pathways of N processing in sediments. Unamended DNF rates determined using similar techniques at other sites ranged from 8 to $330 \mu\text{mol N m}^{-2} \text{h}^{-1}$ (An and Gardner 2002; An et al. 2001; Risgaard-Petersen et al. 2004). The maximum D_{14} rates for the current study were $20 \mu\text{mol N m}^{-2} \text{h}^{-1}$. Denitrification proceeds by direct reduction of NO_3^- supplied from the water column or via coupling to nitrification within the sediment (hereafter "coupled DNF", Nishio et al. 1983). NO_3^- limitation of DNF can be induced by low water column NO_3^- concentrations or by substrate limitation of nitrification (Seitzinger 1994). Water column NO_3^- concentrations in the creek were low at both sites ($1.6 \mu\text{mol L}^{-1}$ at DB and $2.2 \mu\text{mol L}^{-1}$ at GD; Joye, unpublished data) and likely limit DNF. NH_4^+ limitation of nitrification has been reported for NH_4^+ concentrations in the range of $70 - 700 \mu\text{mol L}^{-1}$ (Henrikson and Kemp 1988). Though NH_4^+ concentrations in surficial sediments were on the order of $50 \mu\text{mol L}^{-1}$; pore water NH_4^+ concentrations at 15 cm reached mmol L^{-1} concentrations (Weston et al. 2006). This upwardly diffusing NH_4^+ source could support substantial nitrification activity. No nitrification would have occurred in the dark incubations since the cores were anoxic; and reduced manganese fluxes indicated that no anaerobic nitrification coupled to manganese oxide reduction was occurring as was observed by Hulth et al. (1999).

During times of active BMA photosynthesis, the vertical extent of the oxic zone increases, which can lead to higher volumetric rates of nitrification and coupled DNF (Rysgaard et al. 1993; Dong et al. 2000). However, at the same time, BMA compete with nitrifiers and denitrifiers for NH_4^+ and NO_3^- respectively, which could further exacerbate NO_3^- limitation of DNF (Rysgaard et al. 1993; Cabrita and Brotas 2000; An and Joye 2001). Rates of D_{14} were relatively low in diel and dark treatments (Table 2.3), likely due to NO_3^- limitation driven primarily by competition for NO_3^- with phototrophs in the former case and by extremely low nitrification rates (and resulting low NO_3^- concentration) in the latter case.

Low D_{14} rates at the anthropogenically impacted DB site could also result from inhibition of coupled DNF by the high porewater H_2S concentrations (Table 2.1; Joye and Hollibaugh 1995; Weston et al. 2006). Sulfide inhibits primarily the first step of nitrification (Joye and Hollibaugh 1995), and even low H_2S concentrations ($20 \mu\text{mol L}^{-1}$) directly inhibit DNF (Joye 2002).

The NO_3^- amendment led to increased rates of D_{15} that were similar to rates reported at other sites (An and Gardner 2002; An et al. 2001; Risgaard-Petersen et al. 2004). Rates of D_{15} in dark treatments were significantly ($p < 0.05$) higher than rates in diel treatments for DB in January and August 2002 (Table 2.3). We hypothesize that under diel-day conditions BMA out-competed denitrifiers for the added NO_3^- . Increased BMA production, and subsequent deeper O_2 penetration depths, increased NO_3^- diffusion distances and further separated denitrifiers from their substrate (Rysgaard et al. 1993). Furthermore, denitrifiers are also capable of aerobic respiration (a process that yields more energy than DNF), and under sufficient O_2 concentrations, denitrifiers are likely to use aerobic respiration instead of DNF (Payne 1981).

Competition between dissimilatory nitrate reduction pathways

Under dark conditions microorganisms compete with each other for available NO_3^- . In the current study under amended conditions, D_{15} rates were 166 and 280 $\mu\text{mol N m}^{-2} \text{h}^{-1}$ for GD and DB respectively in August 2002; while DNRA rates were 23 and 38 $\mu\text{mol N m}^{-2} \text{h}^{-1}$. DNRA comprised about 11% of the dissimilatory NO_3^- reduction at each site. The factors that control the balance of DNF and DNRA are poorly constrained and several possible regulatory scenarios have been suggested.

Temperature may influence partitioning between dissimilatory NO_3^- reduction pathways. Previous studies showed DNF was the dominant process for NO_3^- reduction at low temperatures and DNRA became dominant at higher temperatures (King and Nedwell 1984; Ogilvie et al. 1997). The temperatures for our experiments ranged from 15.5 to 20.5°C in winter and 21.1 to 28.6°C in summer. Winter temperatures were frequently in the range favoring DNF (King and Nedwell 1984; Ogilvie et al. 1997; Kelly-Gerreyn et al. 2001), and summer temperatures were always in the range favoring DNRA. However, our results indicate that DNRA remained of secondary importance relative to DNF throughout the year. Differential O_2 controls have also been hypothesized to influence the relative importance of DNF and DNRA (Fazzolari et al. 1998) because DNRA is less sensitive to O_2 than DNF. Given the anoxic condition of the water column in the dark incubations, differential O_2 sensitivity did not influence the balance of DNF and DNRA.

Sulfide negatively affects DNF inhibiting the first step of nitrification (Joye and Hollibaugh 1995) and both the NO and N_2O reductase of denitrifying bacteria (Sørensen et al. 1980). Alternatively, H_2S can stimulate DNRA by acting as an electron donor for the reduction of NO_3^- to NH_4^+ (Brunet and Garcia-Gil 1996). Sulfide concentrations may therefore influence the balance between DNF and DNRA (An and Gardner 2002). In the slurry experiment, H_2S concentrations of only $20 \mu\text{mol L}^{-1}$ led to increased accumulation of N_2O (Fig. 2.4C and D). In agreement with other studies showing a negative correlation between H_2S and DNF, total DNF rates in the slurry experiment decreased with increasing H_2S concentrations (Sørensen et al. 1980; An and Gardner 2002; Joye 2002). However, DNRA rates did not correlate with H_2S concentration as observed previously (Brunet and Garcia-Gil 1996; An and Gardner 2002).

The negative correlation between NO_3^- consumption rates and H_2S concentration suggests H_2S impacted NO_3^- reduction at the initial reductive step from NO_3^- to NO_2^- . In the $20 \mu\text{mol L}^{-1}$ H_2S treatment, 82% of the initial NO_3^- was consumed during the incubation (Fig. 2.4A and B). In the $500 \mu\text{mol L}^{-1}$ treatment, the NO_3^- consumption decreased to 0 and 21% for DB and GD respectively and no NO_3^- consumption was observed in the $5000 \mu\text{mol H}_2\text{S L}^{-1}$ treatment. The decreased NO_3^- consumption indicates that H_2S can completely inhibit both DNF and DNRA. High porewater H_2S concentrations occur at these study sites (Table 2.1; Weston et al. 2006); the range of H_2S concentrations in the winter of 2002 was 20 to $1000 \mu\text{mol L}^{-1}$ in the surface (0-2 cm) sediments, and increased in August 2002 to 200 to $3000 \mu\text{mol L}^{-1}$ at the same depth. While H_2S concentrations of $20 \mu\text{mol L}^{-1}$ would not completely block DNF or DNRA, higher concentrations observed by Weston et al. (2006) at deeper depths and at different times of the year could certainly inhibit these dissimilatory processes.

Another factor previously hypothesized to regulate the importance of DNF versus DNRA is the electron donor to electron acceptor ratio (Tiedje et al. 1982; Tiedje 1994). Although this hypothesis was not derived empirically, it has been corroborated by field studies (Bonin 1996; Fazzolari et al. 1998; Nedwell et al. 1999). DNRA provides slightly more energy per mole of NO_3^- reduced than does DNF. Under highly reduced conditions, a lack of electron acceptors could limit growth (Tiedje et al. 1982) and since DNRA consumes more electrons than DNF, it should be more favorable. Thus, when the DOC/NO_3^- ratio is relatively high, DNRA would be favored.

In the slurry experiments, the balance of DNF and DNRA was examined by explicitly manipulating the DOC/NO_3^- ratio. Unlike H_2S addition, DOC addition did not alter N_2O production but the production of $^{30}\text{N}_2$ decreased substantially as DOC increased (Fig. 2.5A).

Both DNF and DNRA rates correlated with DOC/NO₃⁻ ratios (Figs. 2.5B and C). At high DOC/NO₃⁻ ratios, electron acceptor (NO₃⁻) availability should limit dissimilatory NO₃⁻ reduction while at low DOC/NO₃⁻ ratios, reductant (DOC) availability may be limiting. Our results confirm the Tiedje et al. (1982) hypothesis and show a direct correlation between the DOC/NO₃⁻ ratio and the DNRA/DNF rate ratio (Fig. 2.5D).

Uncertainties regarding the mechanistic relationship between DNF and DNRA are further complicated by evidence of the anammox process (Fig. 2.2F). While anammox accounted for 24 and 67% of the N₂ produced in sediments from two continental shelf sites (Thamdrup and Dalsgaard 2002), the contribution of the process in intertidal sediments has not been previously reported. The minimum relative contribution of anammox to N₂ production in our August 2002 DB incubation was about 6.4%. This is equivalent to about 2.2% of the ¹⁵NO₃⁻ reduced (Fig. 2.2F). Accumulation of ²⁹N₂ significantly ($p < 0.01$) exceeded the ²⁹N₂ possibly originating from any residual ¹⁴NO₃⁻. An anammox rate of 0.05 μmol m⁻² h⁻¹ is a minimum estimate because this rate is based solely on ²⁹N₂ production. During a ¹⁵NO₃⁻ tracer experiment where DNRA was also important, anammox may also produce ³⁰N₂ but this cannot be distinguished from ³⁰N₂ produced via DNF. The temporary accumulation of NO₂⁻ observed in August 2002 (Fig. 2.2D) was also reported in other studies (Dalsgaard and Thamdrup 2002; Thamdrup and Dalsgaard 2002); these authors suggested that NO₃⁻ reduction to NO₂⁻ was coupled to organic matter oxidation, and that NO₂⁻ was then used to oxidize NH₄⁺.

We propose a similar progression of NO₃⁻ reduction for these sediments, with NO₂⁻ accumulating due to serial substrate utilization of the intermediate products (Payne 1981). Denitrifiers possessing NO₃⁻ reductase reduce NO₃⁻ preferentially because the reduction of NO₃⁻ to NO₂⁻ confers more energy per mole N ($G^{\circ} = -161 \text{ kJ mol}^{-1}$) than the reduction of NO₂⁻ to NO

($G^{\circ} = -76.2 \text{ kJ mol}^{-1}$; Tiedje 1994). After NO_3^- is depleted, NO_2^- is reduced (Payne 1981). Some denitrifiers (and bacteria capable of anammox) may lack NO_3^- reductase and these microbes consume accumulated NO_2^- . The accumulation of NO_2^- has been observed in ^{15}N -amendment experiments that utilize a relatively high concentration of $^{15}\text{NO}_3^-$ (Dalsgaard et al. 2005). This accumulation occurred during the initial phase of the amendment, while NO_3^- concentrations were in excess, and it is likely that during this period NO_2^- was not utilized as an electron acceptor (Dalsgaard et al. 2005) or that the reduction rate of NO_3^- to NO_2^- exceeded the reduction rate of NO_2^- .

Contemporaneous DNF and anammox complicates the interpretation of data obtained using the IPT (Kartal et al. 2007). An alternative form of the IPT equation permits estimation of DNF rates in the presence of anammox (Risgaard-Petersen et al. 2003). However, in August 2002, sediments in the DB dark incubations also exhibited DNRA activity. Recent evidence indicates that anammox bacteria are capable of DNRA and can supply themselves with NH_4^+ under NH_4^+ -limited conditions (Kartal et al. 2007). The same study pointed out that under these conditions, the alternative IPT fails to account for the concomitant production of $^{30}\text{N}_2$ by DNF and anammox. In the presence of DNRA, both DNF and anammox are capable of producing all three isotopic species of N_2 so it is impossible to apply the alternative IPT equation presented by Risgaard-Peterson (2003). Given that anammox has not previously been documented in intertidal creek bank sediments, multiple tracers (i.e. $^{15}\text{NO}_3^-$, $^{15}\text{NH}_4^+$) were not employed in the current study. The use of multiple tracers would have allowed for the application of the modified IPT method and for the contributions of DNF, DNRA, and anammox to be more fully examined. As our understanding of coastal nitrogen cycling increases, it is important to probe for all existing pathways and adapt the protocols accordingly.

An additional source of DNRA activity in these sediments is the presence and activity of vacuolate sulfur oxidizing bacteria (VSOB). Sediment cores collected from DB and GD that were stored for several weeks at in situ temperatures but not used in experiments developed white filamentous bacterial surface mats, indicative of VSOB (likely *Beggiatoa* spp.). Some VSOB migrate between depths of high NO_3^- concentrations and high H_2S concentrations and couple the reduction of NO_3^- to the oxidation of HS^- , producing NH_4^+ and S^0 , which is ultimately oxidized to SO_4^{2-} (Zopfi et al. 2001). Based on the observed filamentous bacterial mats, we propose that VSOB likely carried out DNRA in these sediments (Otte et al. 1999; Sayama et al. 2005; Preisler et al. 2007). However, VSOB activity does not adequately explain the increase in water column NO_2^- or the production of $^{29}\text{N}_2$.

Fluxes between the sediment and water column play an important role in estuarine nutrient cycles. Under light replete conditions, autotrophic metabolism dominated and BMA formed an effective cap at the sediment water interface regulating the flux of nutrients across the interface by direct uptake of nutrients and by increasing the depth of the oxic zone. Under dark conditions, heterotrophic metabolism led to release of nutrients from the sediment to the water column and dissimilatory processes dominated the nitrogen cycle. Under anoxic conditions, DNF, DNRA, and anammox competed for substrate. Although evidence for DNF, DNRA and anammox was present, the co-occurrence of all three processes (August 2002) made it virtually impossible to determine absolute process rates or to quantify the relative contributions of individual processes to total NO_3^- reduction with the use of only a single tracer. Future studies in coastal sediments should consider these three pathways of NO_3^- reduction, and additional approaches are necessary to investigate process interactions when all three processes co-occur. It appears a suite of factors (including H_2S and DOC/NO_3^-) influenced these dissimilatory

processes and though DNF was the dominant dissimilatory sink for NO_3^- , the apparent importance of DNRA and anammox illustrate the need for further detailed, process-oriented investigations into the fate of NO_3^- in coastal sediments.

ACKNOWLEDGMENTS

We thank M. Erickson and P. Olecki for help in the field and laboratory. This research was supported by the National Science Foundation's Georgia Coastal Ecosystems Long Term Ecological Research Program (OCE 99-82133 and OCE 06-20959) and National Oceanic and Atmospheric Administration Sea Grant Programs in Georgia (award numbers NA06RG0029-R/WQ11 and R/WQ12A) and South Carolina (award number: NA960PO113).

LITERATURE CITED

- Aller, R. 1994. Bioturbation and remineralization of sedimentary organic matter: Effects of redox oscillation. *Chemical Geology* 114: 331-345.
- Álvarez-Salgado, X., and A. Miller. 1998. Simultaneous determination of dissolved organic carbon and total dissolved nitrogen in seawater by high temperature catalytic oxidation: Conditions for precise shipboard measurements. *Marine Chemistry* 62: 325-333.
- An, S., and W. Gardner. 2002. Dissimilatory nitrate reduction to ammonium (DNRA) as a nitrogen link, versus denitrification as a sink in a shallow estuary (Laguna Madre/Baffin Bay, Texas). *Marine Ecology Progress Series* 237: 41-50.
- An, S., W. Gardner, and T. Kana. 2001. Simultaneous measurement of denitrification and nitrogen fixation using isotope pairing with membrane inlet mass spectrometry analysis. *Applied and Environmental Microbiology* 67: 1171-1178.

- An, S., and S. Joye. 2001. Enhancement of couple nitrification-denitrification by benthic photosynthesis in shallow estuarine sediments. *Limnology and Oceanography* 46: 62-74.
- Bonin, P. 1996. Anaerobic nitrate reduction to ammonium in two strains isolated from coastal marine sediment: A dissimilatory pathway. *FEMS Microbiology Ecology* 19: 27-38.
- Brunet, R., and L. Garcia-Gil. 1996. Sulfide-induced dissimilatory nitrate reduction ammonia in anaerobic freshwater sediments. *FEMS Microbiology Ecology* 21: 131-138.
- Cabrita, M., and V. Brotas. 2000. Seasonal variation in denitrification and dissolved nitrogen fluxes in intertidal sediments of the Tagus estuary, Portugal. *Marine Ecology Progress Series* 202: 51-65.
- Cline, J. 1969. Spectrophotometric determination of hydrogen sulfide in natural waters. *Limnology and Oceanography* 14: 454-458.
- Cook, P., A. Revill, E. Butler, and B. Eyre. 2004. Carbon and nitrogen cycling on intertidal mudflats of a temperate Australian estuary. II. Nitrogen cycling. *Marine Ecology Progress Series* 280: 39-54.
- Dalsgaard, T., and B. Thamdrup. 2002. Factors controlling anaerobic ammonium oxidation with nitrite in marine sediments. *Applied and Environmental Microbiology* 68: 3802-3808.
- Dalsgaard, T., B. Thamdrup, and D. Canfield. 2005. Anaerobic ammonium oxidation (anammox) in the marine environment. *Research in Microbiology* 156: 457-464.
- Dong, L., D. Thornton, D. Nedwell, and G. Underwood. 2000. Denitrification in sediments of the River Colne estuary, England. *Marine Ecology Progress Series* 203: 109-122.

- Eyre, B., and A. Ferguson. 2002. Comparison of carbon production and decomposition, benthic nutrient fluxes and denitrification in seagrass, phytoplankton, benthic microalgae- and macroalgae-dominated warm-temperate Australian lagoons. *Marine Ecology Progress Series* 229: 43-59.
- Eyre, B., S. Rysgaard, T. Dalsgaard, and P. Christensen. 2002. Comparison of isotope pairing and N_2/Ar methods for measuring sediment denitrification rates – assumptions, modifications, and implications. *Estuaries* 25: 1077-1087.
- Fazzolari, E., B. Nicolardot, and J. Germon. 1998. Simultaneous effects of increasing levels of glucose and oxygen partial pressures on denitrification and dissimilatory nitrate reduction to ammonium in repacked soil cores. *European Journal of Soil Biology* 34: 47-52.
- Henrikson, K., and W. Kemp. 1988. Nitrification in estuarine and coastal marine sediments: Methods, patterns and regulating factors. In T. Blackburn and J. Sørensen. [eds.] Nitrogen Cycling in Coastal Marine Environments. Proceedings of the SCOPE Symposium 33. John Wiley & Sons.
- Holmes, R., J. McClelland, D. Sigman, B. Fry, and B. Peterson. 1998. Measuring $^{15}N-NH_4^+$ in marine, estuarine, and fresh water: An adaptation of the ammonia diffusion method for samples with low ammonium concentrations. *Marine Chemistry* 60: 235-243.
- Howarth, R., R. Marino, J. Lane, and J. Cole. 1988. Nitrogen fixation in freshwater, estuarine and marine ecosystems: 1. Rates and importance. *Limnology and Oceanography* 33: 669-687.
- Huettel, M., H. Roy, E. Precht, and S. Ehrenhauss. 2003. Hydrodynamical impact on biogeochemical processes in aquatic sediments. *Hydrobiologia* 494: 231-236.

- Hulth, S., R. Aller, and F. Gilbert. 1999. Coupled anoxic nitrification/manganese reduction in marine sediments. *Geochimica et Cosmochimica Acta* 63: 49-66.
- Jahnke, R., J. Nelson, R. Marinelli, and J. Eckman. 2000. Benthic flux of biogenic elements on the Southeastern US continental shelf: Influence of pore water advective transport and benthic microalgae. *Continental Shelf Research* 20: 109-127.
- Jensen, L. 1984. Antimicrobial action of antibiotics on bacterial and algal carbon metabolism: On the use of antibiotics to estimate bacterial uptake of algal extracellular products (EOC). *Archive Fur Hydrobiologie* 99: 423-432.
- Jørgensen, B., and J. Sørensen. 1985. Seasonal cycles of O₂, NO₃⁻, and SO₄²⁻ reduction in estuarine sediments: The significance of a NO₃⁻ reduction maximum in spring. *Marine Ecology Progress Series* 24: 65-74.
- Joye, S. 2002. Denitrification in the marine environment, pp. 1010-1019. In G. Collins [ed.] *Encyclopedia of Environmental Microbiology*. John Wiley & Sons, Inc.
- Joye, S., and J. Hollibaugh. 1995. Sulfide inhibition of nitrification influences nitrogen regeneration in sediments. *Science* 270: 623-625.
- Joye, S., M. Mazzotta, and J. Hollibaugh. 1996. Community metabolism in microbial mats: The occurrence of biologically-mediated iron and manganese reduction. *Estuarine, Coastal and Shelf Science* 43: 747-766.
- Kana, T., M. Sullivan, J. Cornwell, and K. Groszkowski. 1998. Denitrification in estuarine sediments determined by membrane inlet mass spectrometry. *Limnology and Oceanography* 43: 334-339.

- Kartal, B., M. Kuypers, G. Lavik, J. Schalk, H. Op den Camp, M. Jetten, and M. Strous. 2007. Anammox bacteria disguised as denitrifiers: Nitrate reduction to dinitrogen gas via nitrite and ammonium. *Environmental Microbiology* 9: 635-642.
- Kelly-Gerreyn, B., A. Trimmer, and D. Hydes. 2001. A diagenetic model discriminating denitrification and dissimilatory nitrate reduction to ammonium in a temperate estuarine sediment. *Marine Ecology Progress Series* 220: 33-46.
- King, D., and D. Nedwell. 1984. Changes in nitrate-reducing community of an anaerobic sediment in response to seasonal selection by temperature. *Journal of General Microbiology* 130: 2935-2941.
- Koike, I., and A. Hattori. 1978. Simultaneous determinations of nitrification and nitrate reduction in coastal sediments by a ^{15}N dilution technique. *Applied and Environmental Microbiology* 25: 853-857.
- Mackin, J. and R. Aller. 1984. Ammonium adsorption in marine sediments. *Limnology and Oceanography* 29: 250-257.
- Moore, W. 1996. Large groundwater inputs to coastal waters revealed by ^{226}Ra enrichments. *Nature* 380: 612-614.
- Morin, J. and J. Morse. 1999. Ammonium release from resuspended sediments in the Laguna Madre estuary. *Marine Chemistry* 65: 97-110.
- Nedwell, D., T. Jickells, M. Trimmer, and R. Sanders. 1999. Nutrients in estuaries, pp. 44-92. In D. Nedwell and D. Raffaelli [eds.] *Estuaries: Advances in Ecological Research* vol. 29. Academic Press.
- Nielsen, L. 1992. Denitrification in sediment determined from nitrogen isotope pairing. *FEMS Microbiology Letters* 86: 347-362.

- Nishio, T., I. Koike, and A. Hattori. 1983. Estimates of denitrification and nitrification in coastal and estuarine sediments. *Applied and Environmental Microbiology* 45: 444-450.
- Nixon, S. 1995. Coastal marine eutrophication: A definition, social causes, and future concerns. *Ophelia* 41: 199-219.
- Nixon, S., C. Oviatt, and S. Hale. 1976. Nitrogen regeneration and the metabolism of coastal marine bottom communities, pp. 269-283. In J. Anderson and A. Macfadyen. [eds.] The role of terrestrial and aquatic organisms in decomposition processes. Blackwell.
- Ogilvie, B., M. Rutter, and D. Nedwell. 1997. Selection by temperature of nitrate reducing bacteria from estuarine sediments: Species composition and competition for nitrate. *FEMS Microbiology Ecology* 23: 11-22.
- Otte, S., J. Kuenen, L. Nielsen, H. Paerl, J. Zopfi, H. Schulz, A. Teske, B. Strotmann, V. Gallardo, and B. Jørgensen. 1999. Nitrogen, carbon, and sulfur metabolism in natural *Thioploca* samples. *Applied and Environmental Microbiology* 65: 3148-3157.
- Paerl, H., L. Valdes, J. Pinckney, M. Piehler, J. Dyble, and P. Moisander. 2003. Phytoplankton photopigments as indicators of estuarine and coastal eutrophication. *Bioscience* 53: 953-964.
- Payne, W. 1981. Denitrification. Wiley.
- Porubsky, W., L. Velasquez, and S. Joye. 2008. Nutrient-replete benthic microalgae as a source of dissolved organic carbon to coastal waters. *Estuaries and Coasts* 31: 860-876.
- Preisler, A., D. de Beer, A. Lichtschlag, G. Lavik, A. Boetius, and B. Jørgensen. 2007. Biological and chemical sulfide oxidation in a *Beggiatoa* inhabited marine sediment. *The International Society for Microbial Ecology Journal* 1: 341-353.

- Risgaard-Petersen, N., L. Nielsen, S. Rysgaard, T. Dalsgaard, and R. Meyer. 2003. Application of the isotope pairing technique in sediments where anammox and denitrification coexist. *Limnology and Oceanography-Methods* 1: 63-73.
- Risgaard-Petersen, N., R. Meyer, M. Schmid, M. Jetten, A. Enrich-Prast, S. Rysgaard, and N. Revsbech. 2004. Anaerobic ammonium oxidation in an estuarine sediment. *Aquatic Microbial Ecology* 36: 293-304.
- Rysgaard, S., N. Risgaard-Petersen, L. Nielsen, and N. Revsbech. 1993. Nitrification and denitrification in lake and estuarine sediments measured by the ^{15}N dilution technique and isotope pairing. *Applied and Environmental Microbiology* 59: 2093-2098.
- Sayama, M., N. Risgaard-Petersen, L. Nielsen, H. Fossing, and P. Christensen. 2005. Impact of bacterial NO_3^- transport on sediment biogeochemistry. *Applied and Environmental Microbiology* 71: 7575-7577.
- Seitzinger, S. 1994. Linkages between organic matter mineralization and denitrification in eight riparian wetlands. *Biogeochemistry* 25: 19-39.
- Solorzano, L. 1969. Determination of ammonia in natural waters by the phenol hypochlorite method. *Limnology and Oceanography* 14: 799-801.
- Sørensen, J., J. Tiedje, and R. Firestone. 1980. Inhibition by sulfide of nitric and nitrous oxide reduction by denitrifying *Pseudomonas fluorescens*. *Applied and Environmental Microbiology* 39: 105-108.
- Steward, J., R. Virnstein, M. Lasi, L. Morris, J. Miller, L. Hall, and W. Tweedale. 2006. The impacts of the 2004 hurricanes on hydrology, water quality, and seagrass in the central Indian River Lagoon, Florida. *Estuaries and Coasts* 29(6A): 954-965.

- Strickland, J., and T. Parsons. 1972. A practical handbook of seawater analysis, 2nd ed. Bulletin of the Fisheries Research Board of Canada.
- Sundbäck, K., A. Miles, and E. Göransson. 2000. Nitrogen fluxes, denitrification and the role of microphytobenthos in microtidal shallow-water sediments: an annual study. *Marine Ecology Progress Series* 200: 59-76.
- Thamdrup, B., and T. Dalsgaard. 2002. Production of N₂ through anaerobic ammonium oxidation coupled to nitrate reduction in marine sediments. *Applied and Environmental Microbiology* 68: 1312-1328.
- Thauer, R., K. Jungermann, and K. Decker. 1977. Energy conservation in chemotrophic anaerobic bacteria. *Micobiological Reviews* 41: 100-180.
- Tiedje, J. 1994. Denitrifiers, pp. 245-267. In R. Weaver et al. [eds.] *Methods of Soil Analysis*, Part 2. Soil Science Society of America.
- Tiedje, J., A. Sexston, D. Myrold, and J. Robinson. 1982. Denitrification: Ecological niches, competition, and survival. *Antonie van Leeuwenhoek Journal of Microbiology* 48: 569-583.
- van de Graaf, A., A. Mulder, P. de Bruijn, M. Jetten, L. Robertson, and J. Kuenen. 1995. Anaerobic oxidation of ammonium is a biologically mediated process. *Applied and Environmental Microbiology* 61: 1246-1251.
- Velasquez, L. 2005. Benthic primary production in coastal salt marsh systems. MS Thesis. University of Georgia, Athens, GA.
- Veuger, B., B. Eyre, D. Maher, and J. Middelburg. 2007. Nitrogen incorporation and retention by bacteria, algae, and fauna in a subtropical intertidal sediment: An in situ ¹⁵N-labeling study. *Limnology and Oceanography* 52: 1930-1942.

- Weston, N. B. and S. B. Joye. 2005. Temperature driven accumulation of labile dissolved organic carbon in marine sediments. *Proceedings of the National Academy of Sciences of the United States of America* 102: 17036-17040.
- Weston, N., W. Porubsky, V. Samarkin, S. MacAvoy, M. Erickson, and S. Joye. 2006. Porewater stoichiometry of terminal metabolic products, sulfate, and dissolved organic carbon and nitrogen in estuarine intertidal creek-bank sediments. *Biogeochemistry* 77: 375-408.
- Wetz, M., and P. Wheeler. 2007. Release of dissolved organic matter by coastal diatoms. *Limnology and Oceanography* 52: 798-807.
- Windom, H., H. McKeller Jr., C. Alexander Jr., A. Craig, A. Abusam, and M. Alford. 1998. Indicators of trends toward coastal eutrophication. Land Use-Coastal Ecosystem Study, State of Knowledge Report.
- Zopfi, J., T. Kjær, L. Nielsen, and B. Jørgensen. 2001. Ecology of *Thioploca* spp.: Nitrate and sulfur storage in relation to chemical microgradients and influence of *Thioploca* spp. on the sedimentary nitrogen cycle. *Applied and Environmental Microbiology* 67: 5530-5537.
- Zumft, W. 1992. The denitrifying prokaryotes, pp. 554-582. In A. Balows, H. Trüper, M. Dworkin, W. Harder, and K. Schleifer. [eds.] The prokaryotes. A handbook on the biology of bacteria: Ecophysiology, isolation, identification, applications, 2nd ed., vol. 1. Springer-Verlag.

Table 2.1. Integrated concentrations of pore water biogeochemical constituents in the upper 10 cm of the sediment (Values taken from Weston et al. 2006). **Bold** values indicate significantly higher concentrations at DB relative to GD ($p < 0.05$). Units in $\mu\text{mol cm}^{-2}$, except ^a mmol cm^{-2} and ^b $\text{mg chl } a \text{ m}^{-2}$.

Location	Date	NO _x	NH ₄ ⁺	DOC	H ₂ S	Cl ^{-a}	chl <i>a</i> ^b
DB	Jan-02	0.05	7.37	63.66	4.43	3.55	59.52
	Aug-02	0.01	11.40	41.90	119.62	3.78	45.53
	Jan-04	0.01	10.34	42.21	4.14	3.10	55.15
GD	Feb-02	n.d.	3.75	43.33	10.89	3.94	54.81
	Aug-02	0.01	2.21	31.92	4.71	3.84	56.28

Table 2.2. Benthic flux rates for Dover Bluff (DB) and Grave's Dock (GD). Mean rates in $\mu\text{mol m}^{-2} \text{h}^{-1}$, n indicates the number of time periods considered in the mean, and numbers in parentheses are ± 1 standard error. "Cores n =" indicates the number of Diel and Dark cores for each experimental date. "0 NO_3^- " and "100 NO_3^- " indicate the amount of NO_3^- added ($\mu\text{mol L}^{-1}$; i.e. baseline and amended rates respectively).

Date	Treatment	Tracer	n	NO_x	NH_4^+	O_2	DIC	DOC	DON
January 2002 (DB)	Diel-day	0 NO_3^-	4	-12.4 (7.0)	-31.8 (26.9)	1439.2 (1220.0)	-4621.2 (2870.5)	577.8 (577.4)	622.5 (547.7)
	Diel-night		3	-1.7 (6.8)	-49.7 (43.2)	-643.1 (464.6)	2277.3 (1514.2)	-1174.1 (465.3)	-624.3 (686.8)
	Dark		8	-4.8 (5.3)	2.1 (31.4)	-420.6 (113.2)	-27.7 (774.2)	-127.1 (240.4)	101.5 (266.3)
Cores $n=2$									
	Diel-day	100 NO_3^-	3	-430.6 (52.5)	5.3 (19.0)	-2154.2 (40.1)	2948.9 (1209.8)	-	103.5 (68.5)
	Diel-night		2	-626.5 (267.4)	-23.6 (53.8)	-877.7 (241.2)	3192.4 (2322.2)	-	39.3 (229.7)
	Dark		4	-450.8 (183.3)	-24.5 (125.6)	-128.8 (168.3)	-299.8 (1508.4)	-	104.4 (207.7)
August 2002 (DB)	Diel-day	0 NO_3^-	2	-62.2 (58.3)	-75.9 (42.3)	2550.5 (294.3)	-4177.1 (784.6)	559.8 (283.6)	-
	Diel-night		4	-21.0 (17.4)	-50.6 (60.0)	-959.8 (567.3)	1478.6 (855.3)	-177.8 (918.0)	-
	Dark		6	-24.4 (11.6)	11.4 (69.6)	-534.8 (287.1)	1625.9 (392.4)	334.0 (187.4)	-
Cores $n=3$									
	Diel-day	100 NO_3^-	2	-596.6 (562.7)	0.7 (7.4)	4679.6 (1165.0)	-4344.9 (1652.6)	3579.4 (2907.4)	-
	Diel-night		2	6.5 (224.7)	-7.4 (9.3)	-3355.7 (189.6)	4922.4 (1030.1)	-2610.2 (2878.6)	-
	Dark		4	-298.5 (449.3)	143.7 (341.5)	-29.2 (24.1)	293.7 (4176.9)	-270.9 (1049.2)	-
January 2004 (DB)	Diel-day	0 NO_3^-	4	6.2 (7.8)	-17.7 (12.4)	1146.2 (787.1)	-109.5 (559.5)	-	-7.7 (77.2)
	Diel-night		4	-2.3 (1.8)	1.2 (8.3)	-876.2 (210.0)	997.8 (197.1)	-	-28.5 (94.9)
	Dark		8	-0.5 (1.3)	48.4 (11.2)	-343.2 (131.6)	702.1 (248.2)	-	-20.8 (60.8)
Cores $n=3$									
	Diel-day	100 NO_3^-	4	-177.1 (13.9)	-23.1 (22.6)	2642.5 (419.0)	-1492.1 (376.7)	-	72.1 (30.4)
	Diel-night		2	-87.4 (25.1)	18.9 (25.3)	-1316.6 (125.9)	812.1 (71.7)	-	-71.4 (44.9)
	Dark		8	-85.3 (11.2)	60.7 (19.6)	-9.3 (33.3)	287.1 (100.7)	-	-9.0 (38.2)
February 2002 (GD)	Diel-day	0 NO_3^-	3	-14.0 (9.5)	-5.0 (5.5)	2750.9 (1056.7)	-1825.6 (643.6)	44.9 (108.0)	60.8 (46.2)
	Diel-night		3	12.1 (10.0)	3.8 (4.9)	-1461.2 (598.4)	1298.4 (368.6)	-41.4 (150.3)	-48.2 (72.4)
	Dark		6	-0.7 (2.3)	1.6 (4.6)	-355.8 (202.8)	-429.2 (1005.3)	104.9 (112.9)	-04.9 (45.6)
Cores $n=2$									
	Diel-day	100 NO_3^-	3	-417.4 (214.3)	5.4 (2.7)	493.8 (424.8)	278.1 (238.0)	345.3 (401.2)	100.7 (57.7)
	Diel-night		3	-298.1 (88.2)	-2.7 (2.9)	-1391.1 (798.3)	524.8 (438.9)	245.1 (112.4)	75.4 (50.7)
	Dark		6	-151.9 (68.4)	21.9 (8.5)	-252.6 (100.9)	652.9 (440.6)	153.2 (192.0)	42.7 (31.6)
August	Diel-day	0 NO_3^-	2	-12.9 (12.6)	-58.7 (130.8)	1839.3 (107.7)	-2780.4 (694.5)	310.3 (261.6)	-

2002 (GD)	Diel-night		4	-13.9 (6.9)	21.1 (30.6)	-719.1 (324.8)	796.4 (384.6)	-188.2 (262.5)	-
	Dark		6	-05.8 (1.8)	-26.2 (27.7)	-535.0 (157.9)	568.4 (150.5)	57.0 (129.1)	-
Cores $n=3$									
	Diel-day	100 NO ₃ ⁻	2	-686.6 (107.2)	22.0 (22.9)	2751.3 (304.3)	-2306.1 (473.3)	909.2 (471.8)	-
	Diel-night		2	55.6 (92.2)	-3.4 (2.1)	-2346.4 (213.3)	2951.0 (314.2)	-607.9 (478.4)	-
	Dark		4	-404.9 (109.0)	108.9 (48.3)	-53.4 (38.3)	1027.3 (565.7)	97.3 (193.6)	-
January 2004 (GD)	Diel-day	0 NO ₃ ⁻	4	-2.2 (2.0)	-1.6 (8.9)	1522.3 (686.3)	-891.7 (482.2)	-	229.5 (182.0)
	Diel-night		4	-1.6 (2.4)	-13.3 (13.0)	-673.1 (107.8)	598.0 (132.7)	-	-66.5 (72.3)
	Dark		8	-0.2 (1.5)	-3.1 (9.8)	-269.1 (84.2)	263.1 (68.3)	-	42.4 (76.4)
Cores $n=3$									
	Diel-day	100 NO ₃ ⁻	4	-201.2 (38.4)	3.1 (12.9)	2335.9 (294.1)	-1820.3 (378.2)	-	5.9 (33.0)
	Diel-night		2	-91.8 (10.3)	-16.8 (15.6)	-1134.9 (105.1)	1028.2 (148.0)	-	17.3 (45.6)
	Dark		8	-60.1 (10.8)	42.1 (34.7)	-30.3 (47.0)	121.8 (119.1)	-	-16.0 (39.1)

Table 2.3. Denitrification rates for DB and GD on several dates. Units are $\mu\text{mol N m}^{-2} \text{h}^{-1}$, n is the number of replicates and numbers in parentheses are ± 1 standard error. Stats indicate significant ($p < 0.05$) differences between the following: a – D_{14} and D_{15} , b – dark D_{14} and diel D_{14} , c – dark D_{15} and diel D_{15} , d – DB and GD for a given value.

<u>January 2002</u>					
DB	D_{14}	D_{15}	GD	D_{14}	D_{15}
Dark ($n=2$)	5.36 (1.67)	98.54 (9.85)	Dark ($n=2$)	0.73 (0.04)	18.93 (1.05)
stats	a	a,c	stats	-	-
Diel ($n=2$)	2.38 (0.60)	10.36 (3.79)	Diel ($n=2$)	0.74 (0.33)	9.88 (4.90)
stats	-	c	stats	-	-
<u>August 2002</u>					
DB	D_{14}	D_{15}	GD	D_{14}	D_{15}
Dark ($n=3$)	15.74 (0.72)	280.30 (26.72)	Dark ($n=3$)	9.66 (1.87)	166.04 (37.34)
stats	a,b,d	a,c	stats	d	
Diel ($n=2$)	1.32 (0.00)	29.87 (5.21)	Diel ($n=2$)	4.17 (1.16)	24.28 (0.97)
stats	b	c	stats	-	
<u>January 2004</u>					
DB	D_{14}	D_{15}	GD	D_{14}	D_{15}
Dark ($n=3$)	0.50 (0.05)	23.34 (3.88)	Dark ($n=3$)	0.51 (0.23)	14.13 (3.49)
stats	a	a	stats	a	a
Diel ($n=3$)	0.87 (0.25)	14.01 (3.23)	Diel ($n=2$)	0.00 (0.13)	7.00 (1.88)
stats	a	a	stats	-	

FIGURE LEGENDS

Figure 2.1. Sampling locations in Georgia and South Carolina, USA. GD and DB denote Grave's Dock and Dover Bluff respectively.

Figure 2.2A-F. Concentration versus time for (A & B) O₂ and H₂S, (C & D) NO₂⁻ and NO₃⁻, and (E & F) ²⁹N₂, ³⁰N₂ and NH₄⁺, for site DB, August 2002. Left and right panels indicate diel and dark treatments respectively, gray boxes in the left panels indicate periods of darkness. Note x-axis has been contracted to better illustrate the post-amendment conditions. Vertical dashed-line indicates ¹⁵NO₃⁻ amendment, error bars = ± 1 SE.

Figure 2.3A-F. Concentration versus time for (A & B) O₂ and H₂S, (C & D) NO₂⁻ and NO₃⁻, and (E & F) ²⁹N₂, ³⁰N₂ and NH₄⁺, for site GD, August 2002. Left and right panels indicate diel and dark treatments respectively, gray boxes in the left panels indicate periods of darkness. Note x-axis has been contracted to better illustrate the post-amendment conditions. Vertical dashed-line indicates ¹⁵NO₃⁻ amendment, error bars = ± 1 SE.

Figure 2.4A-D. Nitrogen cycling rates from sulfide manipulation experiments for DB 0-3 cm (A and C) and GD 0-3 cm (B and D). Note compression of the x-axis in all panels. The ¹⁵N-N₂ rate corresponds to the ²⁹N₂ production rate plus 2 times the ³⁰N₂ production rate; Total DNF is the sum of the N₂O and ¹⁵N-N₂ production rates in terms of N. Error bars are ± 1 SE (*n* = 3).

Figure 2.5A-D. Nitrogen cycling rates for DOC/NO₃⁻ ratio manipulation experiments for DB 0-3 cm. Trend lines represent linear relationships. DNF is the sum of the N₂O and ¹⁵N-N₂ production

rates in terms of N; DNRA is the production rate of total NH_4^+ ($\text{NH}_4^+_{\text{DISS}} + \text{NH}_4^+_{\text{ADS}}$). Error bars are ± 1 SE ($n = 3$).

Figure 2.1.

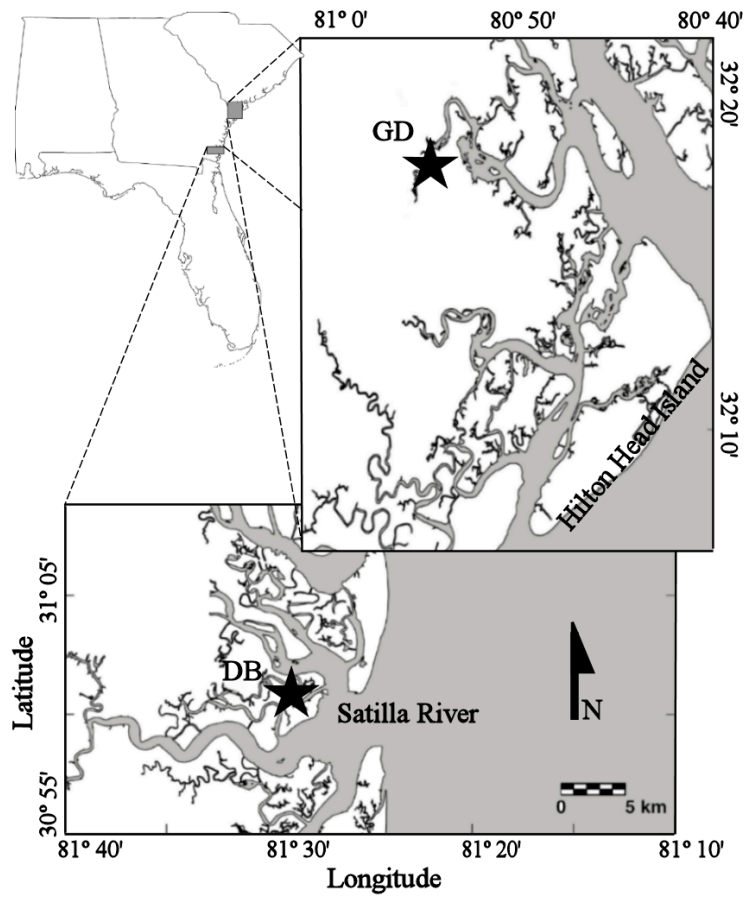


Figure 2.2A-F.

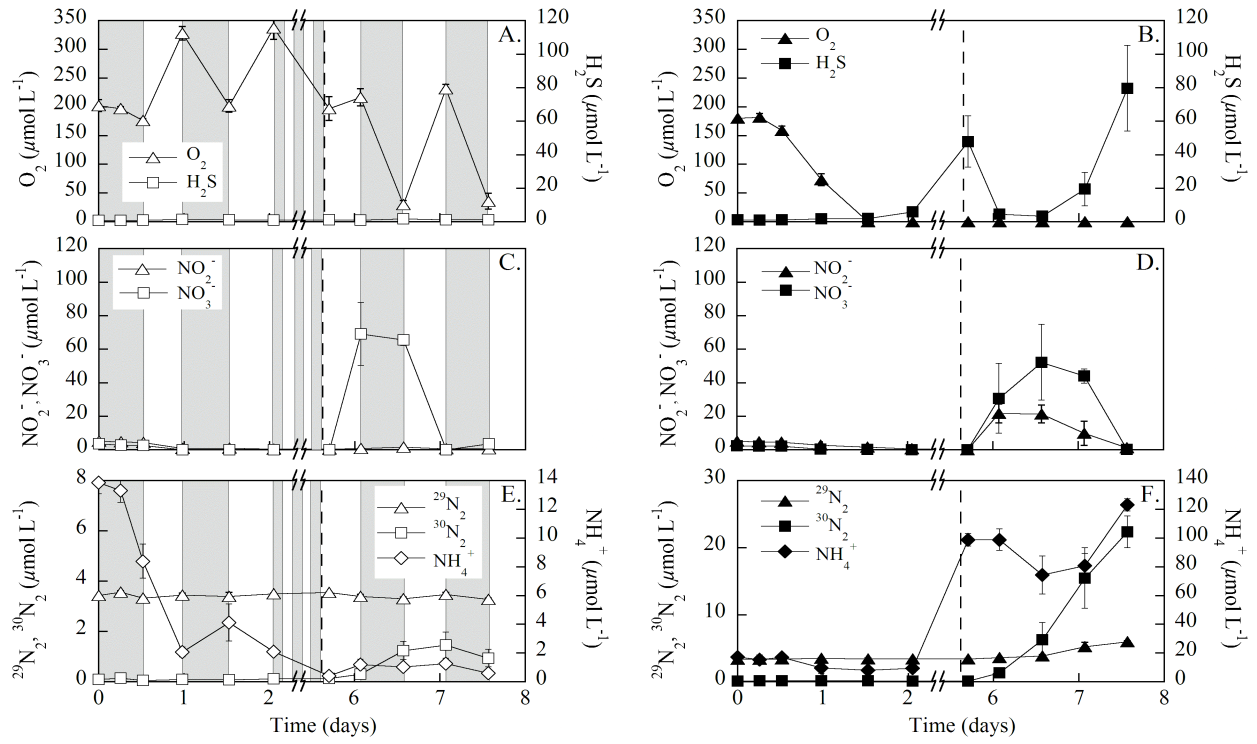


Figure 2.3A-F.

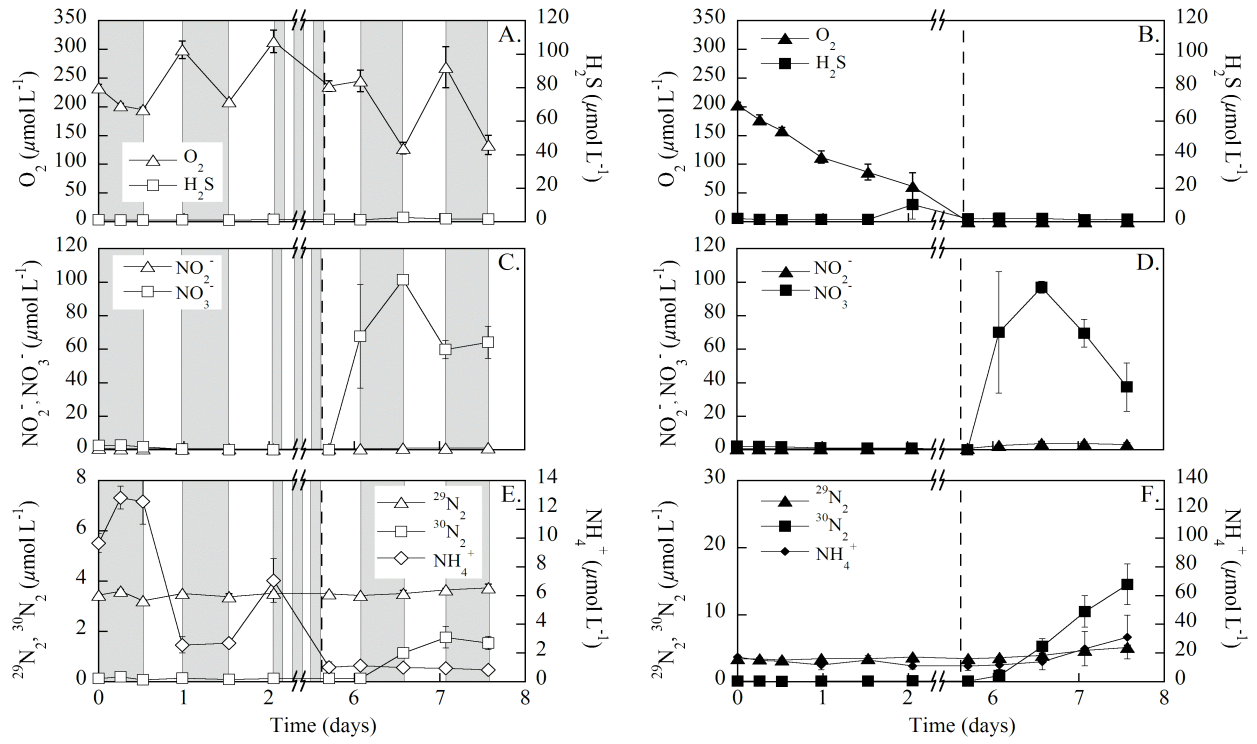


Figure 2.4A-D.

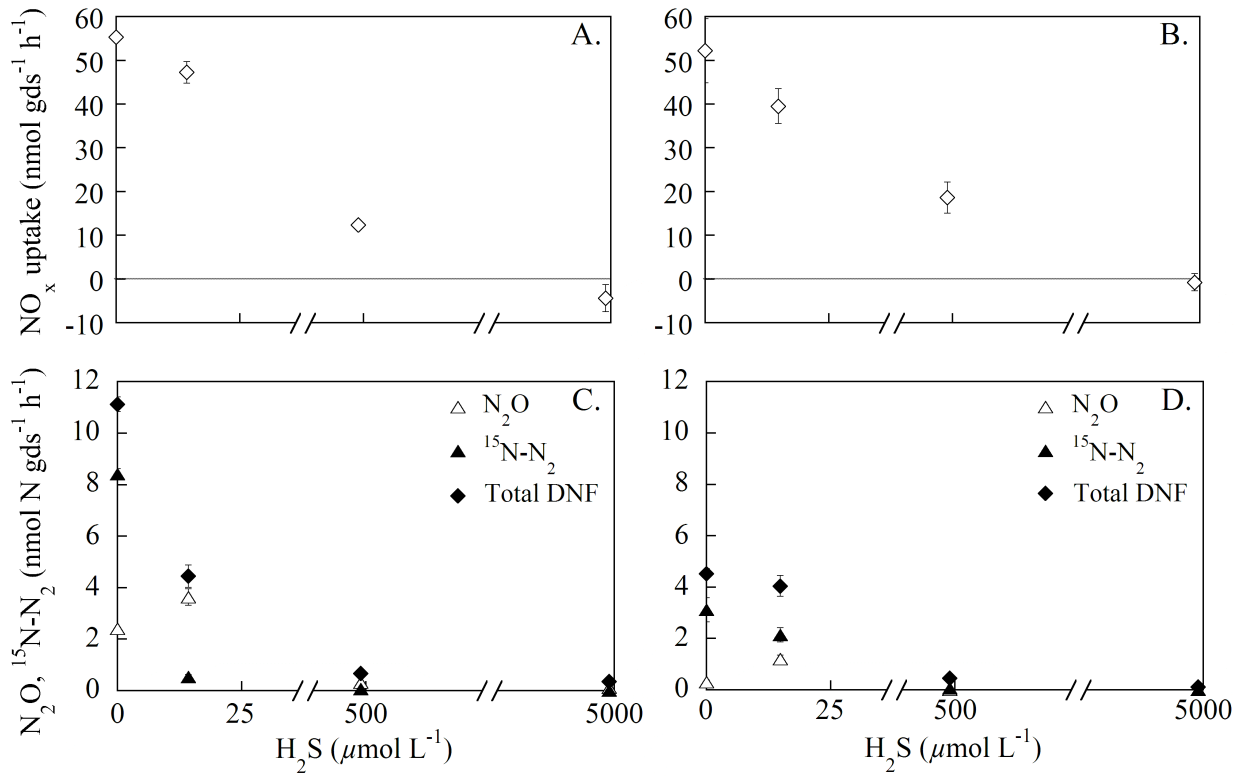
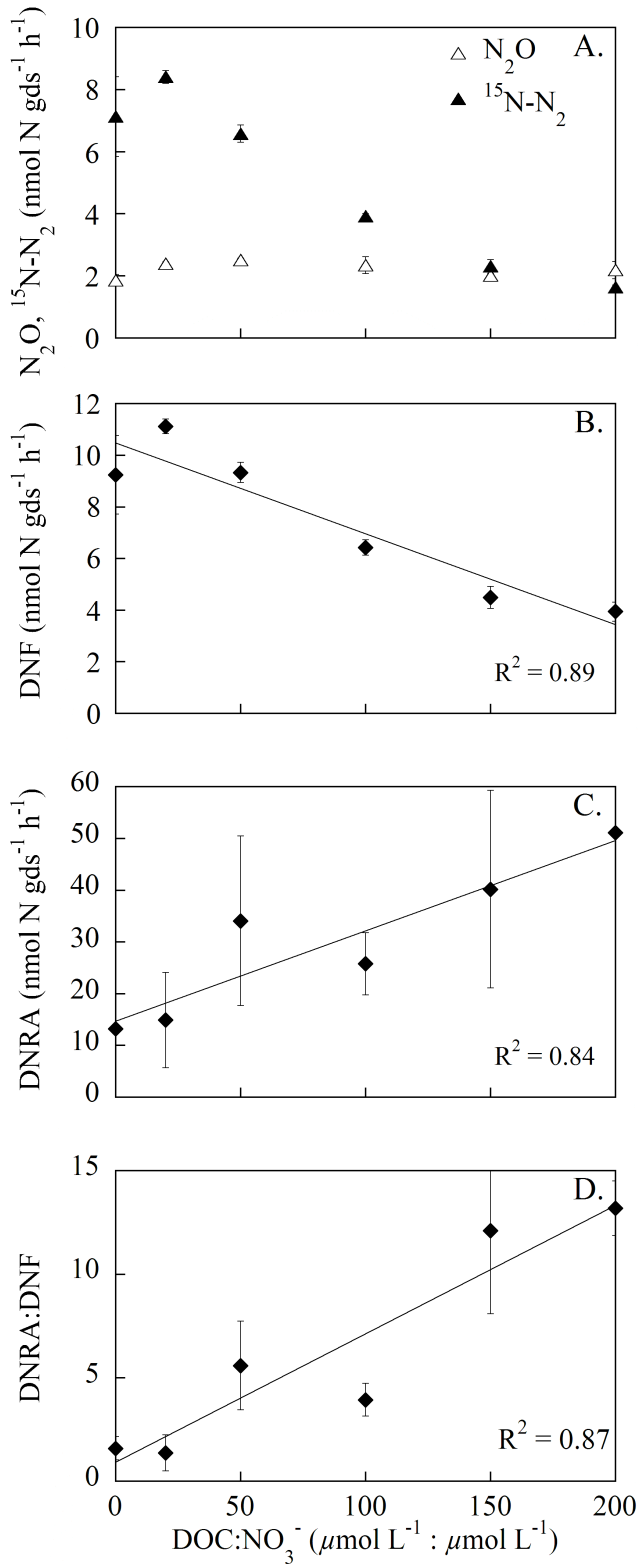


Figure 2.5A-D.



CHAPTER 3

NUTRIENT REplete BENTHIC MICROALGAE AS A SOURCE OF DISSOLVED ORGANIC CARBON TO COASTAL WATERS¹

¹Porubsky, W., L. Velasquez, and S. Joye. 2008. *Estuaries and Coasts*. 31:860-876.

Reprinted here with permission of publisher.

ABSTRACT

Dissolved organic carbon (DOC) flux dynamics were examined in the context of other biogeochemical cycles in intertidal sediments inhabited by benthic microalgae. In August 2003, gross oxygenic photosynthetic (GOP) rates, oxygen penetration depths, and benthic flux rates were quantified at 7 sites along the Duplin River, GA. Sediments contained abundant benthic microalgal (BMA) biomass with a maximum chlorophyll *a* concentration of 201 mg chl *a* m⁻². Oxygen microelectrodes were used to determine GOP rates and O₂ penetration depth, which were tightly correlated with light intensity. Baseline and ¹⁵N-nitrate amended benthic flux core incubations were employed to quantify benthic fluxes and to investigate the impact of BMA on sediment water exchange under nitrogen (N) limited and N-replete conditions. Unamended sediments exhibited tight coupling between GOP and respiration and served as a sink for water column dissolved inorganic nitrogen (DIN) and a source of silicate and dissolved inorganic carbon (DIC). The BMA response to the N addition indicated sequential nutrient limitation, with N limitation followed by silicate limitation. In diel (light-dark) incubations, biological assimilation accounted for 83 to 150% of the nitrate uptake while denitrification (DNF) and dissimilatory nitrate reduction to ammonium (DNRA) accounted for < 7%; in contrast, under dark conditions DNF and DNRA accounted for > 40% of the NO₃⁻ uptake. The N addition shifted the metabolic status of the sediments from a balance of autotrophy and heterotrophy to net autotrophy under diel conditions, and the sediments served as a sink for water column DIN, silicate, and DIC, but became a source of DOC, suggesting that the increased BMA production was decoupled from sediment bacterial consumption of DOC.

INTRODUCTION

Intertidal sediments are sites of organic matter deposition and degradation (Blackburn and Henrikson 1983; Sigmon and Cahoon 1997). The remineralization of organic matter in sediments serves as a primary source of regenerated inorganic nutrients to the water column (Aller and Beninger 1981; Flint and Kamykowski 1984; Sigmon and Cahoon 1997) and also supports benthic primary production (Flint and Kamykowski 1984; Krom 1991; Anderson et al. 2003). Many intertidal sediments are home to a diverse suite of benthic microalgae (BMA), including hundreds of species of pennate diatoms (Williams 1962) that occupy a μm to mm thick layer at the sediment surface. Benthic microalgal production can rival macrophytic and planktonic production in some systems (Pinckney and Zingmark 1993b) and may account for up to one-third of gross primary production in estuarine systems (Pinckney and Zingmark 1993a). Epipellic diatoms often dominate the BMA community (Williams 1962) because their tidally-induced migratory behavior affords an advantage under dynamic conditions where variable light intensity, potentially high salinities, exposure, desiccation and scouring tides could limit, suspend, and export less well adapted BMA (Aleem 1949; Pomeroy 1959; Sundbäck and Granéli 1988; Cabrita and Brotas 2000).

Benthic microalgae exert both direct and indirect controls on the fluxes of nutrients and dissolved organics between the sediment and water column (Sundbäck and Granéli 1988; Joye et al. 2003). BMA directly assimilate inorganic nutrients from the water column (Kelderman et al. 1988; Rysgaard et al. 1993; Sigmon and Cahoon 1997) and also assimilate nutrients regenerated in the sediments, thus retaining nutrients in the benthos (Sundbäck and Granéli 1988; Sigmon and Cahoon 1997; McGlathery et al. 2004). The assimilatory demands of BMA can regulate fluxes of inorganic nitrogen (NO_3^- and NH_4^+) as well as dissolved silicate ($\text{H}_2\text{SiO}_4^{2-}$) (Sigmon

and Cahoon 1997). Direct release of DOC by epipelagic diatoms to support motility is accomplished by secretion of extracellular polymeric substances (EPS; Edgar and Pickett-Heaps 1984; Perkins et al. 2001); this DOC represents a source of labile organic matter for heterotrophic consumption or efflux from the sediment to the water column (Middelburg et al. 2000). Resuspension of BMA can serve as an additional link between benthic production and the water column under certain conditions (de Jonge and van Beusekom 1995).

Benthic flux core incubations were used to quantify flux rates of inorganic nutrients and dissolved inorganic and organic carbon (DIC and DOC) under natural and nitrate amended conditions. A ^{15}N -labeled NO_3^- addition was used to distinguish between assimilatory (biological uptake, including BMA and bacterial assimilation) and dissimilatory (DNF and DNRA) pathways of nitrate reduction. Under diel (light-dark) light conditions, BMA were hypothesized to be the dominant sink for water column and sediment derived DIN, out-competing dissimilatory nitrate reduction processes. We hypothesized that BMA production would be stimulated by the DIN addition and that tight coupling between BMA production and heterotrophic bacterial consumption would continue. Under dark conditions, dissimilatory nitrate reduction processes (denitrification and dissimilatory nitrate reduction to ammonium) were hypothesized to be the dominant sink for the added NO_3^- .

MATERIALS AND METHODS

Study sites

The Duplin River, which forms the western boundary of Sapelo Island (GA, USA), has a watershed that encompasses 11 km² of *Spartina alterniflora* dominated salt marsh and mud flat (80%) and open water (20%) (Fig. 3.1; Pomeroy and Imberger 1981). The river has an average

salinity of 25.7, lacks a typical freshwater source, and is not salinity stratified (Ragotzkie 1955). Semi-diurnal tides with a neap range of ~1.5 m and spring range of ~2.5 m dominate the area. Creek bank sediments are free of macrophytes; however, they are covered by dense accumulations of BMA, primarily diatoms (Pomeroy et al. 1981; Velasquez 2005).

Study areas were selected within the upper reaches of the Duplin River (Fig. 3.1); three sites on the western fork (“West Fork”) and three sites on the eastern fork (“East Fork”). There were no differences in water column biogeochemical signatures (nutrient and organic carbon concentrations) between the two sections of the river (Joye, unpublished data). An additional site on the western fork, designated LF5, was sampled for ^{15}N tracer experiments (Fig. 3.1). All experiments occurred during August 2003.

Experimental design

Benthic fluxes were determined during re-circulated, flow-through incubations of sediment cores ($n = 3$ cores for the West and East forks for a total of $n = 6$, and $n = 3$ per treatment for a total of $n = 6$ for site LF5). The clear acrylic core tubes were 40 cm in height and contained the top 20 cm of sediment, above which ~20 cm of water (approximately 2.25-2.5 liters) was re-circulated. The core tubes were 12 cm in diameter, resulting in a sediment surface area of 0.011 m^2 . Creek bank sediment cores were collected at low tide and were free of macrophytes and visible burrows. Creek water collected at the same time as sediment cores was filtered ($0.7 \mu\text{m}$ GF/F filter) prior to being re-circulated through the cores via a peristaltic pump; the flow speed was $\sim 30 \text{ ml min}^{-1}$, the re-circulated water entered the core approximately 1.5 cm above the sediment surface and exited the core approximately 18 cm above the sediment surface.

The peristaltic pump was maintained at the height of the cores to ensure no pressure gradient formed in the tubing.

Cores collected from the West and East forks were used to determine benthic flux rates under conditions that simulated natural diel variability. Cores collected from site LF5 were divided into two treatments; a “diel” treatment included the influence of regular day-night diel light cycles (~13 hours light, ~11 hours dark) and a “dark” treatment in which cores were maintained under continual darkness (24 hours). Results from the diel treatments were further classified by the timing within the diel cycle, fluxes measured under illuminated conditions were designated “diel-day” and fluxes under dark conditions were designated “diel-night”.

All sediment cores were incubated on a flow-through water table to regulate temperature and under natural sunlight but were screened to mimic in situ light levels. Light levels were determined in the field with a LI-COR model LI-190SA Quantum Sensor (LI-COR, Inc., Lincoln, NE). Diel treatments were maintained at light levels representative of those at the sediment water interface at high tide ($\sim 2 \times 10^{-4}$ mol photons $\text{m}^{-2} \text{s}^{-1}$, as calculated from turbidity, photosynthetically active radiation, and water column depth; data not shown). West and East fork cores were sampled every 12 hours, before sunrise (05:30) and at sunset (20:00), for approximately 3.5 days; whereas cores from site LF5 were sampled similarly over 7 days. The average % change in concentrations during any one 12-hour flux period was approximately 10% under baseline conditions.

Flux experiments for the LF5 cores occurred in two phases. The first phase of the incubation determined baseline fluxes in both diel and dark treatments. The second phase consisted of a $\text{K}^{15}\text{NO}_3^-$ addition that increased the overlying water NO_3^- concentration to $\sim 100 \mu\text{mol L}^{-1}$. The amendment was made following the dawn sampling on the fourth day of the

experiment, after dark treatments became hypoxic, defined here as $[O_2] < 50 \mu\text{mol L}^{-1}$. The first phase is hereafter referred to as “baseline” and the second phase is referred to as “amended”.

Fluxes were calculated as the linear change in overlying water species concentration per sediment surface area per time (Eq. 3.1):

$$FluxRate_i = \frac{[C_{FINAL} \times Vol] - [(C_{INITIAL} \times 0.96) + (C_{Tzero} \times 0.04)] \times Vol}{AREA \times (T_{FINAL} - T_{INITIAL})} \quad (3.1)$$

The *FluxRate* of constituent *i* is in $\text{mmol m}^{-2} \text{h}^{-1}$, *C* is in mmol L^{-1} ; *Vol* is in L, *AREA* is in m^2 , and *T* is in hours. Flux calculations were corrected for dilution caused by replacement of sampled overlying water with filtered time zero water which was approximately 4% of the total overlying water volume per time point (i.e., $[(C_{INITIAL} \times 0.96) + (C_{Tzero} \times 0.04)]$, see Eq. 3.1 and below).

Negative numbers indicate fluxes into the sediment (uptake) and positive numbers indicate fluxes out of the sediment (release). Reported flux rates from diel-day and diel-night treatments are the average rate for each indicated period (i.e., diel-day reported flux is the average of the sunrise-sunset concentration/time/surface area calculations over multiple days).

Sample collection

Approximately 100 ml of the water overlying the core was collected at each time point using a 60 ml syringe attached in-line with the flow-through system. The volume removed was replaced with filtered (time zero) creek water. The impact of the sampling was examined on a per sampling timepoint basis, i.e. the impact of removing 5% of the volume was evaluated with regard to the potential impact to the overlying water concentration, the impact was always on the order of $< 2\%$ so this was not included in the flux calculations as it did not increase variability significantly. Dissolved oxygen (O_2) was measured with a galvanic dissolved oxygen probe (Orion, model no. 084260). pH was determined using a Sensorex[®] 450C flat surface combination

pH/reference electrode. Sulfide concentration was determined using the Cline method (Cline 1969). A sub-sample for dissolved inorganic carbon (DIC) quantification was transferred into a 7 ml glass vial by overflowing the volume of the vial one and a half times and was preserved with 25 μL of HgCl_2 before sealing without a headspace. DIC concentrations were determined on an infrared carbon analyzer (Shimadzu[®] TOC-5000).

A filtered sample (National Scientific[®], Target 0.2 μm pore size) was transferred to a 20 ml glass vial and acidified with 100 μL of concentrated nitric acid for determination of dissolved organic carbon (DOC) concentrations. DOC was measured using a Shimadzu[®] total organic carbon analyzer (TOC-5000).

A sample was filtered into a 30 mL high density polyethylene bottle and stored at 4°C in the dark for subsequent determination of nutrient concentrations (nitrite (NO_2^-), nitrate + nitrite (NO_x), and silicate ($\text{H}_2\text{SiO}_4^{2-}$)). A 5 mL aliquot of the filtered sample was immediately subsampled for determination of NH_4^+ concentration (Solorzano 1969). Nitrite and NO_x ($= \text{NO}_2^- + \text{NO}_3^-$) concentrations were determined by vanadium reduction and NO detection using an Antek[®] 745 $\text{NO}_3^-/\text{NO}_2^-$ reduction assembly and 7050 NO analyzer. NO_3^- concentration was calculated as the difference between NO_x and NO_2^- . Silicate concentration was determined on a Lachat QuikChem[®] FIA+ 8000 Series (QuikChem[®] Method Silicate 31-114-27-1-D). Phosphate concentrations were determined using the molybdate blue technique (Strickland and Parsons 1972).

¹⁵N tracer experiments

A $\text{K}^{15}\text{NO}_3^-$ amendment ($\sim 100 \mu\text{mol L}^{-1}$ final concentration of overlying water, of 99 atom % $\text{K}^{15}\text{NO}_3^-$) was added to the water overlying the LF5 cores to examine the fate and

consequences of a NO_3^- pulse. The ^{15}N was tracked into three pools: 1) N_2 , by measuring the mass 29 and 30 N_2 using the MIMS, 2) NH_4^+ by measuring the atom % ^{15}N of the overlying water NH_4^+ and 3) benthic microalgae (BMA), by measuring the atom % ^{15}N in collected BMA at the termination of the incubation.

A water sample for determination of dissolved N_2 concentration and isotopic composition was collected in a ground glass-stoppered tube by overflowing the volume of the tube (8 mL) one and a half times and was then preserved with HgCl_2 and stored under water at the sampling temperature. The concentration of $^{28}\text{N}_2$, $^{29}\text{N}_2$, and $^{30}\text{N}_2$ were quantified from the ratio of each component to argon ($^x\text{N}_2/\text{Ar}$) using a membrane inlet mass spectrometer (MIMS) (Kana et al. 1998; Eyre et al. 2002). Rates of $^{14}\text{NO}_3^-$ based DNF (D_{14}) were determined by the isotope pairing technique (IPT; Nielsen 1992). The production of $^{29}\text{N}_2$ and $^{30}\text{N}_2$ can be related to the D_{14} rate by Eq. 3.2 (Nielsen 1992):

$$D_{14} = \frac{{}^{29}\text{N}_2 \text{ rate}}{2 \times {}^{30}\text{N}_2 \text{ rate}} \times (2 \times {}^{30}\text{N}_2 \text{ rate} + {}^{29}\text{N}_2 \text{ rate}) \quad (3.2)$$

This calculation is only valid if the following conditions hold true: 1) the production of $^{28}\text{N}_2$ is not affected by the $^{15}\text{N}\text{-NO}_3^-$ addition, 2) $^{28}\text{N}_2$, $^{29}\text{N}_2$, and $^{30}\text{N}_2$ are binomially distributed and 3) the $^{15}\text{NO}_3^-/^{14}\text{NO}_3^-$ ratio remains constant in the NO_3^- reduction zone. Another requirement is that metabolic rates do not change during the incubation. To ensure that these conditions were met in the current study D_{14} rates were calculated from the first three time points following the $^{15}\text{NO}_3^-$ addition thus eliminating periods when NO_3^- may have limited DNF and when metabolic rates changed substantially. Total DNF (D_{15}) rates were calculated as the sum of the D_{14} rate and the production rate of $^{15}\text{N}\text{-N}_2$ (i.e., $^{29}\text{N}_2 + (2 \times {}^{30}\text{N}_2)$); thus, the D_{14} rate represents an unamended rate and the D_{15} rate represents the NO_3^- amended rate. The contribution of DNF to NO_3^-

reduction following the tracer addition (as a percentage) was calculated as the flux of $^{15}\text{N-N}_2$ ($\text{mmol N m}^{-2} \text{ h}^{-1}$) divided by the flux of $^{15}\text{NO}_3^-$ ($\text{mmol N m}^{-2} \text{ h}^{-1}$) multiplied by 100.

At the termination of the experiment the concentration and isotopic composition of water column NH_4^+ was determined (Holmes et al. 1998). Rates of dissimilatory nitrate reduction to ammonium (DNRA) were estimated from the accumulation of $^{15}\text{NH}_4^+$ during the tracer incubation period. The initial concentration of $^{15}\text{NH}_4^+$ was calculated from the natural abundance of ^{15}N in NH_4^+ (NA) and the concentration of NH_4^+ prior to the $^{15}\text{NO}_3^-$ addition:

$\left[^{15}\text{NH}_4^+ \right]_{nit} = \left[\text{NH}_4^+ \right]_{total} \times NA$. The final concentration of $^{15}\text{NH}_4^+$ was calculated from the atom % ^{15}N measured at the termination of the experiment and the final concentration of NH_4^+ :

$\left[^{15}\text{NH}_4^+ \right]_{in} = \left[\text{NH}_4^+ \right]_{in} \times (\text{atom \% } ^{15}\text{N} / 100)$. The rate of DNRA was calculated from the initial and final $^{15}\text{NH}_4^+$ concentrations (Eq. 3.3):

$$DNRA = \frac{\left[^{15}\text{NH}_4^+ \right]_{FINAL} \times Vol - \left[^{15}\text{NH}_4^+ \right]_{INITIAL} \times Vol}{AREA \times (T_{FINAL} - T_{INITIAL})} \quad (3.3)$$

$DNRA$ is the rate of DNRA in $\text{mmol } ^{15}\text{NH}_4^+ \text{ m}^{-2} \text{ h}^{-1}$, Vol is in L, $AREA$ is in m^2 , and T is in hours.

The contribution of DNRA to NO_3^- reduction was calculated as the estimated rate of DNRA ($\text{mmol N m}^{-2} \text{ h}^{-1}$) divided by the average flux of NO_3^- ($\text{mmol N m}^{-2} \text{ h}^{-1}$) multiplied by 100 (for diel treatments, the flux of NO_3^- was averaged for both diel-day and diel-night periods).

Determination of nitrate assimilation in the diel treatment was complicated by the presence of nitrification following the first 28 hours of amended incubation. The NO_3^- assimilation was calculated in two ways: 1) prior to observed increases in NO_3^- concentration (nitrification) during diel-night periods (i.e., only considering the first 28 hours of the amended period) and 2) using an average of the diel-night NO_3^- release as an estimate of nitrification rate and correcting the diel-day periods for nitrification (Table 3.3). The NO_3^- assimilation rate

reflects both BMA and bacterial assimilation, however, BMA uptake likely dominates the term since the NO_3^- was added to the overlying water during the light period and thus BMA may have had greater initial access to the addition. Therefore, biological uptake is hereafter referenced in terms of BMA (see Discussion for further details). In calculation 1), the rate of NO_3^- uptake was used to calculate the mass of NO_3^- removed during the first 28 hours after the N addition.

Denitrification and DNRA rates, averaged for the amended incubation period, were used to obtain a maximum amount of $^{15}\text{NO}_3^-$ reduced via dissimilatory pathways. The dissimilatory removal and the amount of NO_3^- remaining in the overlying water were subtracted from the total addition to give a maximum amount of $^{15}\text{NO}_3^-$ available to BMA. The $^{15}\text{NO}_3^-$ was presumed to be evenly taken up by BMA across the surface area of the core and by correcting for the total time of the diel-day periods of the incubation; we obtained a maximum rate of BMA uptake during the day (“BMA Assim. 1”; Table 3.3). The mass of NO_3^- removed by BMA was then compared to the total mass of $^{15}\text{NO}_3^-$ added to obtain a maximum percentage of $^{15}\text{NO}_3^-$ uptake that could be attributed to BMA (“BMA(1)”, Table 3.3). Calculation 2) was applied to the entire amended incubation period (78 hours). For this calculation, it was assumed that BMA did not assimilate NO_3^- at night. Though some evidence for dark BMA NO_3^- uptake exists (Rysgaard et al 1993, Dalsgaard 2003), the dark release of NO_3^- observed in these experiments indicates net NO_3^- production; dark BMA uptake would also lead to underestimates of nitrification rates. The average rate of NO_3^- uptake during the diel-day period, the average rates of DNF and DNRA, and the average rate of NO_3^- release during the last two diel-night periods (which provided an estimate of the net nitrification rate) were used to calculate the BMA contribution to NO_3^-

uptake: $\text{BMA Assim. 2} = (- \text{NO}_3^-_{\text{DIEL-DAY}}) - (+ \text{NO}_3^-_{\text{DIEL-NIGHT}}) - (- \text{DNF}) - (- \text{DNRA})$ where the sign indicates the direction of the flux (– is uptake and + is release), BMA Assim. 2 is the total

potential uptake of NO_3^- attributed to BMA, $\text{NO}_3^-_{\text{DIEL-DAY}}$ is the rate of NO_3^- flux during the diel-day period, $\text{NO}_3^-_{\text{DIEL-NIGHT}}$ is the rate of NO_3^- flux during the diel-night period and represents an estimate of potential nitrification, and DNF and DNRA are average calculated potential rates. Similar to calculation 1, the mass of NO_3^- removed by BMA was then compared to the total mass of $^{15}\text{NO}_3^-$ added (minus that remaining in the water column) to obtain a maximum percentage of $^{15}\text{NO}_3^-$ uptake that could be attributed to BMA (“BMA(2)”, Table 3.3).

At the end of the incubations, BMA were collected for atom % ^{15}N determination using a modification of the method reported by Williams (1963) (C. Currin, personal communication). The water overlying the core was removed, sand (pre-baked at 500°C) was applied on the surface of the sediment, and a wet (sprayed with filtered creek water) section of Nitex[®] bolting cloth (63 μm pore size) was placed atop the sand. The sediment surface was then shaded to induce vertical migration of the BMA. After approximately 6 hours, the mesh was collected and rinsed into a 500 mL bottle. The rinse water was then collected on an ashed GF/F filter under low vacuum. The filter was examined under a dissecting microscope and large detritus and invertebrates were removed so that only diatoms remained. The filters were then wrapped in aluminum foil and dried in an oven at 80°C for 24 hours. The ^{15}N isotopic composition of the BMA was determined by isotope ratio monitoring mass spectrometry.

Oxygen microprofiles and primary production rates

Gross oxygenic primary production (GOP) rates were determined using the light-dark shift method (Revsbech and Jorgensen 1983). Intact sediment cores (hereafter referred to as “GOP cores”, 4 cm inner diameter, 5 cm depth) were collected adjacent to flux core collection sites. Clark-type oxygen microelectrodes (UNISENSE[®]) were used to determine O_2

microprofiles and gross primary production rates (Revsbech et al. 1980; Revsbech and Jorgensen 1983; Revsbech et al. 1983; Joye and Lee 2004). Rates of GOP were measured at 100 μm depth intervals and integrated from the sediment surface to the depth of zero O_2 production. GOP rates were determined at 0, 1×10^{-3} and 2×10^{-3} mol photons $\text{m}^{-2} \text{s}^{-1}$, which represent zero irradiance, average daily irradiance experienced at the sediment surface on a cloudless day and maximum irradiance experienced at midday in summer, respectively. Following the microelectrode measurements, sediment samples were collected for chlorophyll *a* (chl *a*) and phaeopigment determination (see below). An additional sample from the top centimeter of the core was collected to characterize sediment physical properties including porosity, density and % bulk organic matter.

Sediment samples (top 1 cm) for chl *a* and phaeopigment quantification were collected from field sites on each fork using modified 5 cc syringes. All pigment samples were extracted in 100% acetone in the dark for 24 hours. The supernatant was collected and the absorbance was measured on a spectrophotometer (Strickland and Parsons 1972). Phaeopigment concentration was determined on the same sample following the addition of 100 μL of 1N HCl. The sample was incubated for 2 minutes and the above measurements were repeated.

Statistics

Statistical comparisons of percent organic matter, chl *a* and phaeopigment concentration, chl *a* to phaeopigment ratios and integrated GOP rates between the East and West Fork sites (Table 3.1), were determined by single factor analysis of variance (ANOVA). Single factor ANOVA was also used to compare average fluxes between sites, treatments (i.e., diel-day, diel-night, and dark), and baseline – amended status. DNF rates and the percentage of DNF, DNRA

and NO_3^- assimilation that contributed to NO_3^- uptake were also compared using single factor ANOVA.

RESULTS

Oxygen: Depth profiles, gross oxygenic photosynthesis, and fluxes

Sediment characteristics were similar on both forks of the Duplin River (Table 3.1). Percent organic matter ranged from 11.6 to 14.4% for the East Fork and from 9.8 to 14.9% for the West Fork (Table 3.1), with no significant difference ($p = 0.9$) between the two. Average chl *a* concentrations were significantly higher ($p < 0.05$) for the West Fork with a maximum concentration of 201.2 mg chl *a* m^{-2} (Table 3.1). There was no significant difference between the phaeopigment concentrations on the two forks ($p = 0.09$). The chl *a*/phaeo ratio was significantly higher ($p < 0.01$) on the West Fork indicating high chl *a* production and less BMA senescence.

Representative O_2 microprofiles illustrated the influence of light intensity on both primary production and O_2 penetration depth (Fig. 3.2A-C). Replicate cores from the East Fork indicated spatial variability in both GOP and O_2 penetration depth. Profiles generated at 0 mol photons $\text{m}^{-2} \text{s}^{-1}$ (i.e., O_2 distribution in the absence of benthic photosynthesis) showed a sediment O_2 concentration maximum at the sediment surface and a rapid decrease with depth. Sediment O_2 concentration was lower than the overlying water O_2 concentration and the O_2 penetration depth averaged 1.15 mm (Fig. 3.2A). Profiles determined at zero irradiance showed no difference between sites, indicating that diffusion and sediment characteristics were similar (data not shown). For profiles generated at 1×10^{-3} mol photons $\text{m}^{-2} \text{s}^{-1}$, the surface sediment O_2 maximum exceeded the O_2 concentration in the overlying water (Fig. 3.2B). At a light intensity of 2×10^{-3} mol photons $\text{m}^{-2} \text{s}^{-1}$, the O_2 concentration exhibited a subsurface maximum of 674 to 827 μmol

L^{-1} and the O_2 penetration depth was between 1.7 and 2.2 mm (Fig. 3.2C). Oxygen penetration depths in the 2×10^{-3} mol photons $m^{-2} s^{-1}$ treatment increased significantly relative to the 0 mol photons $m^{-2} s^{-1}$ treatment ($p < 0.05$); however, only one core showed a significant increase in O_2 penetration depth relative to the 1×10^{-3} mol photons $m^{-2} s^{-1}$ treatment ($p < 0.05$).

Integrated GOP rates ranged from 6.1 to 14.2 mmol $O_2 m^{-2} h^{-1}$ for the East Fork (Table 3.1). GOP rates were higher on the West Fork, ranging from 6.4 to 32.9 mmol $O_2 m^{-2} h^{-1}$, with the highest rate on the West Fork being significantly ($p < 0.05$) higher than the highest rate on the East Fork. With the exception of one location on the West fork, GOP rates normalized to chl *a* concentration were comparable among all sites (data not shown).

Oxygen concentrations at the onset of the benthic flux experiments were between 200 and 250 $\mu\text{mol } O_2 L^{-1}$ for all sites and treatments (Fig. 3.3A). Under baseline conditions light treatments showed little variation in O_2 concentration over a diel light-dark cycle. The baseline dark treatment from LF5 exhibited a rapid uptake of O_2 , with complete depletion of O_2 by day 4 (Fig. 3.3A). Following the $^{15}\text{N-NO}_3^-$ addition, the diel treatment from site LF5 illustrated a strong diel cycle: O_2 concentration increased during the diel-day phase and decreased during the diel-night phase (Fig. 3.3A). During the amended portion of the diel LF5 incubation, there was a general trend of increasing O_2 concentration. Following the $^{15}\text{N-NO}_3^-$ addition, O_2 release rates increased by 4 times under diel-day conditions, while O_2 uptake under diel-night conditions increased approximately 2 times (Table 3.2). At the East Fork and LF5 sites, O_2 release rates during the diel-day and uptake rates during the diel-night were comparable indicating a balance between autotrophy and heterotrophy. In contrast, at the West Fork and LF5 sites, diel-night O_2 uptake rates were approximately 1.5 to 2 times the diel-day O_2 release rates indicating net heterotrophy (Table 3.2).

Silicate and phosphate fluxes

Silicate concentration increased for all sites and treatments during the first 3.5 days of the incubation (Fig. 3.3F; Table 3.2). The average $\text{H}_2\text{SiO}_4^{2-}$ concentration increased from 115.9 to 142.1 $\mu\text{mol L}^{-1}$. Following the $^{15}\text{NO}_3^-$ addition to LF5 cores, the silicate concentration in the light treatment continued to increase for approximately 18 hours up to a maximum of 148.4 $\mu\text{mol H}_2\text{SiO}_4^{2-} \text{ L}^{-1}$; this initial increase was followed by an additional 18 hours in which the silicate concentration did not change (Fig. 3.3F). Approximately 36 hours after the $^{15}\text{NO}_3^-$ addition, the silicate concentration decreased rapidly and was 42 $\mu\text{mol H}_2\text{SiO}_4^{2-} \text{ L}^{-1}$ at the end of the incubation (Fig. 3.3F).

Under diel-day conditions, the silicate flux reversed from an average release of 0.1 $\text{mmol H}_2\text{SiO}_4^{2-} \text{ m}^{-2} \text{ h}^{-1}$ to an average uptake of 0.42 $\text{mmol H}_2\text{SiO}_4^{2-} \text{ m}^{-2} \text{ h}^{-1}$ (Table 3.2) following the N amendment. The final concentration in the diel treatment indicated that approximately 71.7% of the $\text{H}_2\text{SiO}_4^{2-}$ was consumed under N-replete conditions. In the dark treatment, the silicate concentration continued to increase following the $^{15}\text{NO}_3^-$ addition and reached a maximum concentration of 227.5 $\mu\text{mol H}_2\text{SiO}_4^{2-} \text{ L}^{-1}$ (Fig. 3.3F), a 96% increase over the initial $\text{H}_2\text{SiO}_4^{2-}$ concentration.

Phosphate fluxes under diel-day and diel-night conditions were insignificant (Table 3.2). Under dark conditions, cores became hypoxic and phosphate fluxes increased significantly. The NO_3^- amendment did not alter phosphate fluxes substantially.

Nitrogen: Fluxes, dissimilatory, and assimilatory processes

Fluxes

The NO_3^- concentration at the start of the incubation averaged $1.5 \mu\text{mol NO}_3^- \text{L}^{-1}$ (Fig. 3.3D). The NO_3^- concentration in the cores from the East and West forks averaged $0.3 \mu\text{mol NO}_3^- \text{L}^{-1}$ at the termination of the incubations (3.5 days), while the LF5 cores (diel and dark treatments) averaged $0.1 \mu\text{mol NO}_3^- \text{L}^{-1}$ following 3.5 days of baseline conditions. The water column NO_3^- concentration increased to an average of $91 \mu\text{mol NO}_3^- \text{L}^{-1}$ as a result of $^{15}\text{NO}_3^-$ amendment (Fig. 3.3D). Following the amendment the diel treatment exhibited a subtle diel cycle with regard to NO_3^- fluxes (Fig. 3.3D). During the first 24 hours following the addition, the slope of the NO_3^- concentration change was significantly greater during diel-day periods than diel-night periods ($p < 0.05$), indicating higher uptake rates during the day. Following the initial 24 hours, the NO_3^- concentration increased during the diel-night periods, indicating that NO_3^- release exceeded uptake (Fig. 3.3D). The NO_3^- concentration in the dark treatment decreased steadily to approximately $7.9 \mu\text{mol NO}_3^- \text{L}^{-1}$ by the end of the incubation (Fig. 3.3D).

The NH_4^+ concentration averaged $4.9 \mu\text{mol NH}_4^+ \text{L}^{-1}$ for all cores at the start of the incubations (Fig. 3.3E). The NH_4^+ concentration decreased to zero in all cores over the first 2.5 days. Just prior to the $^{15}\text{NO}_3^-$ addition, the NH_4^+ concentration increased to 1.3 and $3.6 \mu\text{mol NH}_4^+ \text{L}^{-1}$ in the diel and dark treatments from LF5 respectively (Fig. 3.3E). The diel treatment maintained a concentration of approximately $1.3 \mu\text{mol NH}_4^+ \text{L}^{-1}$ for the remainder of the incubation. In contrast, the NH_4^+ concentration in the dark treatment increased by an order of magnitude following the NO_3^- addition (Fig. 3.3E), reaching a maximum of $34 \mu\text{mol NH}_4^+ \text{L}^{-1}$, or approximately 25 times the NH_4^+ concentration in the diel treatment.

Sediments generally served as a sink for water column NO_3^- and NH_4^+ under baseline conditions. Baseline NO_3^- uptake rates were low for all treatments and sites (Table 3.2) due to the low initial water column NO_3^- concentration. Baseline NH_4^+ flux rates were similar to NO_3^- flux rates (Table 3.2) but slightly higher due to higher initial concentration in the water column.

As expected, NO_3^- flux rates increased with the addition of $^{15}\text{NO}_3^-$ (Table 3.2) and NO_3^- was consumed rapidly in both diel and dark treatments. NO_3^- uptake rates were highest under diel-day conditions, followed by dark conditions, while diel-night conditions indicated NO_3^- release (Table 3.2). NH_4^+ fluxes in the diel-day treatment switched from uptake to release following the NO_3^- addition, although the fluxes were small relative to dark fluxes (Table 3.2). In dark treatments, NH_4^+ uptake ($-0.001 \text{ mmol m}^{-2} \text{ h}^{-1}$) reversed to NH_4^+ release ($0.07 \text{ mmol m}^{-2} \text{ h}^{-1}$) (Table 3.2) but the timing of the NH_4^+ flux reversal began prior to the NO_3^- addition and correlated instead with O_2 concentration reaching hypoxic levels.

Dissimilatory and assimilatory nitrate reduction

The isotope pairing technique (Nielsen 1992) was used to determine D_{14} rates, D_{15} rates, and the percentage of D_{14} that was coupled to nitrification (Fig. 3.4). The average D_{14} rate for the diel treatment was about $1.02 \mu\text{mol N m}^{-2} \text{ h}^{-1}$ and the average D_{14} rate in the dark was about $3.73 \mu\text{mol N m}^{-2} \text{ h}^{-1}$; the dark rate was not significantly different from the diel rate ($p > 0.05$). D_{15} rates were 20 and 39 times higher than D_{14} rates for diel and dark treatments respectively and the D_{15} rate in the dark treatment was significantly higher than in the diel treatment (Fig. 3.4, $p < 0.05$). The percentage of D_{14} coupled to nitrification was 42 and 31% in diel and dark treatments, respectively (Fig. 3.4), and there was no significant difference between the treatments ($p > 0.05$).

In the dark treatment, coupled D_{14} occurred at the beginning of the incubation while the cores were still oxic.

Dissimilatory and assimilatory contributions to NO_3^- reduction rates under amended conditions varied between treatments (Table 3.3). Dissimilatory NO_3^- reduction rates in the diel treatment were significantly lower than in the dark treatment with the DNF and DNRA rates 10 and 3 times lower respectively. In the diel treatment, calculation 1) (see methods) yielded a maximum of 83% of the $^{15}\text{NO}_3^-$ uptake rate attributed to BMA. The calculated BMA(1) uptake rate under diel-day conditions ($0.52 \text{ mmol N m}^{-2} \text{ h}^{-1}$, average for the first 30 hours) was approximately $120 \pm 21.3\%$ of the total diel-day NO_3^- uptake rate ($0.43 \text{ mmol N m}^{-2} \text{ h}^{-1}$, average for the entire amended diel incubation, Table 3.3). Calculation method 2, which included nitrification, yielded a maximum of $142 \pm 23.8\%$ of the added NO_3^- that could be taken up by the BMA; as the BMA(2) uptake rate under diel-day conditions ($0.63 \text{ mmol N m}^{-2} \text{ h}^{-1}$) exceeded the observed total diel-day NO_3^- uptake rate ($0.43 \text{ mmol N m}^{-2} \text{ h}^{-1}$, Table 3.3); the additional NO_3^- available for assimilation was derived from nitrification. In the dark treatment, 41% of the $^{15}\text{NO}_3^-$ added was reduced by DNF, and a minimum of 1.2% of the added $^{15}\text{NO}_3^-$ was reduced by DNRA (Table 3.3). These two processes accounted for the reduction of less than 6% of the added $^{15}\text{NO}_3^-$ in the diel treatment (Table 3.3). Incorporation of ^{15}N into BMA biomass in the diel treatment was 8 times higher than the dark treatment (Table 3.3). Dissimilatory processes were significantly less important in diel treatments, while BMA incorporation of ^{15}N was significantly higher ($p < 0.01$).

Dissolved inorganic and organic carbon fluxes

Baseline DIC concentrations were similar among all sites and treatments (Fig. 3.3B). DIC concentration increased for all baseline treatments during the first 3.5 days, with the largest increase occurring in the dark treatment. Following the nitrogen addition, the DIC concentration from the LF5 diel treatment continued to increase for approximately 36 hours (Fig. 3.3B). After that, the DIC concentration exhibited a strong diel cycle inverse to that of O₂ (Fig. 3.3A and B). In general, the DIC concentration in the diel treatment decreased during the last 2.5 days of the incubation, as uptake during the diel-day exceeded release during the diel-night. The DIC concentration in the dark treatment from LF5 continued to increase following the NO₃⁻ addition and showed little change in the flux. The DOC concentration remained stable for the East and West fork sites (Fig. 3.3C). Prior to the ¹⁵NO₃⁻ amendment, the DOC concentration in the LF5 dark treatment was also stable, but the diel treatment from LF5 showed a slight decrease in DOC concentration (Fig. 3.3C). Following the ¹⁵NO₃⁻ amendment, the DOC concentration increased significantly in the diel and dark treatments from LF5 (Fig. 3.3C).

Baseline fluxes of DIC and DOC varied among treatments (Table 3.2). DIC release occurred under both diel-day and diel-night conditions in the diel treatment and in the dark treatment from LF5. Baseline DIC release rates were highest under diel-night conditions at the East Fork, and reached a maximum of 1.95 mmol DIC m⁻² h⁻¹ (Table 3.2). Diel treatments from the East and West forks showed release of DOC during the diel-day and uptake of DOC during the diel-night (diel day-night differences were significant for the West Fork, $p = 0.03$, but not for the East Fork, $p = 0.6$), with release and uptake rates of comparable magnitude. The baseline diel treatment from LF5 showed uptake of DOC during the diel-day and diel-night, while DOC release occurred in the dark treatment.

The $^{15}\text{NO}_3^-$ addition altered fluxes of DIC and DOC (Table 3.2). DIC flux rates increased following the NO_3^- addition (Table 3.2). The uptake of DIC under amended diel-day conditions was greater than the DIC release under amended diel-night conditions, again suggesting a shift toward net autotrophy (Table 3.2). There was no significant difference between the baseline and amended dark DIC flux (Table 3.2). Following the $^{15}\text{NO}_3^-$ amendment, DOC fluxes reversed from uptake of $-0.13 \text{ mmol DOC m}^{-2} \text{ h}^{-1}$ to a release of $1.01 \text{ mmol DOC m}^{-2} \text{ h}^{-1}$ under diel-day conditions, while under diel-night conditions DOC release increased from 0.12 to $0.36 \text{ mmol DOC m}^{-2} \text{ h}^{-1}$ (Table 3.2). There was no significant difference between the baseline and amended dark DOC flux (Table 3.2).

DISCUSSION

A pulse of NO_3^- altered benthic fluxes and led to a reversal in $\text{H}_2\text{SiO}_4^{2-}$, DIC and DOC fluxes in the diel-day treatments. In diel treatments, the NO_3^- addition shifted the system from a balance of autotrophy and heterotrophy to net autotrophy. Following the NO_3^- addition, the BMA community was relieved of NO_3^- limitation and primary production increased leading to a subsequent drawdown of water column silicate. This pattern indicated sequential limitation of the BMA community by nitrogen and then silicate. The NO_3^- addition altered the DOC flux in the diel treatments and led to increases in both BMA production (during the day) and heterotrophic activity (during the night) with increased BMA production outpacing increased heterotrophic activity. In the dark treatment, the NO_3^- addition increased net heterotrophy and stimulated dissimilatory pathways of NO_3^- reduction, including DNF and DNRA.

Baseline N fluxes

Sediments serve as a site for regeneration of nutrients in coastal areas and are usually an important source of inorganic nutrients to the water column (Blackburn and Henrikson 1983; Sundbäck and Granéli 1988). However, the presence of an active BMA community may limit the role of the sediment as a source of regenerated nutrients due to BMA-mediated assimilation of inorganic nutrients from both the water column and the porewater (Sundbäck and Granéli 1988; Krom 1991; Joye et al. 1996). The impact of infauna has been shown to enhance sediment water column exchange through both grazing of BMA and enhanced transport through bioirrigation; however, benthic diatoms can also mask the impact of infauna-enhanced exchange (Marinelli 1992). Macrofauna, such as fiddler crabs, were excluded from the current incubations and even though meiofauna like nematodes were almost certainly present in the cores, the fluxes were largely influenced by BMA alone. Under baseline conditions in diel treatments, BMA assimilated inorganic nutrients from the sediment and the water column, as shown by the initial decreases in water column NO_3^- and NH_4^+ concentrations (Fig. 3.3D and E) and the lack of DIN release from the sediments during both the diel-day and diel-night periods of the incubation. High concentrations of ammonia ($> 1 \text{ mmol N L}^{-1}$) that can have negative effects on BMA population density (Admiraal et al. 1984) were not evident in this study. While high NH_4^+ concentrations can have a negative impact on the NO_3^- uptake of some phytoplankton, BMA have been shown to uptake NO_3^- under higher NH_4^+ concentrations than phytoplankton (Admiraal et al. 1987) as was the case here where both NO_3^- and NH_4^+ were removed from the overlying water. In the dark treatment, NO_3^- and NH_4^+ uptake was observed during the first 2.5 days of the incubation and N was retained within the sediments even under dark conditions for approximately 12 hours following the complete drawdown of water column DIN (Fig. 3.3D and

E). BMA can effectively assimilate NH_4^+ in the dark, with the implication being that even during extended periods of darkness (25 to 60 hours), BMA can still impact benthic DIN fluxes, as was seen here (Rysgaard et al. 1993).

In addition to limiting nutrient fluxes by direct assimilation, BMA indirectly influenced benthic fluxes by producing O_2 and thus increasing the depth of the oxic zone (Rysgaard et al. 1995; Sundbäck and Granéli 1988). The O_2 produced by BMA photosynthesis impacts benthic fluxes in two ways: 1) larger oxic zones correspond to longer diffusion distances between anoxic sediments and the water column (Rysgaard et al. 1995); and 2) the O_2 produced by BMA serves as an oxidant for reduced nutrients and metals via secondary metabolic pathways (i.e. nitrification, manganese (II) oxidation, iron (II) oxidation, and sulfide oxidation) (Rysgaard et al. 1995; Joye et al. 2003). Oxygen microelectrodes provided direct evidence for the link between BMA primary production and O_2 penetration depth (Fig. 3.2). Under baseline diel-day conditions, a larger oxic zone and longer diffusion distances between anoxic sediments and the water column, in conjunction with BMA assimilation, limited the flux of reduced inorganic nutrients to the overlying water column.

Amended N fluxes

The efficient recycling of inorganic nutrients under baseline conditions indicated potential nutrient limitation of the BMA. Previous studies have suggested nutrient limitation of BMA in both temperate (Sundbäck and Granéli 1988; Rysgaard et al. 1995) and tropical/sub-tropical (Dizon and Yap 1995; Heil et al. 2004; Clavier et al. 2005; Veuger et al. 2007) systems. Other work has implicated nutrient limitation as a potential source of seasonal variations in BMA population density (Admiraal and Peletier 1980). Inorganic N concentrations obtained during

August of 2003 (data not shown) indicated low DIN (NO_3^- and NH_4^+) in the Duplin River (1.6 and $4.2 \mu\text{mol N L}^{-1}$, respectively), low NO_3^- in porewater ($< 1.0 \mu\text{mol N L}^{-1}$), and high porewater NH_4^+ concentration ($130 \mu\text{mol N L}^{-1}$ averaged for the top 10cm). Short-term depletion of porewater NH_4^+ by BMA has been shown to occur with NH_4^+ concentrations decreasing by ~50% in the top 3 cm of sediment cores incubated under illuminated conditions relative to dark treatments ($179 \pm 10 \mu\text{mol N L}^{-1}$ illuminated vs. $367 \pm 18 \mu\text{mol N L}^{-1}$ dark; Thornton et al. 1999). The BMA community on Sapelo Island, GA was formerly hypothesized to be N limited (Darley et al. 1981; Pomeroy et al. 1981).

Previous work has shown varying BMA responses to nutrient (N, P, and trace metals) additions. Filamentous cyanobacterial and diatom primary productivity was enhanced in response to increased supplies of both DIN and dissolved inorganic phosphorus (DIP) (Nilsson et al. 1991). However, only moderate increases in primary production of estuarine microbial mats were observed in response to DIN and DIP additions (Paerl et al. 1993). The complexity of phytoplankton nutrient limitation was illustrated by Pinckney et al. (1995) when DIN additions stimulated both cyanobacteria and diatoms, but both high DIN and DIP preferentially increased diatom abundance. Nutrient additions consisting of DIP only stimulated cyanobacteria and led to an increase in N fixation. Although the current data presented here indicates primary N limitation, the potential for secondary nutrient limitation exists.

The low DIN concentration typical in the Duplin River presented an excellent opportunity to investigate the role of nutrient availability on BMA production and the impact of increased NO_3^- on benthic fluxes. The pulsed NO_3^- addition used here is similar in duration and magnitude to natural supply resulting from groundwater or storm induced inputs (McClelland et al. 1997; Paerl 1997; McClelland and Valiela 1998). While some sources of pulsed nutrient

inputs, such as storm events (Paerl et al. 2001; Pinckney et al. 2001) lead to increased turbidity (Paerl et al. 2001; Steward et al. 2006), groundwater inputs generally do not. The increase in turbidity during a storm event would limit benthic primary production by light attenuation and dissimilatory processes (DNF and DNRA) would dominate; while in a scenario where the dominant DIN delivery pathway was via groundwater or a similar low turbidity source, the opposite would be expected with benthic primary production being an important sink for DIN under light replete conditions. Additional consideration must be given to the location of the DIN delivery, in the current experiment, the DIN is supplied to the overlying water thus giving BMA greater initial access. If the DIN was supplied to the subsurface, to mimic subterranean groundwater discharge, deeper microbial communities would have greater initial access to the DIN.

Sequential nutrient limitation of benthic primary production

The response of the BMA community to the NO_3^- addition provided evidence of sequential nutrient limitation, with the BMA exhibiting primary N limitation followed by secondary silicate limitation. Phosphorus concentrations in these sediments are surprisingly high, possibly due the presence of shallow Miocene phosphorite-rich sediments, and no hint of DIP limitation was present in these experiments. Phosphate fluxes were extremely low (on the order of $\mu\text{mol m}^{-2} \text{h}^{-1}$) and only increased under hypoxic conditions. Phosphate fluxes were not impacted by the NO_3^- addition on the time scale of these experiments.

Silicate has been implicated as a potential limiting nutrient for BMA growth and the impact of silicate availability becomes more important when other nutrients (i.e. nitrogen) are not limiting (Ragueneau et al. 1994; Sigmon and Cahoon 1997). The sequence of nutrient

limitation may also be indicative of the BMA's (primarily benthic diatoms) ability to sequester N intracellularly which allows for immediate uptake, while silicate uptake lags behind due to an inability to store silicate in a similar manner (Doering et al. 1989; Sigmon and Cahoon 1997). After alleviation of N limitation, water column silicate concentrations decreased rapidly from 125 to 40 $\mu\text{mol H}_2\text{SiO}_4^{2-} \text{ L}^{-1}$ (Fig. 3.3E); and the flux of silicate reversed from a release of 0.10 to an uptake of 0.42 $\text{mmol H}_2\text{SiO}_4^{2-} \text{ m}^{-2} \text{ h}^{-1}$ ($p < 0.01$, Table 3.2). The ratio of nitrogen to silicate uptake approached the Redfield ratio of 1:1 (Redfield 1958) following the NO_3^- addition (Table 3.2). Silicate fluxes from the sediment have been shown to decrease more than 80% under light replete conditions due to BMA uptake (Kelderman et al. 1988; Sigmon and Cahoon 1997). The current results document a reversal of $\text{H}_2\text{SiO}_4^{2-}$ fluxes in response to NO_3^- addition (Table 3.2) leading to a significant sink for water column $\text{H}_2\text{SiO}_4^{2-}$ under N-replete conditions. The potential drawdown of water column $\text{H}_2\text{SiO}_4^{2-}$ in eutrophic systems could lead to changes in phytoplankton community assemblages, with potentially harmful phytoplankton benefiting from decreased competition by planktonic diatoms.

The distribution of silicate in the Duplin River suggests a source in the headwater marshes and subsequent transport downstream and export to nearby receiving waters (Doboy Sound), with an estimated exchange of 125 mol Si day^{-1} (Imberger et al. 1983). In this closed system experiment, the NO_3^- addition led to uptake of approximately 72% of the water column $\text{H}_2\text{SiO}_4^{2-}$ over 3 days (Fig. 3.3E); and while the BMA significantly lowered the water column $\text{H}_2\text{SiO}_4^{2-}$ concentration under experimental conditions, could the BMA have a similar impact on the water column of the Duplin under N-replete conditions? This question is important because the water column $\text{H}_2\text{SiO}_4^{2-}$ concentration impacts the distribution of pelagic diatom species, which under silicate limitation could be out competed, leading to community shifts in the

phytoplankton assemblage from diatoms to harmful forms of algae such as dinoflagellates (Hecky and Kilham 1988; Sigmon and Cahoon 1997). To answer this question we estimated the impact of BMA uptake on the water column NO_3^- and $\text{H}_2\text{SiO}_4^{2-}$ pools. The flux rate for each species under diel-day conditions was used in addition to the water depth during neap low tide (0.35 m) and spring high tide (2.49 m), and the water column concentration of each species following the NO_3^- addition (Fig. 3.5). Assuming a residence time of 6 hours for each tide, the uptake of NO_3^- and $\text{H}_2\text{SiO}_4^{2-}$ under spring high tide conditions could account for approximately 1.2 and 0.7% of each respective pool. Under neap low tide conditions, the uptake of NO_3^- and $\text{H}_2\text{SiO}_4^{2-}$ could account for 8.2 and 4.8% of each respective water column pool (Fig. 3.5). While this represents a significant sink of NO_3^- and $\text{H}_2\text{SiO}_4^{2-}$, it is unlikely that the BMA community could impact the $\text{H}_2\text{SiO}_4^{2-}$ or NO_3^- concentration of the Duplin under even N-replete conditions during the day. Additionally, the BMA are susceptible to light limitation in addition to N limitation, in most estuarine systems, the turbidity of the system will also limit the BMA community's ability to significantly impact the water column $\text{H}_2\text{SiO}_4^{2-}$ concentration.

The fate of nitrate: assimilation vs. dissimilatory reduction

Under illuminated conditions, BMA assimilation accounted for 83 to 142% of the NO_3^- uptake (Table 3.3), with dissimilatory pathways (DNF and DNRA) accounting for less than 7% combined. Recent work has shown that bacteria and cyanobacteria can account for 35-100% of the total microbial (BMA inclusive) N (as NH_4^+) uptake (Veuger et al. 2007) in shallow sediments. However, it is important to note that the method utilized by Veuger et al. (2007) consisted of injecting $^{15}\text{NH}_4^+$ into the sediment (6 – 8 cm depth) which effectively bypassed the BMA present in the uppermost layer of the sediment and would preferentially favor

incorporation of the tracer into the bacterial population deeper in the sediments. The current study consisted of a $^{15}\text{NO}_3^-$ addition to the water column, which would preferentially favor the BMA community residing in the surface of the sediment and decrease the likelihood of bacterial incorporation.

BMA assimilation was confirmed from the atom % ^{15}N of the BMA community (Table 3.3); 16.5% of the BMA-N was ^{15}N in the diel treatment. The inclusion of the estimated nitrification rate in the BMA uptake estimate helps to explain why only 16.5% of the BMA-N was ^{15}N , as BMA assimilated both added $^{15}\text{NO}_3^-$ and $^{14}\text{NO}_3^-$ produced via nitrification, with the potential pool of $^{14}\text{NO}_3^-$ being approximately 8-9 times larger than the $^{15}\text{NO}_3^-$ addition. Further dilution of the BMA ^{15}N signal would result from incorporation of regenerated $^{14}\text{NH}_4^+$. Although BMA have been shown to operate as a link between the water column and the sediments via turnover and remineralization of incorporated nitrogen (Tobias et al. 2003), over the timescale of this experiment, BMA served as a sink of N and no subsequent release was observed.

Dissimilatory processes contributed significantly more to the N cycle under dark conditions (Table 3.3), accounting for a maximum of approximately 42% of the NO_3^- uptake. D_{15} rates (Fig. 3.4) determined in this study agree with rates measured in other studies (Kana et al. 1998; An and Gardner 2002). The D_{15} rate removed 40% of the water column NO_3^- during the 3 day incubation (Table 3.3). Although there was evidence of DNRA activity ($^{15}\text{NH}_4^+$ recovery), DNF accounted for approximately 35 times more NO_3^- reduction in the dark (Table 3.3). The estimate of DNRA was based on $^{15}\text{NH}_4^+$ recovered from the water column and as such it represents a lower estimate of DNRA since it does not consider $^{15}\text{NH}_4^+$ contained in the porewater or adsorbed to the sediment. Others have reported that DNRA was responsible for 2 to

5 times more NO_3^- reduction than DNF (An and Gardner 2002), however, that was not the case here.

Dissolved organic carbon dynamics

The $^{15}\text{NO}_3^-$ addition alleviated the N limitation of the BMA, and as a result, BMA production increased. This increase in BMA production under diel-day conditions corresponded to a significant reversal in DOC flux. Prior to NO_3^- addition, sediments were a sink for DOC ($-0.13 \text{ mmol DOC m}^{-2} \text{ h}^{-1}$); after NO_3^- addition, sediments became a source of DOC ($1.01 \text{ mmol DOC m}^{-2} \text{ h}^{-1}$, Table 3.2). Diatoms species release between ~ 5 and 20% of the total C fixed as DOC (Wetz and Wheeler 2007) and with specific regard to benthic production, BMA can be a significant source of DOC in estuarine systems (Peterson and Howarth 1987; Pinckney and Zingmark 1993b); with epipellic diatoms identified as an important source of DOC in intertidal environments (Decho 1990; Taylor 1999; Middelburg et al. 2000). BMA-related DOC efflux can occur as simple exudation of excess production (as DOC) during times of nutrient limitation as cellular C/N ratios become unfavorable (Cook et al. 2004). In addition, motile BMA (in this case epipellic diatoms) secrete extracellular polymeric substances (EPS) (Goto et al. 1999; Underwood and Kromkamp 1999), which function in motility, adhesion, antidessication, and nutrient absorption (Hoagland et al. 1993), as well as colloidal organic carbon (colloidal-OC) which represents low molecular weight amino acids and glucose (Decho 1990). Some data suggest that up to 73% of BMA total gross primary production is excreted as DOC (Goto et al. 1999).

This EPS and exuded colloidal-OC serve as an important source of organic carbon to heterotrophic organisms (Decho and Lopez 1993; Goto et al. 1999) and bacteria have been shown to rapidly assimilate DOC released by BMA (Jensen 1984; Middelburg et al. 2000). van

Duyf et al. (1993) demonstrated a correlation between bacterial biomass and chl *a* and phaeopigment concentrations in the sediment providing intriguing evidence for a link between benthic primary production and bacterial production. However, under diel-day conditions, the DOC was not rapidly consumed as predicted by tight coupling between BMA production and bacterial consumption (Canfield and Des Marais 1993; Joye et al. 1996), but was instead released from the sediment into the water column. Decoupling of organic matter (OM) production by BMA and heterotrophic bacterial consumption of OM under diel-day conditions could possibly result from nutrient limitation of the heterotrophic bacteria.

While tight coupling between BMA production and bacterial consumption has been demonstrated (Canfield and Des Marais 1993; Joye et al. 1996) these studies did not examine such coupling under conditions of N-replete conditions. Under N-limited conditions, we observed tight coupling between daytime production and nighttime respiration, however, following N addition, production and respiration were decoupled, resulting in DOC release. Potential explanations for the observed decoupling of BMA DOC release and bacterial DOC consumption include: 1) differences in the relative growth rate of BMA and bacteria, 2) differential nutrient limitation (i.e. BMA were N limited and bacteria were limited by P or some other nutrient) and 3) competition for the added N.

The response time for different ecosystem components to changes in nutrient concentrations can play a major role in shaping the overall ecosystem response to a nutrient addition. Nitrate uptake rates following the N addition increased for both diel-day and dark treatments; diel-day N uptake rates were approximately 2 times higher than dark rates (diel-day: $-0.42 \text{ mmol NO}_3^- \text{ m}^{-2} \text{ h}^{-1}$; dark: $-0.17 \text{ mmol NO}_3^- \text{ m}^{-2} \text{ h}^{-1}$; Table 3.2). While others have shown that denitrifying bacteria are capable of rapid response to increases in NO_3^- availability (Kana et

al. 1998; Joye and Paerl 1993) it appears that the BMA also possess the ability to rapidly take up additional NO_3^- . As previously stated, some BMA possess the ability to store NO_3^- intracellularly, which may also confer an advantage over some heterotrophic bacteria (Doering et al. 1989; Sigmon and Cahoon 1997). The relative response times for BMA and bacteria could also explain a decoupling in BMA production and bacterial utilization of DOC, if the BMA response is much faster than bacteria, a decoupling between DOC production and consumption would be observed.

Differential nutrient limitation can also impact the way an ecosystem responds to increased nutrient supply. While it appears that the BMA were primarily N-limited, this same conclusion is not necessarily true of the bacterial population. In saltmarshes, the macrophytes may be N limited while the heterotrophic bacteria are DIP limited (Sundareshwar et al. 2003). The N/P ratio of the incoming nutrients can impact not only which ecosystem components can respond to the addition, but it can also impact the communities that constitute each component. An increase in DIP supply, for example, may lead to a shift in the BMA community toward cyanobacteria that are capable of N fixation (Pinckney et al. 1995); whereas an increase in both N and DIP may confer an advantage to both diatoms and cyanobacteria (Pinckney et al. 1995). If the BMA were N limited and the bacteria were P limited, the N addition would stimulate BMA production of DOC, but would not support increased bacterial consumption of DOC.

Competition for a limiting nutrient that is common to more than one ecosystem component (i.e., limiting to both BMA and bacteria) can also influence the way an ecosystem responds to an increase in nutrient supply. The role of bacteria as organic matter remineralizers has given way to a more complete view of bacteria as potential consumers of inorganic nutrients (Azam et al. 1983; van Duyl et al. 1993; Allen et al. 2001). Bacteria assimilate N from organic

and inorganic sources and may mineralize organic N and then assimilate the resulting NH_4^+ (Tupas and Koike 1990, 1991; Lomstein et al 1998). In general, higher C/N ratios of organic substrates lead to lower N regeneration by bacteria (Hollibaugh 1978), indicating that bacteria retain N under N limiting conditions. Under diel-day conditions, heterotrophic bacteria may have been out-competed by BMA for available N, which limited bacterial utilization of the BMA produced DOC. Alternatively, another nutrient (P) may have limited bacterial consumption of DOC. It is interesting to note that water column DOC uptake reversed under diel-night conditions decreased (-0.73 to $0.56 \text{ mmol DOC m}^{-2} \text{ h}^{-1}$) following the N addition, while at the same time DIC release increased (1.70 to $3.14 \text{ mmol DIC m}^{-2} \text{ h}^{-1}$, Table 3.2). This can be attributed to a decrease in the heterotrophic bacteria dependence on water column DOC following the N addition as more BMA produced DOC was available in the sediment. The increase in BMA DOC production in the sediment appeared to allow sediment heterotrophic bacteria to increase DIC production while depending less on water column DOC uptake. If the BMA out-compete the bacteria for the added N in the diel treatment, the BMA production of DOC would exceed the bacterial consumption, as the bacteria would remain N limited.

This study showed that BMA exerted strong direct and indirect influences on the fluxes of nutrients and organics. In laboratory whole core incubations, BMA controlled water column nutrient concentrations and significantly reduced the release of inorganic nutrients under light replete conditions. The addition of inorganic N to the water column stimulated BMA primary production and additionally led to a significant decrease of water column silicate. The BMA community exhibited sequential nutrient limitation with N being the primary limiting nutrient followed by silicate. While under baseline conditions there was tight coupling between organic carbon production and consumption, following NO_3^- addition, organic carbon production during

the diel-day outpaced consumption and led to DOC release from the sediments. The observed decoupling of BMA production and bacterial consumption of DOC illustrates a potentially important aspect of ecosystem response to increased nutrient loads, and could have resulted from differences in relative growth rates, differences in the limiting nutrient for BMA and bacteria, or direct competition for a common limiting nutrient. Under dark conditions, dissimilatory processes played an important role in nitrate reduction as hypothesized, however under light replete conditions, BMA out competed heterotrophic bacteria, and specifically dissimilatory nitrate reducers, for available nitrate.

ACKNOWLEDGMENTS

We thank M. Erickson, M. Price, and N. Weston for assistance in the field and in the laboratory; and I. Anderson, N. Weston, T. Hollibaugh, E. Howard, R. Jahnke and two anonymous reviewers for providing comments that substantially improved this paper. This research was supported by the National Science Foundation's Georgia Coastal Ecosystems Long Term Ecological Research Program (OCE 99-82133 and OCE 06-20959).

LITERATURE CITED

- Admiraal, W., and H. Peletier. 1980. Influence of seasonal variation of temperature and light on the growth of cultures and natural populations of intertidal diatoms. *Marine Ecology Progress Series* 2: 35-43.
- Admiraal, W., H. Peletier, and T. Brouwer. 1984. The seasonal succession patterns of diatom species on an intertidal mudflat: An experimental analysis. *Oikos* 42: 30-40.

- Admiraal, W., C. Riaux-Gobin, and R. Laane. 1987. Interactions of ammonium, nitrate, and D- and L- amino acids in the nitrogen assimilation of two species of estuarine benthic diatoms. *Marine Ecology Progress Series* 40: 267-273.
- Aleem, A. 1950. The diatom community inhabiting the mud-flats at Whitstable. *New Phytologist* 49: 174-187.
- Allen, A., M. Booth, M. Frischer, P. Verity, J. Zehr, and S. Zani. 2001. Diversity and detection of nitrate assimilation genes in marine bacteria. *Applied and Environmental Microbiology* 67: 5343-5348.
- Aller, R., and L. Benninger. 1981. Spatial and temporal patterns of dissolved ammonium, manganese and silica fluxes from bottom sediments of Long Island Sound, USA. *Journal of Marine Research* 39: 295-314.
- An, S., and W. Gardner. 2002. Dissimilatory nitrate reduction to ammonium (DNRA) as a nitrogen link, versus denitrification as a sink in a shallow estuary (Laguna Madre/Baffin Bay, Texas). *Marine Ecology Progress Series* 237: 41-50.
- An, S., and S. Joye. 2001. Enhancement of couple nitrification-denitrification by benthic photosynthesis in shallow estuarine sediments. *Limnology and Oceanography* 46: 62-74.
- Anderson, I., K. McGlathery, and A. Tyler. 2003. Microbial mediation of "reactive" nitrogen transformations in a temperate lagoon. *Marine Ecology Progress Series* 246: 73-84.
- Azam, F., T. Fenchel, J. Field, J. Gray, L. Meyer-Reil, and F. Thingstad. 1983. The ecological role of water-column microbes in the sea. *Marine Ecology Progress Series* 10: 257-263.
- Blackburn, T., and K. Henriksen. 1983. Nitrogen cycling in different types of sediments from Danish waters. *Limnology and Oceanography* 28: 477-493.

- Blanton, J., J. Amft, F. Andrade, M. Ferreira, and E. Fernandes. 2005. Exchange processes between intertidal areas and tidal creeks: The Duplin River Study. *The LTER Network News* 18: 11-12
- Cabrita, M., and V. Brotas. 2000. Seasonal variation in denitrification and dissolved nitrogen fluxes in intertidal sediments of the Tagus estuary, Portugal. *Marine Ecology Progress Series* 202: 51-65.
- Canfield, D., and D. Des Marais. 1993. Biogeochemical cycles of carbon, sulfur, and free oxygen in a microbial mat. *Geochimica et Cosmochimica Acta* 57: 3971-3984.
- Clavier, J., G. Boucher, L. Chauvaud, R. Fichez, and S. Chifflet. 2005. Benthic response to ammonium pulses in a tropical lagoon: Implications for coastal environmental processes. *Journal of Experimental Marine Biology and Ecology* 316: 231-241.
- Cline, J. 1969. Spectrophotometric determination of hydrogen sulfide in natural waters. *Limnology and Oceanography* 14: 454-458.
- Cook, P., A. Reville, E. Butler, and B. Eyre. 2004. Carbon and nitrogen cycling on intertidal mudflats of a temperate Australian estuary. II. Nitrogen cycling. *Marine Ecology Progress Series* 280: 39-54.
- Dalsgaard, T. 2003. Benthic primary production and nutrient cycling in sediments with benthic microalgae and transient accumulation of macroalgae. *Limnology and Oceanography* 48: 2138-2150.
- Darley, W., C. Montague, F. Plumley, W. Sage, and A. Psalidas 1981. Factors limiting edaphic algal biomass and productivity in a Georgia salt marsh. *Journal of Phycology* 17: 122-128.

- Decho, A. 1990. Microbial extracellular secretion in ocean environments: Their role in food webs and marine processes. *Oceanography and Marine Biology: An Annual Review* 28: 73-153.
- Decho, A., and G. Lopez. 1993. Exopolymer microenvironments of microbial flora: Multiple and interactive effects on trophic relationships. *Limnology and Oceanography* 38: 1633-1645.
- de Jonge, V., and J. van Beusekom. 1995. Wind- and tide-induced resuspension of sediment and microphytobenthos from tidal flats in the Ems estuary. *Limnology and Oceanography* 40: 766-778.
- Dizon, R., and H. Yap. 1999. Short-term responses of coral reef microphytobenthic communities to inorganic nutrient loading. *Limnology and Oceanography* 44: 1259-1267.
- Doering, P., C. Oviatt, L. Beatty, V. Banzon, R. Rice, S. Kelly, B. Sullivan, and J. Frithsen. 1989. Structure and function in a model coastal ecosystem: Silicon, the benthos, and eutrophication. *Marine Ecology Progress Series* 52: 287-299.
- Edgar, L., and J. Pickett-Heaps. 1984. Diatom locomotion, pP. 48-88. In D. Chapman and F. Round [eds.] *Progress in Phycological Research*, Volume 3. Biopress, Bristol.
- Eyre, B., S. Rysgaard, T. Dalsgaard, and P. Christensen. 2002. Comparison of isotope pairing and N₂/Ar methods for measuring sediment denitrification rates – assumptions, modifications, and implications. *Estuaries* 25: 1077-1087.
- Flint, R. and D. Kamykowski. 1984. Benthic nutrient regeneration in south Texas coastal waters. *Estuarine Coastal and Shelf Science* 18: 221-230.
- Goto, N., T. Kawamura, O. Mitamura, and H. Terai. 1999. Importance of extracellular organic carbon production in the total primary production by tidal-flat diatoms in comparison to phytoplankton. *Marine Ecology Progress Series* 190: 289-295.

- Gould, W., and G. McCready. 1982. Denitrification in several soils: Inhibition by sulfur anions. *Canadian Journal of Microbiology* 28: 334-340.
- Granéli, W., and K. Sundbäck. 1986. Can microbenthic photosynthesis influence the below-halocline oxygen conditions in the Kettegat? *Ophelia* 26: 195-206.
- Hecky, R., and P. Kilham. 1988. Nutrient limitation of phytoplankton in freshwater and marine environments: A review of recent evidence on the effects of enrichment. *Limnology and Oceanography* 33: 796-822.
- Heil, C., K. Chaston, A. Jones, P. Bird, B. Longstaff, S. Costanzo, and W. Dennison. 2004. Benthic microalgae in coral reef sediments of the southern Great Barrier Reef, Australia. *Coral Reefs* 23: 336-343.
- Hoagland, K., J. Rosowski, M. Gretz, and S. Roemer. 1993. Diatom extracellular polymeric substances: Function, fine structure, chemistry, and physiology. *Journal of Phycology* 29: 537-566.
- Hollibaugh, J. 1978. Nitrogen regeneration during the degradation of several amino acids by plankton communities collected near Halifax, Nova Scotia, Canada. *Marine Biology* 45: 191-201.
- Holmes, R., J. McClelland, D. Sigman, B. Fry, and B. Peterson. 1998. Measuring $^{15}\text{N-NH}_4^+$ in marine, estuarine, and fresh water: An adaptation of the ammonia diffusion method for samples with low ammonium concentrations. *Marine Chemistry* 60: 235-243.
- Imberger, J., T. Berman, R. Christian, E. Sherr, D. Whitney, L. Pomeroy, R. Wiegert, and W. Wiebe. 1983. The influence of water motion on the distribution and transport of materials in a salt marsh estuary. *Limnology and Oceanography* 28: 201-214.

- Jensen, L. 1984. Antimicrobial action of antibiotics on bacterial and algal carbon metabolism: On the use of antibiotics to estimate bacterial uptake of algal extracellular products (EOC). *Archiv fur Hydrobiologie* 99: 423-432.
- Joye, S. and J. Hollibaugh. 1995. Sulfide inhibition of nitrification influences nitrogen regeneration in sediments. *Science* 270: 623-625.
- Joye, S., M. Mazzotta, and J. Hollibaugh. 1996. Community metabolism in microbial mats: The occurrence of biologically-mediated iron and manganese reduction. *Estuarine Coastal and Shelf Science* 43: 747-766.
- Joye, W., and R. Lee. 2005. Benthic microbial mats: Important sources of fixed nitrogen and carbon to the Twin Cays, Belize ecosystem. *Atoll Research Bulletin* 528: 1925-1937.
- Joye, S., W. Porubsky, N. Weston, and R. Lee. 2003. Benthic microalgal production and nutrient dynamics in intertidal sediments, pp. 67-70. In J. Rullkötter [ed.] *BioGeoChemistry of Tidal Flats*, Forschungszentrum Terramare Berichte Nr. 12, Proceedings of a Workshop held at the Hanse Institute of Advanced Study, Delmenhorst, Germany, May 14-17 2003, ISSN 1432-797X.
- Kana, T., M. Sullivan, J. Cornwell, and K. Groszkowski. 1998. Denitrification in estuarine sediments determined by membrane inlet mass spectrometry. *Limnology and Oceanography* 43: 334-339.
- Kelderman, P., H. Lindeboom, and J. Klein. 1988. Effects of nutrient enrichment on microalgal community composition in a coastal shallow-water sediment system: An experimental study. *Botanica Marina* 34: 341-358.

- Krom, M. 1991. Importance of benthic productivity in controlling the flux of dissolved inorganic nitrogen through the sediment-water interface in a hypertrophic marine ecosystem. *Marine Ecology Progress Series* 78: 163-172.
- Lomstein, B., A. Jensen, J. Hansen, J. Andreasen, L. Hansen, J. Berntsen, and H. Kunzendorf. 1998. Budgets of sediment nitrogen and carbon cycling in the shallow water of Knebel Vig, Denmark. *Aquatic Microbial Ecology* 14: 69-80.
- McClelland, J., I. Valiela, and R. Michener. 1997. Nitrogen-stable isotope signatures in estuarine food webs: A record of increasing urbanization in coastal watersheds. *Limnology and Oceanography* 42: 930-937.
- McClelland, J., and I. Valiela. 1998. Linking nitrogen in estuarine producers to land-derived sources. *Limnology and Oceanography* 43: 577-585.
- McGlathery, K., K. Sundback, and I. Anderson. 2004. The importance of primary producers for benthic nitrogen and phosphorous cycling, pp: 231-262. In S. Nielsen, G. Banta, and M. Foldager [eds.] *Estuarine Nutrient Cycling: The Influence of Primary Producers*. Kluwer, Boston.
- Middelburg, J., C. Barranguet, H. Boschker, P. Herman, T. Moens, and C. Heip. 2000. The fate of intertidal microphytobenthos carbon: An in situ ¹³C-labeling study. *Limnology and Oceanography* 45: 1224-1234.
- Nielsen, L. 1992. Denitrification in sediment determined from nitrogen isotope pairing. *FEMS Microbiology Ecology* 86: 347-362.
- Nilsson, P., B. Jönsson, I. Swanberg, and K. Sundbäck. 1991. Response of a marine shallow-water sediment system to an increased load of inorganic nutrients. *Marine Ecology Progress Series* 71: 275-290.

- Paerl, H., S. Joye, and M. Fitzpatrick. Evaluation of nutrient limitation of CO₂ and N₂ fixation in marine microbial mats. *Marine Ecology Progress Series* 101: 297-306.
- Paerl, H. 1997. Coastal eutrophication and harmful algal blooms: Importance of atmospheric deposition and groundwater as “new” nitrogen and other nutrient sources. *Limnology and Oceanography* 42: 1154-1165.
- Paerl, H., J. Bales, L. Ausley, C. Buzzelli, L. Crowder, L. Eby, J. Fear, M. Go, B. Peierls, T. Richardson, and J. Ramus. 2001. Ecosystem impacts of three sequential hurricanes (Dennis, Floyd, and Irene) on the United States’ largest lagoonal estuary, Pamlico Sound, NC. *Proceedings of the National Academy of Science* 98: 5655-5660.
- Perkins, R., G. Underwood, V. Brotas, G. Snow, B. Jesus, and L. Ribeiro. 2001. Responses of microphytobenthos to light: Primary production and carbohydrate allocation over an emersion period. *Marine Ecology Progress Series* 223: 101-112.
- Peterson, B., and R. Howarth. 1987. Sulfur, carbon, and nitrogen isotopes used to trace organic matter flow in the salt-marsh estuaries of Sapelo Island, Georgia. *Limnology and Oceanography* 32: 1195-1213.
- Pinckney, J., and R. Zingmark. 1993a. Biomass and production of benthic microalgal communities in estuarine habitats. *Estuaries* 16: 887-897.
- Pinckney, J., and R. Zingmark. 1993b. Modeling the annual production of intertidal benthic microalgae in estuarine ecosystems. *Journal of Phycology* 29: 396-407.
- Pinckney, J., H. Paerl, and M. Fitzpatrick. Impacts of seasonality and nutrients on microbial mat community structure and function. *Marine Ecology Progress Series* 123: 207-216.
- Pinckney, J., H. Paerl, P. Tester, and T. Richardson. 2001. The role of nutrient loading and eutrophication in estuarine ecology. *Environmental Health Perspectives* 109: 699-706.

- Pomeroy, L. 1959. Algal productivity in salt marshes of Georgia. *Limnology and Oceanography* 4: 386-397.
- Pomeroy, L., W. Darley, E. Dunn, J. Gallagher, E. Haines, and D. Whitney. 1981. Primary production, pp. 39-67. *In* L. Pomeroy, and R. Wiegert [eds.] *The Ecology of a Salt Marsh*. Springer-Verlag, New York.
- Pomeroy, L., and J. Imberger. 1981. The physical and chemical environment, pp. 21-36. *In* L. Pomeroy, and R. Wiegert [eds.] *The Ecology of a Salt Marsh*. Springer-Verlag, New York.
- Ragueneau, O., E. De Blas Varela, P. Treguer, B. Queguiner, and Y. Del Amo. 1994. Phytoplankton dynamics in relation to the biogeochemical cycle of silicon in a coastal ecosystem of western Europe. *Marine Ecology Progress Series* 43: 63-69.
- Redfield, A. 1958. The biological control of chemical factors in the environment. *American Scientist* 46: 205-222.
- Revsbech, N., J. Sørensen, T. Blackburn, and J. Lomholt. 1980. Distribution of oxygen in marine sediments measured with microelectrodes. *Limnology and Oceanography* 25: 403-411.
- Revsbech, N., and B. Jørgensen. 1983. Photosynthesis of benthic microflora measured with high spatial resolution by the oxygen microprofile method: Capabilities and limitations of the method. *Limnology and Oceanography* 28: 749-756.
- Revsbech, N., B. Jørgensen, T. Blackburn, and Y. Cohen. 1983. Microelectrode studies of photosynthesis and O₂, H₂S and pH profiles of a microbial mat. *Limnology and Oceanography* 28: 1062-1074.
- Rysgaard, S., P. Christensen, and L. Nielsen. 1995. Seasonal variation in nitrification and denitrification in estuarine sediment colonized by benthic microalgae and bioturbating infauna. *Marine Ecology Progress Series* 126: 111-121.

- Rysgaard, S., N. Risgaard-Petersen, L. Nielsen, and N. Revsbech. 1993. Nitrification and denitrification in lake and estuarine sediments measured by the ^{15}N dilution technique and isotope pairing. *Applied and Environmental Microbiology* 59: 2093-2098.
- Sigmon, D., and L. Cahoon. 1997. Comparative effects of benthic microalgae and phytoplankton on dissolved silica fluxes. *Aquatic Microbial Ecology* 13: 275-284.
- Solorzano, L. 1969. Determination of ammonia in natural waters by the phenylhypochlorite method. *Limnology and Oceanography* 14: 799-801.
- Steward, J., R. Virnstein, M. Lasi, L. Morris, J. Miller, L. Hall, and W. Tweedale. 2006. The impacts of the 2004 hurricanes on hydrology, water quality, and seagrass in the central Indian River Lagoon, Florida. *Estuaries and Coasts*. 29(6A): 954-965.
- Strickland, J., and T. Parsons. 1972. A practical handbook of seawater analysis, 2nd ed. Bulletin of the Fisheries Research Board of Canada.
- Sundbäck, K., and W. Granéli. 1988. Influence of microphytobenthos on nutrient fluxes between sediment and water: A laboratory continuous flow study. *Marine Ecology Progress Series* 43: 63-69.
- Sundareshwar, P., J. Morris, E. Koepfler, and B. Fornwalt. 2003. Phosphorous limitation of coastal ecosystem processes. *Science* 299: 563-565.
- Taylor, I., D. Paterson, and A. Mehlert. 1999. The quantitative variability and monosaccharide composition of sediment carbohydrates associated with intertidal diatom assemblages. *Biogeochemistry* 45: 303-327.
- Thornton, D., G. Underwood, and D. Nedwell. 1999. Effect of illumination and emersion period on the exchange of ammonium across the estuarine sediment-water interface. *Marine Ecology Progress Series* 184: 11-20.

- Tiedje, J., A. Sexston, D. Myrold, and J. Robinson. 1982. Denitrification: Ecological niches, competition, and survival. *Antonie van Leeuwenhoek Journal of Microbiology* 48: 569-583.
- Tobias, C., A. Giblin, J. McClelland, J. Tucker, and B. Peterson. 2003. Sediment DIN fluxes and preferential recycling of benthic microalgal nitrogen in a shallow macrotidal estuary. *Marine Ecology Progress Series* 257: 25-36.
- Tupas, L., and I. Koike. 1990. Amino acid and ammonium utilization by heterotrophic marine bacteria grown in enriched seawater. *Limnology and Oceanography* 35: 1145-1155.
- Underwood, G., and J. Kromkamp. 1999. Primary production by phytoplankton and microphytobenthos in estuaries, pp. 93-153. In D. Nedwell, and D. Raffaelli. [eds.] *Advances in Ecological Research: Estuaries* (Vol. 29). Academic Press, New York.
- van Duyl, F., W. van Raaphorst, and A. Kop. 1993. Benthic bacterial production and nutrient sediment-water exchange in sandy North Sea sediments. *Marine Ecology Progress Series* 100: 85-95.
- Velasquez, L. 2005. Benthic primary production in coastal salt marsh systems. M.S. thesis. Univ. of Georgia.
- Veuger, B., B. Eyre, D. Maher, and J. Middelburg. 2007. Nitrogen incorporation and retention by bacteria, algae, and fauna in a subtropical intertidal sediment: An in situ ¹⁵N-labeling study. *Limnology and Oceanography* 52: 1930-1942.
- Wetz, M., and P. Wheeler. 2007. Release of dissolved organic matter by coastal diatoms. *Limnology and Oceanography* 52: 798-807.
- Williams, R. 1962. The ecology of diatom populations in a Georgia salt marsh. Ph. D. thesis. Harvard Univ.

Williams, R. 1963. The use of netting to collect motile benthic algae. *Limnology and Oceanography* 8: 360-361.

SOURCE OF UNPUBLISHED MATERIALS

Joye, S. Unpublished data. Department of Marine Sciences, The University of Georgia, Room 220 Marine Sciences Building, Athens, Georgia, 30602-3636

Table 3.1. Sediment characteristics and gross oxygenic photosynthetic rates for the East and West forks of the Duplin River. ^a and ^b are $p < 0.05$ and $p < 0.01$ respectively and indicate significantly higher values on the West Fork relative to the East Fork. Reported numbers are mean values \pm 1 standard error ($n = 3$).

Site	% Org	Chl a ^a (mg m ⁻²)	Phaeopigments (mg m ⁻²)	Chl a : Phaeo ^b (-)	Integrated
	Matter (%)				Photosynthesis (mmol O ₂ m ⁻² h ⁻¹)
East Fork 1	11.6 \pm 0.1	132.8 \pm 22.9	130.2 \pm 16.1	1.6 \pm 0.1	14.2 \pm 1.6
East Fork 2	13.1 \pm 0.6	75.9 \pm 8.0	89.7 \pm 5.1	1.5 \pm 0.1	7.3 \pm 1.2
East Fork 3	14.4 \pm 0.3	108.5 \pm 3.5	116.1 \pm 4.5	1.6 \pm 0.0	6.1 \pm 0.5
West Fork 1	9.8 \pm 0.2	105.6 \pm 8.8	88.5 \pm 4.9	1.9 \pm 0.1	6.4 \pm 0.6
West Fork 2	14.7 \pm 0.3	193.7 \pm 14.3	100.9 \pm 3.3	2.6 \pm 0.2	10.8 \pm 0.6
West Fork 3	14.9 \pm 0.1	201.2 \pm 7.0	106.3 \pm 5.5	2.6 \pm 0.1	32.9 \pm 2.6

Table 3.2. Benthic flux rates for various species from the East Fork (EF), West Fork (WF), and LF5. B and A indicate baseline and amended rates respectively; rates are in $\text{mmol m}^{-2} \text{h}^{-1}$ and reflect the mean value ($n = 3$) \pm 1 standard error.

Site	Treatment	Tracer	O ₂	DIC	DOC	NO ₃ ⁻	NH ₄ ⁺	PO ₄ ³⁻	H ₂ SiO ₄ ²⁻
EF	Diel-day	B	1.04 (0.96)	-0.21 (0.20)	0.33 (0.66)	-0.002 (0.01)	-0.021 (0.03)	0.001 (0.002)	0.07 (0.03)
	Diel-night	B	-0.88 (0.04)	1.95 (0.48)	-0.34 (0.72)	-0.002 (0.002)	-0.020 (0.02)	-0.001 (0.002)	0.05 (0.05)
WF	Diel-day	B	0.28 (0.58)	0.21 (0.27)	1.56 (1.25)	-0.008 (0.01)	0.002 (0.02)	-0.001 (0.003)	0.04 (0.03)
	Diel-night	B	-0.64 (0.11)	1.65 (0.48)	-1.58 (1.12)	-0.003 (0.003)	-0.020 (0.02)	-0.004 (0.01)	0.02 (0.03)
LF5	Diel-day	B	0.85 (0.86)	0.92 (0.37)	-0.13 (0.97)	-0.002 (0.01)	-0.003 (0.01)	0.006 (0.003)	0.10 (0.04)
	Diel-night	B	-1.44 (0.52)	1.70 (0.52)	-0.73 (1.02)	-0.01 (0.01)	-0.019 (0.02)	-0.003 (0.002)	0.06 (0.04)
	Diel-day	A	3.48 (1.28)	-3.59 (1.93)	1.01 (0.89)	-0.43 (0.12)	0.0003 (0.01)	-0.002 (0.01)	-0.42 (0.19)
	Diel-night	A	-3.08 (0.79)	3.14 (0.60)	0.56 (1.47)	0.05 (0.19)	-0.004 (0.01)	-0.005 (0.002)	-0.13 (0.06)
LF5	Dark	B	-0.43 (0.13)	1.46 (0.46)	0.12 (0.72)	-0.01 (0.003)	-0.001 (0.02)	0.013 (0.01)	0.14 (0.06)
	Dark	A	-0.16 (0.02)	1.59 (0.76)	0.36 (0.82)	-0.174 (0.08)	0.07 (0.08)	0.013 (0.02)	0.23 (0.11)

Table 3.3. Assimilatory and dissimilatory nitrate sinks from site LF5 under amended conditions. ^a and ^b denote $p < 0.05$ and $p < 0.01$ respectively and represent significant differences between diel and dark treatments, * is the average benthic microalgal NO₃⁻ uptake rate for diel-day period (i.e. not including diel-night periods). “BMA Assim.” refers to benthic microalgal assimilation, (1) and (2) designate BMA uptake calculation prior to observed nitrification and corrected for observed nitrification respectively. Rates are in mmol N m⁻² h⁻¹, numbers in parentheses are ± 1 standard error.

Treatment	Rates of NO ₃ ⁻ use				% of NO ₃ ⁻ uptake				atom % ¹⁵ N
	BMA Assim. (1)	BMA Assim. (2)	D ₁₅ ^a	DNRA ^b	BMA(1)	BMA(2)	DNF ^a	DNRA ^b	BMA ^b
Diel	0.522*	0.625*	0.013	0.001	83.40	141.64	2.07	0.16	16.5
	(0.012)	(0.231)	(0.012)	(0.001)					(0.4)
Dark	N/A	N/A	0.113	0.003	N/A	N/A	40.5	1.2	2.6
			(0.023)	(0.004)					(2.5)

FIGURE LEGENDS

Figure 3.1. Sampling locations on the Duplin River, Sapelo Island, Georgia.

Figure 3.2A-C. Oxygen and GOP rates vs. depth profiles, (A) $0 \text{ mol photons m}^{-2} \text{ s}^{-1}$, (B) $1 \times 10^{-3} \text{ mol photons m}^{-2} \text{ s}^{-1}$, (C) $2 \times 10^{-3} \text{ mol photons m}^{-2} \text{ s}^{-1}$. The sediment water interface is indicated as a dashed horizontal line. Core A and core B are replicate cores from the East fork. Like symbols are replicates from the same core. Lines represent average GOP rates for each core ($n = 2$).

Figure 3.3A-F. Concentration vs. time for benthic flux core incubations. For diel treatments, open symbols indicate the previous time period was illuminated (diel-day), closed symbols indicate the previous time period was dark (diel-night). Error bars represent ± 1 standard error. For incubations from site LF5 the NO_3^- addition is indicated by a vertical line.

Figure 3.4. Denitrification rates and the percentage of denitrification coupled to nitrification for incubations from site LF5. Error bars represent ± 1 standard error. * $p < 0.05$.

Figure 3.5. The potential impact of BMA uptake under nitrogen replete conditions on water column NO_3^- and $\text{H}_2\text{SiO}_4^{2-}$ pools for both neap low tide and spring high tide.

Figure 3.2A-C.

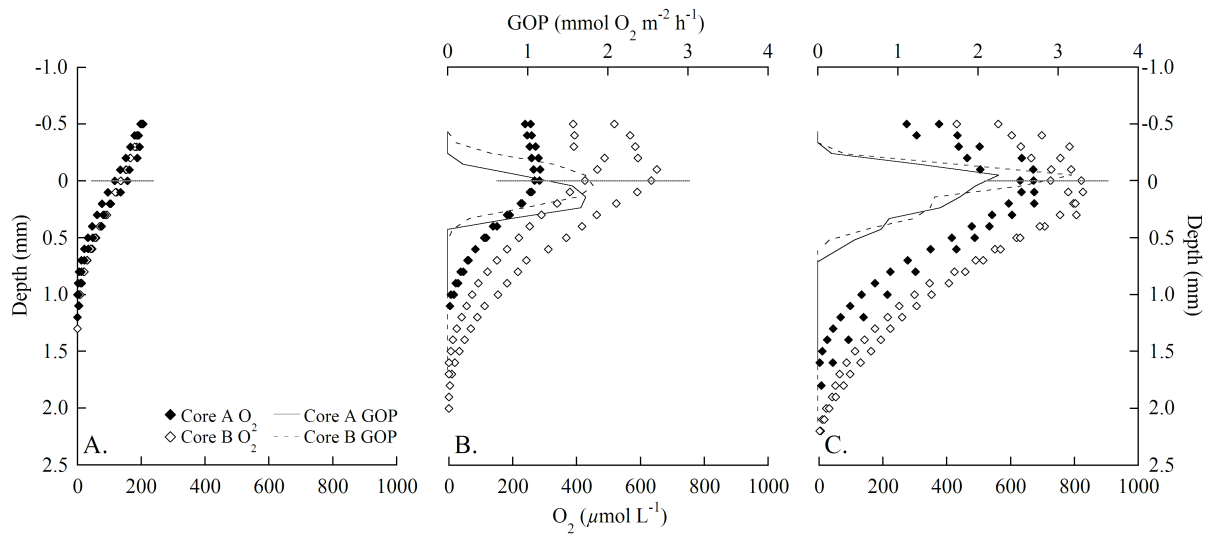


Figure 3.3A-F.

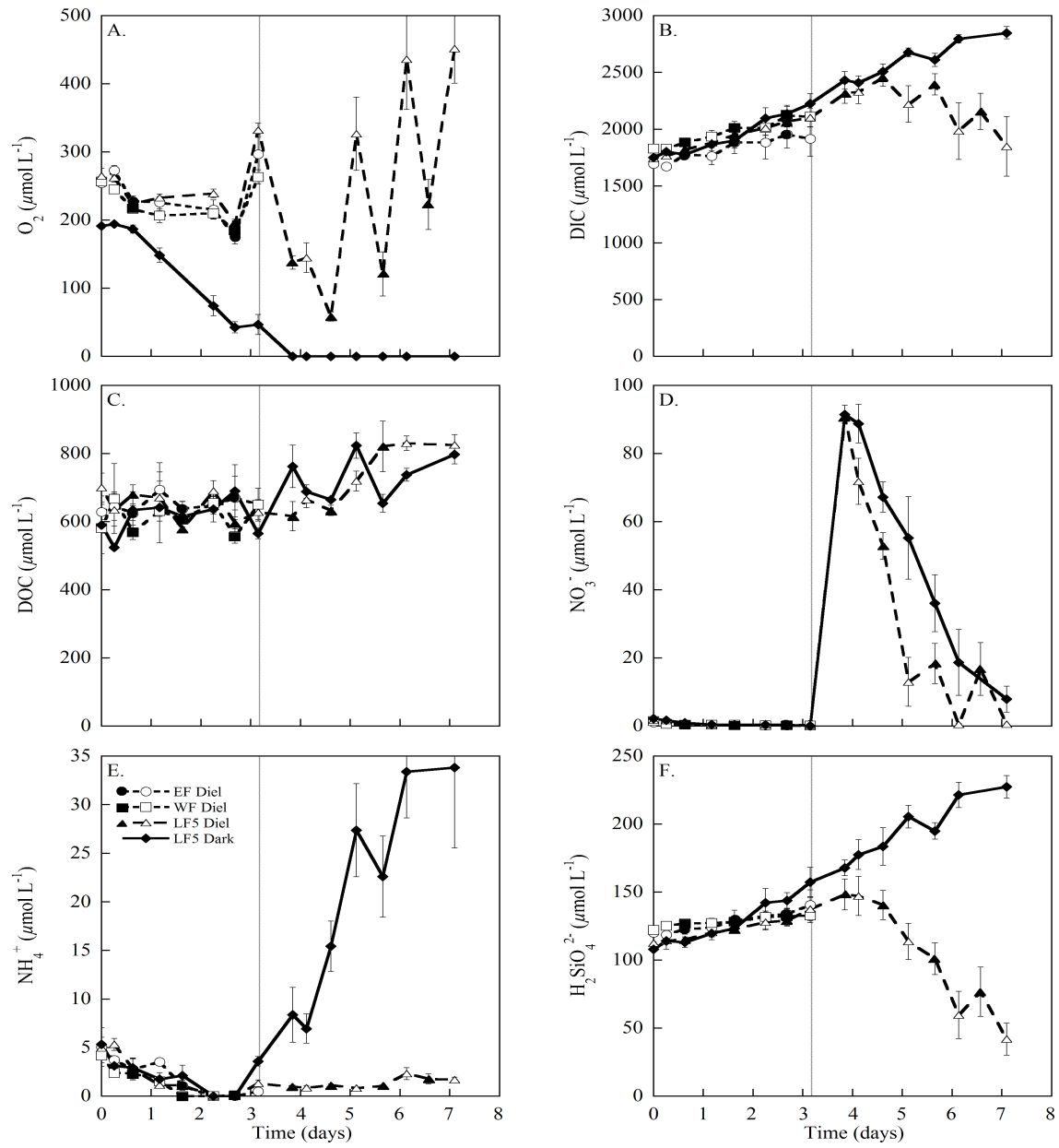


Figure 3.4.

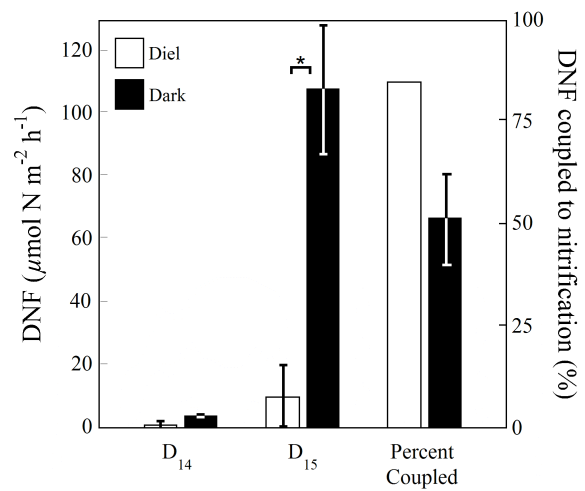
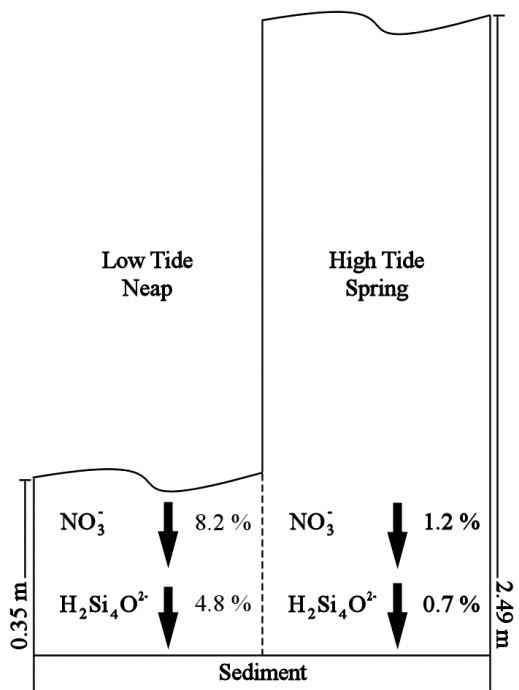


Figure 3.5.



CHAPTER 4

GROUNDWATER AS A POTENTIAL SOURCE OF NUTRIENTS AND DISSOLVED ORGANIC MATTER TO THE OKATEE RIVER ESTUARY, SOUTH CAROLINA¹

¹Porubsky, W., W. Moore, N. Weston, C. Ruppel, and S. Joye. To be submitted to *Limnology and Oceanography*.

ABSTRACT

Thermal infrared (TIR) aerial remote sensing, geochemical characterization and radium isotopes were used to evaluate the role of groundwater as a source of nutrients and organics to the Okatee River estuary, South Carolina (USA). Benthic flux measurements and potential denitrification (pDNF) rate assays tracked the fate of constituents in sediments. TIR surveys confirmed the presence of multiple groundwater discharge sites with high seep densities in Okatee headwaters. Geochemical data indicated significant differences in groundwater chemical composition between the eastern and western sides of the river and radium activity ratios indicated distinct hydrological regimes between these two areas. Groundwater from the western side of the Okatee was characterized by higher concentration of dissolved organic (DOC) and inorganic carbon (DIC), dissolved organic nitrogen (DON), nutrients (i.e., NH_4^+ , PO_4^{3-}) and reduced metabolites (H_2S and CH_4). On the eastern side, groundwater was characterized by higher dissolved oxygen concentration and lower concentrations of DOC, DIC, DON, nutrients and reduced metabolites. Spatial variations in microbially mediated processes (i.e., sulfate reduction), DOC distribution, and/or groundwater residence time contributed to this pattern. Geochemical data, ^{226}Ra activity and radium loading rates illustrated a substantial groundwater contribution of organics, DIC, nutrients, methane and nitrous oxide to the Okatee. Benthic fluxes were significantly lower than radium based inputs, showing that advection of groundwater-derived nutrients dominated fluxes in the system. While pDNF rates could remove a significant portion of the groundwater associated DIN load, in situ DNF rates were much lower thus limiting the impact of DNF.

INTRODUCTION

Coastal regions represent a dynamic interface between the land and the sea, a mixing zone for fresh and oceanic waters. Nutrients and organic materials supplied to coastal ecosystems are derived from both terrestrial and oceanic sources. Of the terrestrial input terms, some, e.g., river inputs, are reasonably well constrained (Cotrim da Cunha et al. 2007). Other sources, such as submarine groundwater discharge (SGD) or atmospheric inputs are poorly constrained both in terms of quantity and bioavailability (Paerl 1997; Burnett et al. 2003). SGD includes fresh groundwater and recirculated seawater and thus covers the flux of typically saline groundwater to coastal waters (Burnett et al. 2003; Moore 2003; Moore et al. 2006). Here we use the term groundwater to include this mixture of fresh groundwater and recirculated seawater. Shallow groundwater is recognized as a dynamic and potentially important source of nutrients to coastal waters (Giblin and Gaines 1990; Kroeger and Charette 2008). Despite significant methodological advances (summarized in Burnett et al. 2003) quantifying groundwater inputs to coastal waters remains a challenge. As a result, they are often the least constrained component of coastal nutrient and carbon budgets (Moore et al. 2006; Burnett et al. 2003).

The four isotopes of radium (^{223}Ra , ^{224}Ra , ^{226}Ra and ^{228}Ra) offer an effective way to track groundwater input (Moore 1996; Rama and Moore 1996). Fluxes of radium (Ra) in a system arise from (1) surface water inflow, (2) sedimentary Ra release and (3) groundwater discharge. By measuring the first two components and estimating surface water residence time, the Ra flux due to groundwater discharge can be constrained. Measuring the Ra isotopic composition and activity in groundwater reveals the volume of groundwater required to support the inferred groundwater-derived Ra flux. Contemporaneous measurement of groundwater constituent concentration permits the estimation of groundwater-derived fluxes. The results of these

geochemical analyses, coupled with similar analyses of surface waters, can be incorporated into simple mixing models to constrain the relative contribution of seawater, rainwater, surficial groundwater, and deep, chemically distinct groundwater to the nutrient budget (Moore et al. 2006).

Though groundwater only accounts for ~6-10% of surface water inputs to coastal waters globally (Burnett et al. 2003; Moore et al. 2008), the nutrient load associated with groundwater inputs may rival riverine inputs because groundwater nutrient concentrations often exceed those in surface water (Moore et al. 2006; Kroeger et al. 2007; Swarzenski et al. 2007). Groundwater originating from developed watersheds often contains even higher concentrations of nutrients and organic matter (LaPointe et al. 1990; Cole et al. 2006). Inputs of nutrient enriched groundwater to coastal receiving waters can alter the rates and types of primary producers that dominate the system (e.g., phytoplankton, seagrass versus macroalgae) (Valiela et al. 1990; Gobler and Sañudo-Wilhemly 2001; Gobler and Boneillo 2003).

We investigated the importance of groundwater-derived inputs to the Okatee River estuary, a coastal ecosystem in South Carolina, United States of America. Thermal infrared remote imaging surveys were used to identify areas of groundwater input. We sampled groundwater from monitoring wells and surface waters within the Okatee estuary to develop a radium budget for the system. We quantified the relationship between the concentrations of dissolved organic carbon (DOC), nutrients, redox metabolites, trace gases and dissolved radium isotopes in shallow groundwater and used these data to develop radium vs. constituent regressions. Using these regressions in conjunction with system-scale radium concentration data, we obtained groundwater derived loading rates of materials to the Okatee. Finally, we measured potential denitrification (pDNF) in sediment slurries to evaluate the ability of Okatee sediments

to remove nitrate and benthic fluxes of nutrients, redox metabolites and organic carbon to compare the importance of diffusive benthic flux as a source for nutrients to the estuary. The data show that groundwater is an important source of nutrients and organic matter to the Okatee estuary.

METHODS

Study Site

The Okatee River (32.34° N, 80.89° W) is a tributary of the Colleton River, which flows into Port Royal Sound on the South Carolina (SC) coast (Fig. 4.1A-F). The Okatee is a small, shallow river surrounded by an extensive *Spartina alterniflora* marsh. *Salicornia* and *Juncus* are found in saltpans and near the upland boundary, respectively. The annual range of temperature, tidal amplitude and salinity are 10-30°C, ~2 m, and 0 to 30, respectively. The population of Beaufort County, home to the Okatee, is one of the fastest growing in SC: the county population increased by roughly 40% from 1990-2000 (<http://www.npg.org/states/sc.htm>). Additional development within the Okatee watershed is expected (Windom et al. 1998) and this development will impact the quality of surface and groundwater in the future.

Remote Sensing

Thermal infrared (TIR) aerial remote sensing surveys were conducted in August 2001 to identify the location and type (e.g., surface, bank or sub-marsh flows) of groundwater inputs. The timing of the surveys was selected to take advantage of the maximum seasonal temperature difference between warm surface water and colder groundwater. The TIR imaging takes advantage of the fact that groundwater temperature is similar over seasons, while surface water

temperature increases significantly during summer. These thermal differences permit visualization of sites where cold groundwater (white/bright areas, Fig. 4.1B-E) discharges into warm surface waters (black areas; Portnoy et al. 1998). The surveys generated a GIS referenced data set of the loci of actively discharging groundwater (Fig. 4.1A-E).

Monitoring wells

Using the TIR data as a guide, two groundwater monitoring well transects were installed in the spring of 2002 (Fig. 4.1F). Upland wells (MW11 and MW12) were installed in the spring of 2003 and the later installation date is reflected in the fewer number of monitoring samples collected (*n* values in Tables 4.1, 4.2, and 4.3). Conventional monitoring wells were vibra-cored in through 4" PVC casing (Schultz and Ruppel 2002). The wells were constructed of 2" Schedule 40 PVC with machine-slotted screens located fully within the saturated zone. A coarse sand filter pack was installed adjacent to the screen to prevent fine sediment particles from fouling the well. Following installation, wells were developed by pumping until the water was clear. For upland wells, a small (30 cm square) cement pad ~10 cm thick was installed to prevent annular flow, and bolted flush caps were used for wellhead protection. For marsh wells, near-surface annular sealants that hydrate properly in saline settings were used, and the wellhead was positioned above the spring high tide line to prevent flooding.

Monitoring wells were sampled quarterly (i.e., spring, summer, fall, winter) at low tide from the spring of 2002 through the winter of 2005. During the first year (2002) wells were sampled twice each quarter (i.e., 8 times per year). Monitoring wells (screened depth: ~1 - 2.5 m) were sampled using standard methods, i.e., one well volume was purged using a battery-powered peristaltic pump and then samples were collected and processed. Two samples were immediately

collected for quantification of dissolved gases. The first sample, for Ar:N₂ analysis, was collected into glass vials ($n = 3$) that were over-filled with groundwater and fixed with ZnCl₂; vials were sealed with a ground glass stopper and stored at field temperature prior to analysis at the UGA laboratory. The second sample (2 mL) was injected into a He-purged, crimp-sealed 14 mL headspace vial which was acidified (0.1 mL conc. H₃PO₄) for determination of N₂O, CH₄ and CO₂ concentration. An additional sample (~200 mL) was collected into a He-purged bottle to minimize oxidation of reduced species and filtered (0.2 μm), fixed (in the field) as noted below, and stored prior to analysis. Creek water samples (~0.5 m depth) were obtained from the Okatee near the bridge along highway 278 (Fig. 4.1A).

Temperature, pH and dissolved oxygen concentration was determined immediately on surface and groundwater samples using an Orion[®] high precision temperature-pH meter and a galvanic oxygen (O₂) sensor (Model 842). A variety of dissolved parameters were quantified to characterize the geochemical signature of the groundwater samples. Dissolved nutrient samples were filtered (0.2 μm) and stored (4°C) prior to analysis (within days to a week). Concentrations of NO_x (= NO₃⁻ + NO₂⁻) and PO₄³⁻ (dissolved inorganic phosphorous, DIP) were determined at the UGA lab using standard protocols on a Lachat autoanalyzer (QuikChem[®] 8000). Ammonium (NH₄⁺) samples were immediately fixed with phenol and concentrations were quantified using the phenol-hypochlorite technique (Soloranzo 1969) as soon as possible (usually within 1-2 days). Samples containing H₂S were diluted to remove analytical interference (Joye et al. 1996).

Samples for the determination of dissolved organic matter were fixed with phosphoric acid (50 μL conc. H₃PO₄ per mL sample). High temperature catalytic combustion and quantification as nitric oxide was used to determine total dissolved nitrogen (TDN) concentration; dissolved organic nitrogen (DON) concentrations were estimated by difference

(TDN – dissolved inorganic nitrogen (DIN) = DON where $\text{DIN} = \text{NO}_x + \text{NH}_4^+$; Álvarez-Salgado and Miller 1998). Dissolved organic carbon (DOC) (high temperature catalytic combustion; Peltzer and Brewer 1993) and dissolved inorganic carbon (DIC) (acidification and infrared detection; Aug. 2002 and after) concentrations were determined using a Shimadzu TOC5000[®] (Bouillon et al. 2003). Prior to August 2002, DIC was determined as CO_2 concentration using gas chromatography (see below). Sulfate (SO_4^{2-}) and chloride (Cl^-) concentrations were determined on acidified (50 μL conc. trace metal grade HNO_3 per mL of sample) sub-samples using ion chromatography (Joye et al. 2004). Total dissolved phosphorous (TDP) concentrations were determined by evaporation, ashing, and acid hydrolysis followed by quantification as DIP; dissolved organic phosphorous (DOP) was estimated by difference ($\text{DOP} = \text{TDP} - \text{DIP}$; Monaghan and Ruttenberg 1999). The concentration of dissolved gases was determined by membrane inlet mass spectrometry (MIMS) for N_2 and Ar (Kana et al. 1998) and gas chromatography for N_2O (Joye and Paerl 1994) and CH_4 and CO_2 (Joye et al. 2004). Concentrations of hydrogen sulfide (H_2S ; Cline 1969) and dissolved reduced iron (Fe^{2+} ; Stookey 1979) were determined using colorimetric techniques (Joye et al. 1996).

Radium quantification

Radium isotopes were collected by pumping a known volume of surface water (~25 L) or groundwater (1-4 L) through a pre-filter (2.5 mm glass fiber) and then through a column of MnO_2 -coated acrylic fiber at a rate of $< 1 \text{ L min}^{-1}$ (Moore 1976). Short-lived Ra isotopes (^{223}Ra and ^{224}Ra , half-lives of 11.3 and 3.66 days respectively, Moore 2003) were quantified using delayed-coincidence measurement of their radon daughters (error = 10%; Moore and Arnold 1996). Long-lived Ra isotopes (^{226}Ra and ^{228}Ra , half-lives of 1600 and 5.7 years respectively,

Moore 2003) were determined subsequently using gamma ray spectrometry (error = 7%; Moore 1984). Other Ra sources were evaluated to develop a Ra budget for the system (see Moore et al. 2006 for further details).

Benthic fluxes and sediment denitrification

Benthic fluxes were determined at four sites within the Okatee watershed (Fig. 4.1A) between June 2001 and January 2004. Site t1, located near the freshwater endmember of the Okatee, experiences salinities between 0 and 20. Site 278 lies near the highway US-278 bridge and experiences salinities between 10 and 30. The salinity at Grave's Dock site (GD) is near that of seawater. The fourth site, Pooh Bridge (PB), is on a Malind Creek, a tidal creek that feeds into the Okatee River and has a salinity range similar to site t1 (Weston et al. 2006). Benthic fluxes were determined in flow-through incubations of sediment cores ($n = 2-3$) under simulated diel cycles (Porubsky et al. Chapter 3). Sediment was collected from macrophyte-free creek banks in clear polycarbonate core tubes at low tide and was transported to the UGA lab for incubation (details given in Porubsky et al. Chapter 2).

Additional sediment cores were collected in April and June 2001 (see Fig. 4.1A) to determine rates of potential denitrification (pDNF) using the acetylene (C_2H_2) block technique (Joye and Paerl 1994). Cores were extruded in the laboratory and sub-samples (~3 grams wet sediment, $n = 3$ per depth) were collected at 1 to 5 cm intervals for use in pDNF assays. Sediment was slurried with 15 mL of 0.2 μm filtered, He-purged surface water, amended with NO_3^- and glucose (1 and 2 mmol L^{-1} , respectively), injected with C_2H_2 (10% of bottle volume), and incubated in the dark for 3-5 hours at in situ temperature. Following incubation, a head-

space sample was collected and stored in a He-purged gas tight vial for N₂O analysis (as described above). Rates were time zero corrected and normalized per gram wet sediment (gws⁻¹).

RESULTS

Remote Sensing

The TIR survey illustrated numerous and significant surface and sub-marsh groundwater seeps throughout the Okatee estuary (Fig. 4.1A-E). Approximately 55 sites of groundwater seepage were identified using TIR (Fig. 4.1A); with a higher seep density (~80%) in the upper reaches of the Okatee. System wide, the seeps occurred in approximately equal numbers on the eastern (27) and western (28) sides of the Okatee but in the upper reaches of the Okatee ~60% of the seeps were observed on the western side (Fig. 4.1A).

Groundwater and surface water geochemistry

Surface water collected from the Okatee at the 278 bridge had an average salinity of 10.3, was relatively high in dissolved O₂ (206.3 μmol L⁻¹), had a Cl⁻/SO₄²⁻ ratio (18.92) comparable to seawater (Table 4.1, Pilson 1998), and a dissolved N₂ concentration slightly above equilibrium with the atmosphere (102% saturation, Table 4.3). The Okatee surface water had high concentrations of DIC, DOC, and DON, but low concentrations of DIN and a DIN/DIP below the Redfield N/P of 16:1 (Table 4.2, Redfield 1958).

Due to the similarities in the geochemistry of the upland wells (MW11 and MW12), data from the two wells were averaged (Tables 4.1, 4.2 and 4.3). The upland groundwater had a salinity of 14.2 indicating a contribution of recirculated saline water in the upland aquifer adjacent to the marsh (Table 4.1). Upland groundwater was characterized by extremely low pH,

low dissolved O₂ concentration (71.3 μmol L⁻¹), and high concentrations of dissolved Fe²⁺, DOC, and reduced nitrogen (i.e., NH₄⁺ and DON, Tables 4.1, 4.2 and 4.3). Concentrations of DIP were low, generating a DIN/DIP ratio that was approximately 6 times the Redfield N/P (Table 4.2).

Significant differences in groundwater geochemistry were apparent between the eastern and western sides of the Okatee. The eastern groundwater was characterized by significantly higher salinity ($p < 0.0001$), dissolved O₂ ($p < 0.01$) and reduced iron ($p < 0.05$) concentration and significantly lower H₂S ($p < 0.0001$; Tables 4.1 and 4.3) concentration relative to the western groundwater. The Cl⁻/SO₄²⁻ ratio for eastern groundwater was comparable to seawater, while the Cl⁻/SO₄²⁻ ratio in western groundwater was significantly ($p < 0.0001$) higher than both the eastern groundwater and seawater, indicating a depletion of SO₄²⁻. The greatest depletion was present in well MW05 (Table 4.1 and Fig. 4.3A). Both eastern and western groundwater was significantly elevated in DIC relative to the Okatee ($p < 0.0001$; Table 4.2). The DIC ($p < 0.0001$, Table 4.2) and DOC ($p < 0.0001$, Table 4.2 and Fig. 4.2A) concentrations in western groundwater were significantly higher than in eastern groundwater. Linear regression of all groundwater DOC and DIC concentrations revealed a strong correlation, suggesting they derive from the same source (Fig. 4.3B). DOC was positively correlated to salinity in the western wells, but there was no significant trend in the relationship between DOC and salinity in the upland or eastern groundwater (Fig. 4.2A). The highest DIN concentrations (mainly NH₄⁺) occurred in western groundwater ($p < 0.0001$), with NH₄⁺ concentrations approximately 28 times higher than the Okatee (Table 4.2). DIN and DIP, like DOC, showed no significant relationship to salinity (Fig. 4.2B and C). DON and DIP concentrations showed a similar pattern with highest concentrations present in the western groundwater ($p < 0.01$ and $p < 0.0001$ for DON and DIP respectively; Table 4.2; Fig. 4.2C). The DIN/DIP ratio for both the eastern and western

groundwater was below the Redfield N/P (Table 4.2). Though the mean DIN concentration in western groundwater was 7 times that in eastern groundwater, the DIN/DIP ratio in western groundwater was lower due to higher DIP concentrations (Table. 4.2).

Groundwater from the western side of the Okatee had H₂S concentrations that were ~65 times higher than the eastern groundwater ($p < 0.0001$, Table 4.3). Groundwater from the western side also had generally higher concentrations of dissolved CH₄, although the difference was not significant ($p > 0.05$, Table 4.3). N₂O concentrations (20 to 250 nmol L⁻¹) and N₂ concentrations and % saturation were similar on both sides of the Okatee (Table 4.3).

Radium and nutrient loading relationships

The average ²²⁶Ra activity for the upland groundwater was significantly ($p < 0.01$) higher than the activity from the eastern side but not the western side ($p > 0.05$) of the Okatee (Table 4.1). The average ²²⁸Ra activity for the upland groundwater was significantly ($p < 0.001$) higher than both the eastern and western sides of the Okatee. Groundwater collected from the eastern side of the Okatee had significantly ($p < 0.0001$) lower ²²⁶Ra activities than groundwater collected from the western side (1.58 vs. 3.85 dpm L⁻¹, Table 4.2; Moore et al. 2006). While there were no significant ($p > 0.05$) differences in the ²²⁸Ra activity between the eastern and western groundwater, the significantly ($p < 0.0001$) lower ²²⁶Ra activities in the eastern groundwater resulted in a significantly ($p < 0.0001$) higher average ²²⁸Ra/²²⁶Ra activity ratio (7.67 ± 0.46 eastern vs. 2.73 ± 0.09 western; Moore et al. 2006). The ²²⁸Ra/²²⁶Ra activity ratio for the upland groundwater was not significantly different ($p > 0.05$) from the ²²⁸Ra/²²⁶Ra activity ratio of either the eastern or western groundwater. Significant relationships were observed between geochemical constituents and ²²⁶Ra in groundwater (Fig. 4.4A-F). Higher

^{226}Ra activity correlated with higher concentrations of DOC, DIC, DON, NH_4^+ (DIN), DIP, H_2S , CH_4 and N_2O ; linear regressions between ^{226}Ra and these constituents were used to estimate their groundwater derived flux (Table 4.4).

The daily flux of ^{226}Ra ($3.43 \times 10^8 \text{ dpm d}^{-1}$, Table 4.4) was estimated from the average flux of ^{224}Ra ($1.28 \times 10^9 \text{ dpm d}^{-1}$, Moore et al. 2006) and the measured ratio of $^{224}\text{Ra}/^{226}\text{Ra}$ averaged for all marsh groundwater (3.75, data not shown). This flux was used in conjunction with the linear relationships of ^{226}Ra activity and constituent concentration (Fig. 4.4A-F) to estimate daily fluxes. Constituent fluxes were comparable to those reported in Moore et al. (2006); however, differences arise because the fluxes reported here consider the groundwater parameter concentrations for both the eastern and western sides of the Okatee (Moore et al. 2006 only considered the western side). This discrepancy is most apparent in the DIN and DIP fluxes and the resulting DIN/DIP ratio of 12.80 (compared to 4.8 reported in Moore et al. 2006). The ^{226}Ra -derived fluxes indicate that the groundwater was greater source of DIN than DON (Table 4.4). Groundwater was also a significant source of dissolved gases with a daily flux of ~ 1290 mol CH_4 and 10 mol of N_2O (Table 4.4).

Benthic processes (fluxes and pDNF)

Diffusive benthic fluxes were measured in sediment flow-through core incubations on 4 occasions (Table 4.5). There were no significant seasonal or spatial trends in benthic fluxes. Using the hypsometric curve developed for the Okatee (Blanton et al. 2006) to estimate the area of intertidal, creek-bank sediment ($2 \times 10^5 \text{ m}^2$, taken as the point where the greatest slope of the water level relative to mean low water vs. the water surface area curve (Moore et al. 2006) ends as representative of bank-full), we calculated an integrated flux of nutrients for day and night

periods as well as a net daily flux (day flux + night flux, Table 4.5). Given that the sediments were intertidal, the period of inundation was estimated at 12.4 hours a day (i.e., 6.2 hrs of day submerged and 6.2 hrs of night submerged) and thus the integrated fluxes account for submerged periods only. Integrated DIC fluxes during the day exceeded release during the night, resulting in a negative net daily DIC flux, indicating autotrophic sediments (Table 4.5). The sediments were a net sink for DIN and a net source of organics (DOC and DON) to the Okatee.

Potential DNF rates, determined at sites GD, 278 and t1, decreased with depth. The range of pDNF rates was 0-110 nmol N gws⁻¹ h⁻¹. The average pDNF for all three sites at a depth of 1.5 cm was 38.60 nmol N gws⁻¹ h⁻¹. Using measured sediment density and porosity, and rates from the upper 3.5 cm, an integrated pDNF rate of 7.72 mmol N m⁻² d⁻¹ was obtained. This rate was used in conjunction with the tidal prism area (7.13 x 10⁵ m²) determined by Blanton et al. (2006) as an estimate of the area of active pDNF and yielded a system wide pDNF rate of 5.51 x 10³ mol N d⁻¹. A more conservative estimate confining DNF to the estimated creek-bank area (2 x 10⁵ m²), yields a pDNF rate of 1.54 x 10³ mol N d⁻¹. The tidal prism area DNF estimate represents ~20% of the estimated groundwater derived DIN flux (Table 4.4), while the creek-bank estimate was approximately 3.5 times lower.

DISCUSSION

Mapping locations of SGD

Thermal infrared imaging offers an effective way to identify locations of SGD (Banks et al. 1996; Portnoy et al. 1998; Johnson et al. 2008). The technique depends on temperature differences between groundwater and surface waters and is thus limited to periods when these temperature differences are large enough to distinguish the two water types. TIR can be used as a

powerful tool for mapping SGD sites over large areas in short periods of time. Combining TIR with other techniques for quantifying SGD (such as radium isotopes) increases the utility of the technique by identifying locations of high groundwater input.

TIR results indicated a higher incidence of groundwater seeps in the upper reaches of the Okatee. Approximately 80% of the seeps observed in August 2001 were found in the upper reaches of the Okatee during summer months when SGD is highest (Moore et al. 2006). The active seeps in the upper reaches during August 2001 underscored the importance of characterizing groundwater geochemistry in the upper reaches of the system in order to estimate system wide groundwater-derived inputs. There were no significant differences in seep abundance between the eastern and western sides of the Okatee; however, in the upper reaches approximately 60% of the documented seeps were on the western side. This finding suggests that the western side of the marsh may be a site of greater SGD than the eastern side.

Radium isotopes and hydrology

The radium activities observed in the eastern and western wells can be used to distinguish hydrologic differences between the respective sides of the Okatee. The two radium isotopes, ^{226}Ra and ^{228}Ra , have distinct half-lives of 1600 and 5.7 years, respectively (Moore 2003). They are continually produced from their long-lived parents, ^{232}Th and ^{230}Th . In order to sustain a high dissolved $^{228}\text{Ra}/^{226}\text{Ra}$ activity ratio, the aquifer must be frequently flushed to regenerate the shorter-lived ^{228}Ra (e.g., Moore 2003). Thus, a relatively high dissolved $^{228}\text{Ra}/^{226}\text{Ra}$ activity ratio is indicative of greater flushing. The $^{228}\text{Ra}/^{226}\text{Ra}$ activity ratio was significantly ($p < 0.0001$) higher in the eastern wells than the western wells, indicating that the aquifer on the eastern side was flushed more frequently than the western side. This result contradicts the findings of the TIR

survey of groundwater seeps which indicated ~60% of the seeps in the upper reaches were on the western side of the Okatee. The radium derived evidence for higher flushing of the eastern side is supported by higher O_2 and NO_3^- concentrations and lower concentrations of reduced metabolites (i.e., H_2S and NH_4^+ , Tables 4.2 and 4.3). The higher NO_3^- concentrations observed in the eastern groundwater may have resulted from increased nitrification activity due to the higher supply of O_2 to the eastern side of the marsh (Tobias et al. 2001a; Smith et al. 2006). Conversely, lower incidence of flushing in the aquifer on the western side, and consequently longer groundwater residence times, may promote microbial processes (i.e., SR and DNF) due to increased contact time with substrates (Harvey and Odum 1990; Capone and Slater 1990; Joye and Paerl 1993). Though the $^{228}Ra/^{226}Ra$ activity ratio for the upland wells was not significantly ($p > 0.05$) different from the eastern and western groundwater, the average activities for both ^{228}Ra and ^{226}Ra were higher in the upland groundwater. The higher ^{226}Ra activity suggests that the upland is not a site of frequent flushing; however this observation is contradicted by the contemporaneously high ^{228}Ra activity. One possible explanation is that the upland is a site where the location of the freshwater-saltwater interface can shift resulting in a high rate of radium regeneration with low rates of export.

Groundwater geochemistry

Variability in groundwater derived nutrient inputs result from temporal differences in groundwater nutrient concentrations and advection rates and differences in the loci of groundwater seepage. Only three parameters showed any significant ($p < 0.05$) seasonal variations in the Okatee groundwater: 1) temperature, 2) groundwater from the western side was significantly higher in NO_x^- during winter, and 3) groundwater from the eastern side was

significantly ($p < 0.05$) higher in PO_4^{3-} during summer. Given the small seasonal variations in the groundwater physical/chemical signature, any seasonal differences in groundwater-derived nutrient inputs must result from variations in the flow (i.e., discharge rates) or origin (i.e., eastern vs. western groundwater) of groundwater inputs. Significantly higher nutrient fluxes were reported for the Okatee during summer due to higher discharge rates (Moore et al. 2006).

Spatial variability in groundwater geochemistry was evaluated by contrasting the geochemical signature across sites within the Okatee system. The southern (MW11, MW05, and MW04) and northern (MW12, MW06, MW07, MW08, and MW09) upland to marsh well transects on the western side of the Okatee show a similar geochemical progression from the upland to the marsh. Both upland wells were characterized by extremely low pH and high dissolved reduced Fe^{2+} (Tables 4.1 and 4.3). This combination of acidic conditions and high Fe^{2+} suggests oxidative weathering of iron sulfide rich soils (Giblin and Howarth 1984; Portnoy and Giblin 1997; Hussein and Rabenhorst 1999); however, the high SO_4^{2-} concentration that would result from the oxidative weathering was absent in the upland groundwater (Table 4.1). DIC concentrations were typically lowest in the upland wells, peaked with the highest DIC concentrations found in the mid-marsh groundwater wells (24.45 ± 1.48 and 21.68 ± 1.18 mmol L^{-1} for MW05 and MW06 respectively) and then decreased further from the upland. This groundwater also had the highest DOC concentrations. DIC was linearly related to DOC throughout the Okatee (Fig. 4.3B) indicating that high DIC and DOC concentrations likely from a common source (particulate organic carbon, POC) within the marsh. The large increase in DIC and DOC in the transition from the upland to the marsh indicates that the upland groundwater is not a significant source of DIC or DOC to the marsh groundwater and that cycling of organic matter within the marsh drives the geochemical signature of the groundwater. The high mid-

marsh concentrations of organic and inorganic carbon suggest the dominant source of carbon is also in the mid-marsh, and could reflect the input of marsh grasses, high-tide deposited organic matter, and lower export of carbon from the area.

Further evidence for the role of the marsh in controlling the geochemical signature of the groundwater is evident in the evolution of the upland groundwater chemical signature as it moves through the marsh prior to discharging to the Okatee. Upland groundwater was low in DOC, NO_3^- , and PO_4^{3-} but enriched in NH_4^+ relative to surface water collected from the Okatee (Tables 4.1 and 4.2). Groundwater from the western side of the Okatee had significantly higher concentrations of DIC, DOC, NH_4^+ , DON, PO_4^{3-} , H_2S , CH_4 , and N_2O ($p < 0.0001$ to $p < 0.01$; Tables 4.2 and 4.3) than the upland groundwater flowing into the marsh. The increase in nutrients, dissolved organics, and dissolved gases demonstrates that significant alteration of the groundwater geochemical signature occurs during marsh transit. Estimating groundwater nutrient inputs based on the geochemical composition of the upland groundwater would result in ~2-fold underestimate of organics (DON and DOC) fluxes and a 10, 50 or 100-fold, respectively, underestimation of NH_4^+ , PO_4^{3-} , or DIC fluxes.

There were stark differences between the groundwater geochemistry of the western marsh and the eastern marsh (Tables 4.1, 4.2, and 4.3). The high DOC, DIN and DON concentrations observed in western groundwater were not present in eastern groundwater (Table 4.2). DOC concentrations in the groundwater from the western Okatee were significantly ($p < 0.0001$) higher than those from the eastern Okatee (Table 4.2). High concentrations of presumably labile DOC supported greater rates of heterotrophic metabolism, as evidenced by higher DIC concentrations in western groundwater (Table 4.2, Fig. 4.3B). Because the $\text{Cl}^-/\text{SO}_4^{2-}$ ratio of seawater is constant (Pilson 1998) and since Cl^- is conservative, $\text{Cl}^-/\text{SO}_4^{2-}$ ratio can be

used to calculate SO_4^{2-} depletion, a proxy for microbial sulfate reduction (Weston et al. 2006). The $\text{Cl}^-/\text{SO}_4^{2-}$ ratio in groundwater from the western Okatee was depleted in SO_4^{2-} relative to seawater. Higher DOC concentration in this groundwater apparently supports significant rates of sulfate reduction (Table 4.1 and Fig. 4.3A). Both the $\text{Cl}^-/\text{SO}_4^{2-}$ ratio and higher concentrations of H_2S in the western groundwater provide evidence of active SR (Table 4.3). Consumption of organic matter by sulfate reducers and other heterotrophic bacteria produces NH_4^+ and DON, which were present at high concentrations in western groundwater. Conversely, the groundwater on the eastern side of the Okatee had lower DOC concentrations and insignificant sulfate reduction rates (i.e., $\text{Cl}^-/\text{SO}_4^{2-}$ ratio similar to seawater, Table 4.1 and Fig. 4.3A). Lower concentrations of organic matter and possibly lower rates of heterotrophic metabolism could account for the observed lower concentrations of NH_4^+ and DON in the eastern groundwater.

Alternatively, the disparity between the groundwater geochemical signatures from the western and eastern sides of the Okatee could reflect variations in aquifer flow regime. Such differences could drive differences in microbial activity and geochemistry. Radium data confirm higher frequency of flushing of the aquifer on the eastern side which could serve to simply flush the reduced metabolites from the aquifer more efficiently than on the western side.

Using an average C/N ratio (30.3) for *Spartina alterniflora* leaves, roots, and litter (Cheng et al. 2006), we calculated an expected DIN concentration that would result from organic matter breakdown within the marsh (Table 4.2). The upland wells showed an N deficit, which may reflect the choice of the C/N ratio of the hypothetical source material. High DIC concentrations in the groundwater on both sides of the Okatee result in high expected DIN concentrations with higher expected N on the western side of the Okatee. However, the measured DIN concentrations fall short of the predicted values ($N_{\text{missing}} = 133.50$ and $310.86 \mu\text{mol N L}^{-1}$

for the eastern and western sides respectively; Table 4.2) indicating a sink of DIN (most likely DNF) in the marsh complex. Dissolved N_2 is supersaturated in the groundwater from both sides of the Okatee (Table 4.3) indicating that DNF is a likely source of N_2 in the marsh. Given the larger discrepancy in groundwater DIN concentration in the western marsh, it appears that the DNF sink would have to be larger for the western side. However, DNF is typically sensitive to H_2S concentrations greater than $20 \mu\text{mol L}^{-1}$ (Joye 2002) and NO_x uptake decreased by approximately 50% at H_2S concentrations of $500 \mu\text{mol L}^{-1}$ in surficial sediments from within the Okatee system (Porubsky et al. Chapter 2). The western side is a site of sulfate reduction (Fig. 4.3A) and high groundwater H_2S concentrations ($> 2000 \mu\text{mol L}^{-1}$, Table 4.4) which would be expected to limit the impact of DNF. However, either sulfide-insensitive DNF or other potential NO_3^- sinks, including bacterial assimilation (Veuger et al. 2007), and/or anaerobic ammonium oxidation (anammox; Thamdrup and Dalsgaard 2002; Risgaard-Petersen et al. 2004), could be important.

Radium-based estimates of groundwater fluxes

The use of upland and marsh wells in the current study permits estimation of groundwater derived fluxes that factor in the potential alteration of materials during transit through coastal sediments (Tobias et al. 2001b; Valiela et al. 1990). Sediment processes alter the geochemical signature of the upland groundwater prior to discharge to the coastal ocean (Tobias et al. 2001a), highlighting the need for characterization of groundwater close to the receiving waters. Additionally the contribution of recirculated seawater to SGD would be overlooked by only examining the upland groundwater and ignoring the chemical signature of the groundwater near the site of discharge.

The linear regressions of nutrients, organics and trace gases with ^{226}Ra activity (Figs. 4.4A-F) were used to estimate potential groundwater inputs based on ^{226}Ra flux rates (Table 4.4). The estimated groundwater flux based on balancing the ^{226}Ra activity yields a flux rate of $1.04 \text{ m}^3 \text{ s}^{-1}$ for the Okatee estuary. The estimated fluxes of NH_4^+ , PO_4^{3-} , DOC and DIC were similar to inputs estimated by Moore et al. (2006) using a almost identical groundwater flux rate of $1 \text{ m}^3 \text{ s}^{-1}$ even though those fluxes used nutrient concentrations from the western wells only. The flux estimates in table 4.4 factor in nutrient concentrations in both the eastern and western wells, indicating that inclusion of the eastern wells does not significantly alter the nutrient flux estimates (reported in Moore et al. 2006). Surprisingly, this suggests that the eastern wells do not supply a significant portion of the groundwater derived nutrients entering the Okatee even though the ^{228}Ra data suggest this side of the system is more rapidly flushed. ^{226}Ra derived fluxes of DOC, DON, and NH_4^+ to the Okatee ($\text{mol C or N m}^{-2} \text{ d}^{-1}$) were approximately 13, 4 and 38 times higher, respectively, than wetland to estuary fluxes determined by Tobias et al. (2001b); and approximately 4, 2, and 8 times higher than the same fluxes reported for an area in the northeastern coastal Gulf of Mexico (Santos et al. 2008).

The radium loading approach also permits approximation of groundwater-associated carbon (C) fluxes to the coastal zone. Previously estimated DIC fluxes indicate that ~10% of the DIC in groundwater is exported to the coastal ocean and the remaining 90% is lost to the atmosphere (Cai et al. 2000). While the predicted loss of DIC to the atmosphere leaves a relatively small fraction of groundwater DIC available for transport to the coastal ocean, the high groundwater associated fluxes result in a significant contribution of DIC to coastal ecosystems. Groundwater associated DIC fluxes were significant relative to riverine DIC flux in the South Atlantic Bight (Cai et al. 2003) and groundwater DIC concentrations were significantly higher

then surface water DIC concentrations (Table 4.2; also Cai and Wang 1998; Cai et al. 2003). Radium based estimates of groundwater DIC flux from North Inlet, SC yielded a flux of 171 $\text{mmol m}^{-2} \text{d}^{-1}$ (Cai et al. 2003). The average groundwater DIC concentration from the Okatee system was approximately 10 mmol L^{-1} and the associated areal flux rate of 2456 $\text{mmol m}^{-2} \text{d}^{-1}$ (Table 4.2 and 4.4), which is approximately 14 times higher than the flux from North Inlet. The radium loading approach yielded a DOC areal flux rate of $\sim 146 \text{ mmol m}^{-2} \text{d}^{-1}$ (Table 4.4) which was similar to the DIC flux rate from North Inlet, indicating that the groundwater in the Okatee system can be a significant source of both inorganic and organic carbon to the coastal ocean.

Fluxes of greenhouse gases (CH_4 and N_2O) contribute to global warming and ozone depletion (IPCC 2007). Radium based groundwater CH_4 fluxes ($\sim 2 \text{ mmol m}^{-2} \text{d}^{-1}$, Table 4.4) were approximately 15 times higher than CH_4 emission rates from macrotidal salt marsh sediments in the Bay of Fundy (average $0.13 \text{ mmol m}^{-2} \text{d}^{-1}$; Magenheimer et al. 1996), 53 times higher than CH_4 fluxes from Lanark Spring in Florida (Cable et al. 1996), and equal to CH_4 emission rates from Chesapeake Bay salt marsh sediments ($\sim 2.4 \text{ mmol m}^{-2} \text{d}^{-1}$; Lipschultz 1981). However, groundwater CH_4 fluxes were approximately 80% of CH_4 emission rates reported for salt marshes in Georgia (King and Wiebe 1978) and were 3 to 22 times lower than CH_4 emission rates from a variety of fresh and salt water ecosystems in India with varying degrees of anthropogenic pressure (Purvaja and Ramesh 2001). While CH_4 fluxes were orders of magnitude lower than DIC fluxes, they were comparable to CH_4 emission rates from natural marsh systems and resulted in an average CH_4 concentration ($3.0 \mu\text{mol L}^{-1}$) in Okatee surface water and was near the maximum of the CH_4 concentration range (0.002 to $3.6 \mu\text{mol L}^{-1}$) reported for a series of European estuaries (Middelburg et al. 2002). Similarly, groundwater derived N_2O fluxes (~ 0.03

mmol N m⁻² d⁻¹, Table 4.4) were approximately 5 times the N₂O flux reported for a salt marsh sediments (0.006 mmol N m⁻² d⁻¹, Smith et al. 1983).

Benthic flux based estimates of nutrient flux, N mitigation via DNF

Diffusive fluxes, measured in sediment flux cores, were much smaller than radium derived groundwater nutrient-fluxes (Tables 4.2-4.5). This indicates that advective groundwater transport of nutrients and organics, likely originating within the marsh, dominates inputs to the Okatee. Further evidence for advective groundwater flux was found in creek-bank depth profiles of salinity, DIC, and NH₄⁺ (Figs. 4.5A-F, see Weston et al. 2006 for methods and details). Depth profiles from different heights on the creek bank show a strong contribution of fresh groundwater advection at site PB in February and August of 2002. Profiles from lower on the creek-bank showed a decrease in salinity with depth while profiles collected higher on the creek bank show little variation in salinity with depth (Figs. 4.5A and D). The fresher water at the lower creek bank position had higher DIC and NH₄⁺ concentrations again indicating that groundwater advection is a significant source of inorganics to the Okatee (Figs. 4.5B-C and E-F).

Net DIC fluxes from benthic cores indicated that intertidal sediments were net autotrophic and capable of removing ~266 mol C d⁻¹ within the intertidal area (Table 4.5). Absolute rates of diffusive DIC fluxes were orders of magnitude smaller than radium derived groundwater fluxes for the Okatee and estimated fluxes of DIC for North Inlet, SC (Cai et al. 2003) and radium derived groundwater DIC fluxes for the Okatee. Benthic microalgae (BMA) impact benthic fluxes through both indirect and direct controls (Sundbäck and Granéli 1988; Joye et al. 2003; Porubsky Chapter 3). BMA can assimilate nutrients from the water column and the sediments (Sigmon and Cahoon 1997; Sundbäck and Granéli 1988) and act as a cap at the

sediment water column interface that modulates benthic nutrient fluxes. However, even the most efficient BMA cannot completely consume the groundwater-derived nutrient fluxes in this system.

The average benthic flux of DOC ($3.74 \text{ mmol C m}^{-2} \text{ d}^{-1}$) was approximately 39 times lower than the radium based DOC flux. Sediments occupied by a productive BMA community have been shown to be a source of DOC to the water column (Pinckney and Zingmark 1993; Porubsky et al. Chapter 3). Up to 73% of BMA total gross primary production may be released as DOC (Goto et al. 1999). The DOC released by BMA may be rapidly assimilated by bacteria (Middelburg et al. 2000), however, under nitrogen-replete conditions, BMA-derived DOC may flux to the water column (Porubsky et al. Chapter 3). Both benthic flux core and radium based estimates of DOC flux indicate that sediments and groundwater are important DOC sources to the Okatee. Organic matter inputs could stimulate heterotrophic metabolism in the water column and influence the net metabolic balance of the Okatee system.

The benthos can also impact the metabolism of the system through water column nutrient uptake. The average daytime N/P ratio of the uptake rate from benthic flux cores was approximately 2.6 (Table 4.5). However, net daily benthic fluxes showed N uptake and P release indicating N limitation and excess P (Table 4.5). The N/P ratio of the Okatee (4.91, Table 4.2) was significantly lower than the radium estimated groundwater flux N/P (12.80, Table 4.4) indicating that N was preferentially taken up in the benthos. The ratio of N/P can impact competition between communities for available resources. A low N/P may confer an advantage to N-fixing cyanobacteria (Pinckney et al. 1995) while a high N/P may favor benthic diatoms. Thus the processes occurring within the marsh complex that alter the N/P ratio of the groundwater have implications beyond the sediment-water interface.

Denitrification can potentially alter the N/P ratio and represents a loss of N from the system with implications for mitigation of N loading to coastal zones. While pDNF rates measured in slurry incubations ($7.72 \text{ mmol N m}^{-2} \text{ d}^{-1}$) indicated that DNF could remove a significant amount of the DIN load in the Okatee system (~6-20% depending on area of pDNF used), un-amended DNF rates measured in benthic flux cores from Grave's Dock were much lower (0.01 and $0.23 \text{ mmol N m}^{-2} \text{ d}^{-1}$ for January 2004 and August 2002 respectively, Porubsky et al. Chapter 2). Maximum benthic flux core estimated DNF rates could only remove ~0.6% of the DIN load in the Okatee. Both of these estimates have associated problems, but they are useful to bracket the probable range of DNF rates present in the Okatee. Based on the relationship between DIC and the predicted DIN concentration, Cai et al. (2000) estimated a range of DNF rates of $3\text{-}11 \text{ mmol m}^{-2} \text{ d}^{-1}$ dependent on the C/N ratio selected; with Redfield (C/N = 6.6) resulting in the maximum rate. In the Okatee the slurry determined pDNF rate and DNF rates determined from NO_3^- amended benthic flux cores from August 2002 ($3.99 \text{ mmol N m}^{-2} \text{ d}^{-1}$, Porubsky et al. Chapter 2) fall within this range indicating that, given access to high NO_3^- concentrations, DNF could potentially remove a significant portion of the DIN load. With the DIN pool dominated by reduced species (DON and NH_4^+), DNF is dependent on nitrification to supply substrate. The largest pool of DIN was in the groundwater of the western marsh (Table 4.2), where low dissolved O_2 and high H_2S concentrations likely limited nitrification.

CONCLUSIONS

The hydrology and resulting geochemistry of a complex aquifer system such as the Okatee underscores the necessity for the integration of methods used in this study. While TIR data indicated higher occurrence (i.e., number of seeps) of groundwater delivery on the western

side of the Okatee, $^{228}\text{Ra}/^{226}\text{Ra}$ activity ratios contradicted this finding and indicated that the aquifer on the eastern side was more frequently flushed suggesting greater groundwater delivery. Variations in hydrology, likely combined with organic carbon distribution, impacted the microbial activity and geochemistry. The groundwater in the Okatee carries a marsh-dominated geochemical signature and indicates that processing of materials within the marsh is much more important than input of upland groundwater. Less flushing and more organic matter in the groundwater on the western side lead to higher sulfate reduction rates and concentrations of reduced metabolites than on the eastern side.

Loading rates derived from radium isotope data indicated that even though the eastern side may be more frequently flushed, the significantly higher concentration of organics, DIC and nutrients observed in the western groundwater represent the majority of the advective groundwater-derived input to the Okatee. Diffusive benthic fluxes were significantly smaller than radium-based groundwater inputs and thus were of minor importance to the overall flux of materials to the Okatee. The large amount of ‘missing’ DIN in the upper reaches of the Okatee suggest a significant N sink, and while pDNF rates could account for a large fraction, in situ rates from benthic flux cores were much lower and could not be responsible for the loss. While alternative sinks such as microbial uptake or possibly anammox may account for some of the missing N, the exact fate is not known.

ACKNOWLEDGMENTS

We thank the South Carolina Department of Natural Resources Waddell Mariculture Center for providing facilities and M. Erickson and A. Mahoney for assistance in the field and lab. This publication was sponsored in part by the NOAA Center for Sponsored Coastal Ocean

Research/Coastal Ocean Program, through the South Carolina Sea Grant Consortium, pursuant to National Oceanic and Atmospheric Administration Award NA960PO113 (LU-CES). This work was also supported in part by The National Science Foundation (OCE-9982133 and OCE 0620959 to S.B.J.) and the Georgia Sea Grant Program (awards NA06RG0029-R/WQ11 and R/WQ12A to S.B.J.)

LITERATURE CITED

- Álvarez-Salgado, X., and A. Miller. 1998. Simultaneous determination of dissolved organic carbon and total dissolved nitrogen in seawater by high temperature catalytic oxidation: Conditions for precise shipboard measurements. *Marine Chemistry* 62: 325-333.
- Banks, W., R. Paylor, and W. Hughes. 1996. Using thermal-infrared imagery to delineate ground-water discharge. *Ground Water* 34: 434-443.
- Blanton, J., F. Andrade, and A. Ferreira. 2006. The relationship of hydrodynamics and morphology in tidal-creek and salt-marsh systems in South Carolina and Georgia, pp. 93-107. In G. Kleppel, M. DeVoe, and M. Rawson Jr. [eds.] *Implications of Changing Land Use Patterns to Coastal Ecosystems*. Springer.
- Bouillon, S., M. Frankignoulle, F. Dehairs, B. Velimirov, A. Eiler, G. Abril, H. Etcheber, and A. Borges. 2003. Inorganic and organic carbon biogeochemistry in the Gautami Godavari estuary (Andhra Pradesh, India) during pre-monsoon: The local impact of extensive mangrove forests. *Global Biogeochemical Cycles* Vol. 17, No. 4, 1114, doi:10.1029/2002GB002026.
- Burnett, W., H. Bokuniewicz, M. Huettel, W. Moore, and M. Taniguchi. 2003. Groundwater and pore water inputs to the coastal zone. *Biogeochemistry* 66: 3-33.

- Cable, J., G. Bugna, W. Burnett, and J. Chanton. 1996. Application of ^{222}Rn and CH_4 for assessment of groundwater discharge to the coastal ocean. *Limnology and Oceanography* 41: 1347-1353.
- Cai, W., and Y. Wang. 1998. The chemistry, fluxes, and sources of carbon dioxide in the estuarine waters of the Satilla and Altamaha Rivers, Georgia. *Limnology and Oceanography* 43: 657-668.
- Cai, W., Y. Wang, J. Krest, and W. Moore. 2003. The geochemistry of dissolved inorganic carbon in a surficial groundwater aquifer in North Inlet, South Carolina, and the carbon fluxes to the coastal ocean. *Geochimica et Cosmochimica Acta* 67: 631-637.
- Cai, W., W. Wiebe, Y. Wang, and J. Sheldon. 2000. Intertidal marsh as a source of dissolved inorganic carbon and a sink of nitrate in the Satilla river-estuarine complex in the southeastern U.S. *Limnology and Oceanography* 45: 1743-1752.
- Capone, D., and J. Slater. 1990. Interannual patterns of water table height and groundwater derived nitrate in nearshore sediments. *Biogeochemistry* 10: 277-288.
- Cline, J. 1969. Spectrophotometric detection of hydrogen sulfide in natural waters. *Limnology and Oceanography* 14: 454-458.
- Cole, M., K. Kroeger, J. McClelland, and I. Valiela. 2006. Effects of watershed land use on nitrogen concentrations and $\delta^{15}\text{N}$ nitrogen in groundwater. *Biogeochemistry* 77: 199-215.
- Cotrim da Cunha, L., E. Buitenhuis, C. Le Quéré, X. Giraud, and W. Ludwig. 2007. Potential impact of changes in river nutrient supply on global ocean biogeochemistry. *Global Biogeochemical Cycles* 21, doi:10.1029/2006GB002718.
- Giblin, A., and A. Gaines. 1990. Nitrogen inputs to a marine embayment - the importance of groundwater. *Biogeochemistry* 10: 309-328.

- Giblin, A., and R. Howarth. 1984. Porewater evidence for a dynamic sedimentary iron cycle in salt marshes. *Limnology and Oceanography* 29: 47-63.
- Gobler, C., and G. Boneillo. 2003. Impacts of anthropogenically influenced groundwater seepage on water chemistry and phytoplankton dynamics within a coastal marine system. *Marine Ecology Progress Series* 255: 101-114.
- Gobler, C., and S. Sañudo-Wilhemy. 2001. Temporal variability of groundwater seepage and brown tide blooms in a Long Island embayment. *Marine Ecology Progress Series* 217: 299-309.
- Goto, N., T. Kawamura, O. Mitamura, and H. Terai. 1999. Importance of extracellular organic carbon production in the total primary production by tidal-flat diatoms in comparison to phytoplankton. *Marine Ecology Progress Series* 190: 289-295.
- Harvey, J., and W. Odum. 1990. The influence of tidal marshes on upland groundwater discharge to estuaries. *Biogeochemistry* 10: 217-236.
- Hussein, A., and M. Rabenhorst. 1999. Modeling of sulfur sequestration in coastal marsh soils. *Soil Science Societ of America Journal* 63: 1954-1963.
- IPCC. 2007. Climate Change 2007: The Physical Science Basis – Summary for Policymakers. <http://www.ipcc.ch/SPM2feb07.pdf>.
- Johnson, A., C. Glenn, W. Burnett, R. Peterson, and P. Lucey. 2008. Aerial infrared imaging reveals large nutrient-rich groundwater inputs to the ocean. *Geophysical Research Letters* Vol. 35, L15606, doi:10.1029/2008GL034574.
- Joye, S., and H. Paerl. 1993. Contemporaneous nitrogen fixation and denitrification in intertidal microbial mats: rapid response to runoff events. *Marine Ecology Progress Series* 94: 267-274.

- Joye, S. and H. Paerl. 1994. Nitrogen cycling in marine microbial mats: Rates and patterns of nitrogen fixation and denitrification. *Marine Biology* 119: 285-295.
- Joye, S., M. Mazzotta, and J. Hollibaugh. 1996. Community metabolism in intertidal microbial mats: The importance of iron and manganese reduction. *Estuarine, Coastal and Shelf Science* 43: 747-766.
- Joye, S., A. Boetius, B. Orcutt, J. Montoya, H. Schulz, M. Erickson, and S. Lugo. 2004. The anaerobic oxidation of methane and sulfate reduction in sediments from Gulf of Mexico cold seeps. *Chemical Geology* 205(3/4): 219-238.
- Joye, S., W. Porubsky, N. Weston, and R. Lee. 2003. Benthic microalgal production and nutrient dynamics in intertidal sediments, pp. 67-70. In J. Rullkötter [ed.] *BioGeoChemistry of Tidal Flats*, Forschungszentrum Terramare Berichte Nr. 12, Proceedings of a Workshop held at the Hanse Institute of Advanced Study, Delmenhorst, Germany, May 14-17 2003, ISSN 1432-797X.
- Kana, T., M. Sullivan, J. Cornwell, and K. Groszkowski. 1998. Denitrification in estuarine sediments determined by membrane inlet mass spectrometry. *Limnology and Oceanography* 43: 334-339.
- King, G., and W. Wiebe. 1978. Methane release from soils of a Georgia salt marsh. *Geochimica et Cosmochimica Acta* 42: 343-348.
- Kroeger, K., and M. Charette. 2008. Nitrogen biogeochemistry of submarine groundwater discharge. *Limnology and Oceanography* 53: 1025-1039.
- Kroeger, K., P. Swarzenski, Wm. Greenwood, C. Reich. 2007. Submarine groundwater discharge to Tampa Bay: Nutrient fluxes and biogeochemistry of the coastal aquifer. *Marine Chemistry* 104: 85-97.

- LaMontagne, M., R. Duran, and I. Valiela. 2003. Nitrous oxide sources and sinks in coastal aquifers and coupled estuarine receiving waters. *Science of the Total Environment* 309: 139-149.
- LaPointe, B., J. O'Connell, and G. Garrett, 1990. Nutrient couplings between on-site sewage disposal systems, groundwaters, and nearshore waters of the Florida Keys. *Biogeochemistry* 10: 289-307.
- Lipschultz, F. 1981. Methane release from a brackish intertidal salt-marsh embayment of Chesapeake Bay, Maryland. *Estuaries* 4: 143-145.
- Magenheimer, J., T. Moore, G. Chmura, and R. Daoust. 1996. Methane and carbon dioxide flux from a macrotidal salt marsh, Bay of Fundy, New Brunswick. *Estuaries* 19: 139-145.
- Middelburg, J., C. Barranguet, H. Boschker, P. Herman, T. Moens, and C. Heip. 2000. The fate of intertidal microphytobenthos carbon: An in situ ^{13}C -labeling study. *Limnology and Oceanography* 45: 1224-1234.
- Middelburg, J., J. Nieuwenhuize, N. Iversen, N. Høgh, H. De Wilde, W. Helder, R. Seifert, and O. Christof. 2002. Methane distribution in European tidal estuaries. *Biogeochemistry* 59: 95-119.
- Monaghan, E., and K. Ruttenberg. 1999. Dissolved organic phosphorus in the coastal ocean: Reassessment of available methods and seasonal phosphorus profiles from the Eel River Shelf. *Limnology and Oceanography* 44: 1702-1714.
- Moore, W. 1976. Sampling ^{228}Ra in the deep ocean. *Deep-Sea Res.* 23: 647-651.

- Moore, W. 1984. Radium isotope measurements using germanium detectors. *Nuclear Instruments and Methods* 223: 407-411.
- Moore, W. 1996. Large groundwater inputs to coastal waters revealed by ^{226}Ra enrichments. *Nature* 380: 612-614.
- Moore, W. 2003. Sources and fluxes of submarine groundwater discharge delineated by radium isotopes. *Biogeochemistry* 66: 75-93.
- Moore, W. and R. Arnold. 1996. Measurement of ^{223}Ra and ^{224}Ra in coastal waters using a delayed coincidence counter. *Journal of Geophysical Research* 101: 1321-1329.
- Moore, W., J. Blanton, and S. Joye. 2006. Estimates of flushing times, submarine groundwater discharge, and nutrient fluxes to Okatee Estuary, South Carolina. *Journal of Geophysical Research* 111, C09006, doi: 10.1029/2005JC003041.
- Moore, W., J. Sarmiento, and R. Key. 2008. Submarine groundwater discharge revealed by ^{228}Ra distribution in the upper Atlantic Ocean. *Nature Geoscience* doi: 10.1038/ngeo183.
- Paerl, H. 1997. Coastal eutrophication and harmful algal blooms: Importance of atmospheric deposition and groundwater as “new” nitrogen and other nutrient sources. *Limnology and Oceanography* 42: 1154-1165.
- Peltzer, E. and P. Brewer. 1993. Some practical aspects of measuring DOC sampling artifacts and analytical problems with marine samples. *Marine Chemistry* 41: 243-252.
- Pilson, M. 1998. An introduction to the chemistry of the sea. Prentice Hall, New Jersey.
- Pinckney, J., H. Paerl, and M. Fitzpatrick. 1995. Impacts of seasonality and nutrients on microbial mat community structure and function. *Marine Ecology Progress Series* 123: 207-216.

- Pinckney, J., and R. Zingmark. 1993. Modeling the annual production of intertidal benthic microalgae in estuarine ecosystems. *Journal of Phycology* 29: 396-407.
- Portnoy, J., B. Nowicki, C. Roman, and D. Urish. 1998. The discharge of nitrate-contaminated groundwater from developed shoreline to marsh-fringed estuary. *Water Resources Research* 34: 3095-3104.
- Porubsky, W., L. Velasquez, and S. Joye. 2008. Nutrient-replete benthic microalgae as a source of dissolved organic carbon to coastal waters. *Estuaries and Coasts* doi: 10.1007/s12237-008-9077-0.
- Porubsky, W., N. Weston, and S. Joye. Benthic metabolism and the fate of dissolved inorganic nitrogen in intertidal sediments. *Estuarine, Coastal and Shelf Science, Submitted*.
- Purvaja, R., and R. Ramesh. 2001. Natural and anthropogenic methane emission from coastal wetlands of south India. *Environmental Management* 27: 547-557.
- Rama, and W. Moore. 1996. Using the radium quartet to estimate water exchange and groundwater input in salt marshes. *Geochimica et Cosmochimica Acta* 60: 4645-4652.
- Redfield, A. 1958. The biological control of chemical factors in the environment. *American Scientist* 46: 205-222.
- Risgaard-Peterson, N., R. Meyer, M. Schmid, M. Jetten, A. Enrich-Prast, S. Rysgaard, and N. Revsbech. 2004. Anaerobic ammonium oxidation in an estuarine sediment. *Aquatic Microbial Ecology* 36: 293-304.
- Santos, I., W. Burnett, J. Chanton, B. Mwashote, I. Suryaputra, and T. Dittmar. 2008. Nutrient biogeochemistry in a Gulf of Mexico subterranean estuary and groundwater-derived fluxes to the coastal ocean. *Limnology and Oceanography* 53: 705-718.

- Schultz, G. and C. Ruppel. 2002. Constraints on hydraulic parameters and implications for groundwater flux across the upland-estuary interface. *Journal of Hydrology* 260: 255-269.
- Sigmon, D., and L. Cahoon. 1997. Comparative effects of benthic microalgae and phytoplankton on dissolved silica fluxes. *Aquatic Microbial Ecology* 13: 275-284.
- Smith, R., L. Baumgartner, D. Miller, D. Repert, and J. Böhlke. 2006. Assessment of nitrification potential in groundwater using short term, single-well injection experiments. *Microbial Ecology* 51: 22-35.
- Smith, C., R. DeLaune, and W. Patrick, Jr.. 1983. Nitrous oxide emission from Gulf Coast wetlands. *Geochimica et Cosmochimica Acta* 47: 1805-1814.
- Solorzano, L. 1969. Determination of ammonia in natural waters by the phenolhypochlorite method. *Limnology and Oceanography* 14: 799-801.
- Stookey, L. 1970. Ferrozine – a new spectrophotometric reagent for iron. *Analytical Chemistry* 42: 779-781.
- Sundbäck, K., and W. Granéli. 1988. Influence of microphytobenthos on nutrient fluxes between sediment and water: A laboratory continuous flow study. *Marine Ecology Progress Series* 43:63-69.
- Swarzenski, P., C. Reich, K. Kroeger, and M. Baskaran. 2007. Ra and Rn isotopes as natural tracers of submarine groundwater discharge in Tampa Bay, Florida. *Marine Chemistry* 104: 69-84.
- Thamdrup, B., and T. Dalsgaard. 2002. Production of N₂ through anaerobic ammonium oxidation coupled to nitrate reduction in marine sediments. *Applied and Environmental Microbiology* 68: 1312-1318.

- Tobias, C., I. Anderson, E. Canuel and S. Macko. 2001a. Nitrogen cycling through a fringing marsh-aquifer ecotone. *Marine Ecology Progress Series* 210: 25-39.
- Tobias, C., J. Harvey, and I. Anderson. 2001b. Quantifying groundwater discharge through fringing wetlands to estuaries: Seasonal variability, methods comparison, and implications for wetland-estuary exchange. *Limnology and Oceanography* 46: 614-615.
- Valiela, I., J. Costa, K. Foreman, J. Teal, B. Howes, and D. Aubrey. 1990. Transport of groundwater-borne nutrients from watersheds and their effects on coastal water. *Biogeochemistry* 10: 177-197.
- Veuger, B., B. Eyre, D. Maher, and J. Middelburg. 2007. Nitrogen incorporation and retention by bacteria, algae, and fauna in a subtropical intertidal sediment: An in situ ¹⁵N-labeling study. *Limnology and Oceanography* 52: 1930-1942.
- Weston, N., W. Porubsky, V. Samarkin, M. Erickson, S. MacAvoy, and S. Joye. 2006. Porewater stoichiometry of terminal metabolic products, sulfate, and dissolved organic carbon and nitrogen in estuarine intertidal creek-bank sediments. *Biogeochemistry* 77: 375-408.
- Windom, H., H. McKeller Jr., C. Alexander Jr., A. Craig, A. Abusam, and M. Alford. 1998. Indicators of trends toward coastal eutrophication. Land Use-Coastal Ecosystem Study, State of Knowledge Report.

Table 4.1. Summary of physical and chemical data (Temperature in °C, pH, and DO₂ in μmol L⁻¹), major ions (Cl⁻ and SO₄²⁻ in mmol L⁻¹) and radium activities (²²⁶Ra and ²²⁸Ra dpm L⁻¹) for well and surface water samples collected between March 2002 and December 2005. Averages and standard errors are presented for pooled data from wells on the east (wells 1A, 1B, 2 and 3) and west (wells 4, 5, 6, 7 and 8) sides of the Okatee River and wells adjacent to the upland (wells 11 and 12). See Fig. 4.1 for well locations. *n* = number of measurements. a, b, c, and d designate statistically significant differences between the groundwater from each location (a = Upland wells, b = Okatee @ 278, c = Eastern wells, and d = Western wells), i.e., a = statistically different from location ‘a’ (*p* < 0.05), *a* = (*p* < 0.01), and **a** = (*p* < 0.0001).

Site	Temp	pH	Salinity	DO ₂	Cl ⁻	SO ₄ ²⁻	Cl/SO ₄ ²⁻	²²⁶ Ra	²²⁸ Ra
Upland wells ^a	19.00	4.34	14.15	71.28	198.85	8.98	22.38	5.18	44.87
StErr	0.78	0.32	0.39	28.60	5.46	0.39	0.49	0.91	5.187
<i>n</i>	11	10	13	9	13	13	13	9	9
stats	d	b,c,d	c,d	<i>b</i>	c,d	c,d		<i>b,c</i>	b,c,d
Okatee @ 278 ^b	17.99	7.34	10.31	206.30	182.01	8.98	18.92	0.40	0.99
StErr	1.90	0.16	2.66	28.66	50.19	2.25	1.70	0.04	0.17
<i>n</i>	13	9	15	6	16	16	16	25	25
stats		a,c	c,d	<i>a,c,d</i>	c,d	c,d		<i>a,c</i>	a,c,d
Eastern wells ^c	20.22	6.64	38.49	50.10	574.89	29.09	19.95	1.58	12.07
StErr	0.54	0.09	0.92	11.46	13.07	0.72	0.27	0.14	0.99
<i>n</i>	63	30	65	23	70	70	70	26	26
stats		a,b,d	a,b,d	<i>b,d</i>	a,c,d	a,c,d		<i>a,b,d</i>	<i>a,b</i>
Western wells ^d	20.93	7.04	31.18	4.44	462.62	17.77	27.60	3.85	10.26
StErr	0.45	0.09	0.64	1.42	7.07	0.51	0.82	0.21	0.54
<i>n</i>	68	38	74	4	79	79	79	53	53
stats	a	a,c	a,b,c	<i>a,b,c</i>	a,b,c	a,b,c		b,c	<i>a,b</i>

Table 4.2. Carbon and nutrient concentrations ($\mu\text{mol L}^{-1}$) for well and surface water samples collected between March 2002 and December 2005. Averages and standard errors are presented for pooled data from wells on the east (wells 1A, 1B, 2 and 3) and west (wells 4, 5, 6, 7 and 8) sides of the Okatee River and wells adjacent to the upland (wells 11 and 12). DIN/DIP reflects the molar ratio ($=[(\text{NO}_x^- + \text{NH}_4^+)/\text{PO}_4^{3-}]$) and N_{pred} reflects the expected DIN concentration obtained by dividing the observed DIC concentration by the *Spartina* C/N ratio ($=\text{DIC}/30.3$; Cheng et al. 2006). N_{missing} reflects the amount of DIN that cannot be accounted for, assumed to be removal via denitrification or assimilation during transit through the marsh. n = number of measurements. a, b, c, and d designate statistically significant differences between the groundwater from each location (a = Upland wells, b = Okatee @ 278, c = Eastern wells, and d = Western wells), i.e., a = statistically different from location 'a' ($p < 0.05$), $a = (p < 0.01)$, and $\mathbf{a} = (p < 0.0001)$.

Site	DIC	DOC	NO_x^-	NH_4^+	DON	PO_4^{3-}	DIN/DIP	N_{pred}	N_{missing}
Upland wells ^a	671.27	909.53	3.41	53.23	54.57	0.64	88.50	22.15	-42.41
StErr	114.15	50.66	2.34	9.81	12.17	0.10		3.77	
n	9	12	12	13	8	14		9	
stats	b,c,d	c,d		b,c,d	d	b,c,d			
Okatee @ 278 ^b	2144.47	1309.01	4.52	7.06	55.99	2.36	4.91	324.92	
StErr	488.25	224.37	1.80	1.85	7.07	0.69		73.98	
n	12	15	13	17	13	13		12	
stats	a,c,d	c		a,c,d	d	a,d			
Eastern wells ^c	4866.90	613.37	7.82	21.21	53.70	2.38	12.20	160.62	133.50
StErr	335.16	26.71	2.17	3.51	7.19	0.62		11.06	
n	52	66	54	70	58	56		52	
stats	a,b,d	a,b,d		a,b,d	d	a,d			
Western wells ^d	15975.80	1388.92	4.11	203.18	102.61	24.69	8.40	527.25	310.86
StErr	1093.50	52.90	1.59	18.00	11.66	5.05		36.09	
n	61	75	64	83	54	72		61	
stats	a,b,c	a,c		a,b,c	a,b,c	a,b,c			

Table 4.3. Summary of reduced metabolites (H₂S, Fe²⁺, CH₄, N₂O, and N₂ in μmol L⁻¹) and % saturation of N₂ (%) for well and surface water samples collected between March 2002 and December 2005. Averages and standard errors are presented for pooled data from wells on the east (wells 1A, 1B, 2 and 3) and west (wells 4, 5, 6, 7 and 8) sides of the Okatee River and wells adjacent to the upland (wells 11 and 12). *n* = number of measurements. a, b, c, and d designate statistically significant differences between the groundwater from each location (a = Upland wells, b = Okatee @ 278, c = Eastern wells, and d = Western wells), i.e., a = statistically different from location 'a' (*p* < 0.05), *a* = (*p* < 0.01), and **a** = (*p* < 0.0001).

Site	H ₂ S	Fe ²⁺	CH ₄	N ₂ O	N ₂	N ₂ % _{sat}
Upland wells ^a	9.58	1247.13	0.00	0.02	-	-
StErr	6.80	150.23	0.00	0.00	-	-
<i>n</i>	12	12	4	4	-	-
stats	d	b,c,d	<i>c,d</i>	<i>c,d</i>		
Okatee @ 278 ^b	12.74	17.23	3.00	0.13	560.21	102.04
StErr	10.21	10.10	1.65	0.04	50.90	0.39
<i>n</i>	14	9	9	6	5	5
stats	d	a,c	c,d			c,d
Eastern wells ^c	34.40	59.78	16.94	0.18	471.77	109.27
StErr	19.00	14.92	6.50	0.02	8.05	0.98
<i>n</i>	57	41	40	27	29	30
stats	d	a,b,d	a,b	<i>a</i>		b
Western wells ^d	2210.48	19.22	31.23	0.19	488.11	107.04
StErr	305.97	5.17	8.86	0.03	6.24	0.95
<i>n</i>	65	54	46	28	30	30
stats	a,b,c	a,c	a,b	<i>a</i>		b

Table 4.4. Potential groundwater derived fluxes of nutrients, organics, and dissolved gases in the Okatee estuary assuming an annual average ^{226}Ra flux of 3.43×10^8 (dpm d^{-1} ; calculated from Moore et al. 2006) and estimated from linear regressions (see in Fig. 4.4A-F). C is concentration in $\mu\text{mol L}^{-1}$.

Constituent	C/ ^{226}Ra ($\mu\text{mol dpm}^{-1}$)	Areal flux ($\text{mol m}^{-2} \text{d}^{-1}$)	Total flux ($\text{mol} \times 10^3 \text{d}^{-1}$)	N/P flux ratio (molar)
NH_4^+	75.53	0.036	25.87	12.80
PO_4^{3-}	5.90	0.003	2.02	
DOC	303.56	0.146	103.99	
DIC	5130.2	2.456	1757.46	
DON	10.89	0.005	3.73	
CH_4	3.76	0.002	1.29	
N_2O	0.02	0.000	0.01	

Table 4.5. Summary of benthic fluxes. Individual fluxes are in units of $\text{mmol m}^{-2} \text{d}^{-1}$, integrated average fluxes are in mol d^{-1} for the estimated Okatee creek-bank area (from Blanton et al. 2006). Numbers in parentheses are ± 1 SE.

Date	Site	Treatment	DIC	DOC	NO _x	NH ₄ ⁺	DON	PO ₄ ³⁻
June 2001	GD	Day	-	-3.453 (3.559)	0.003 (0.001)	0.003 (0.027)	0.059 (0.004)	-0.039 (0.114)
	GD	Night	-	3.424 (2.949)	-0.002 (0.003)	-0.016 (0.028)	-0.023 (0.007)	0.063 (0.091)
February 2002	T1	Day	0.137 (0.124)	0.003 (0.182)	0.008 (0.011)	-0.007 (0.003)	-0.024 (0.021)	0.000 (0.001)
	T1	Night	0.028 (0.097)	-0.279 (0.173)	-0.007 (0.006)	0.001 (0.004)	-0.013 (0.013)	0.000 (0.001)
	278	Day	-0.007 (0.147)	0.093 (0.138)	-0.009 (0.005)	-0.078 (0.062)	0.068 (0.127)	-0.002 (0.004)
	278	Night	-0.057 (0.240)	-0.019 (0.108)	0.003 (0.005)	0.024 (0.029)	-0.087 (0.070)	-0.002 (0.002)
	GD	Day	-2.378 (0.570)	0.038 (0.092)	-0.022 (0.007)	-0.007 (0.008)	0.084 (0.063)	-0.001 (0.003)
	GD	Night	1.298 (0.369)	-0.041 (0.150)	0.012 (0.010)	0.004 (0.005)	-0.048 (0.072)	0.000 (0.001)
	PB	Day	0.142 (0.033)	-2.460 (1.239)	0.016 (0.019)	-0.011 (0.009)	0.130 (0.207)	-0.003 (0.002)
	PB	Night	0.044 (0.164)	3.906 (2.140)	-0.041 (0.040)	0.011 (0.008)	-0.099 (0.171)	-0.003 (0.001)
August 2002	GD	Day	-1.608 (1.180)	-0.084 (0.427)	-0.012 (0.007)	-0.003 (0.092)	-	-0.001 (0.001)
	GD	Night	1.312 (0.187)	0.032 (0.130)	-0.022 (0.007)	-0.003 (0.027)	-	-0.001 (0.001)
January 2004	GD	Day	-0.892 (0.483)	-	-0.002 (0.002)	-0.002 (0.009)	0.230 (0.182)	-0.002 (0.013)
	GD	Night	0.690 (0.151)	-	-0.002 (0.003)	-0.016 (0.015)	-0.050 (0.099)	0.001 (0.001)
<i>Integrated whole system fluxes:</i>								
Average	All	Day	-952.52 (533.17)	-704.64 (716.57)	-3.19 (6.04)	-18.61 (13.20)	113.12 (42.78)	-8.54 (6.65)
	All	Night	685.54 (324.88)	1452.36 (983.32)	-9.75 (8.44)	6.56 (6.17)	-45.50 (27.56)	10.21 (11.34)
	All	Net	-266.98 (235.75)	747.72 (820.85)	-12.94 (6.51)	-12.05 (9.95)	67.62 (58.14)	1.67 (4.77)

FIGURE LEGENDS

Figure 4.1A-F. Site map highlighting the location of groundwater inputs, monitoring wells and flux core (t1, 278, GD, and PB) and rate core (t1, 278, and GD) collection sites. (A) System-scale map showing locations of flux and pDNF measurements (labels) and groundwater input (\blacktriangle) based on TIR data. Representative TIR images showing colder ground water (white) contrasting against the warm (black) tidal creek water (images from August 2001) for the sites circled in panel (A). (B) Numerous sub-marsh and creek bed groundwater flows (white arrows) visible in the tidal creek. (C) Several discrete groundwater plumes entering a tidal creek north of the northern well transect. (D) Groundwater inputs along the edges of a tidal creek. (E) Strong groundwater surface plumes in addition to sub-marsh groundwater enter along a small tributary carrying a temperature signal into a larger tidal creek. (F) Expanded view of monitoring well locations.

Figure 4.2A-C. Concentration versus salinity plots for (A) DOC, (B) DIN (predominantly NH_4^+), and (C) DIP (PO_4^{3-}) in the groundwater. Linear relationships for east, west, and upland wells as indicated.

Figure 4.3A-B. (A) Sulfate versus chloride relationships for Okatee wells. The solid line indicates the conservative $\text{SO}_4^{2-}/\text{Cl}^-$ ratio; values that fall below this line indicate SO_4^{2-} depletion. Dashed lines indicate the linear relationship for the east wells and west wells. (B) DOC versus DIC relationship for all Okatee wells.

Figure 4.4A-F. Constituent versus ^{226}Ra activity relationships for the Okatee wells. (A) DOC, (B) DIC, (C) NH_4^+ , (D) DIP, (E) H_2S , and (F) N_2O . Open symbols were excluded from linear relationship analysis.

Figure 4.5A-F. Porewater equilibration depth profiles for site PB in February 2002 (A-C) and August 2002 (D-F). Equilibration meters were placed perpendicular to the creek with “High” designating a profile from near the top of the intertidal creek-bank and “Low” designating a profile from the near the bottom of the intertidal creek-bank.

Figure 4.1A-F.

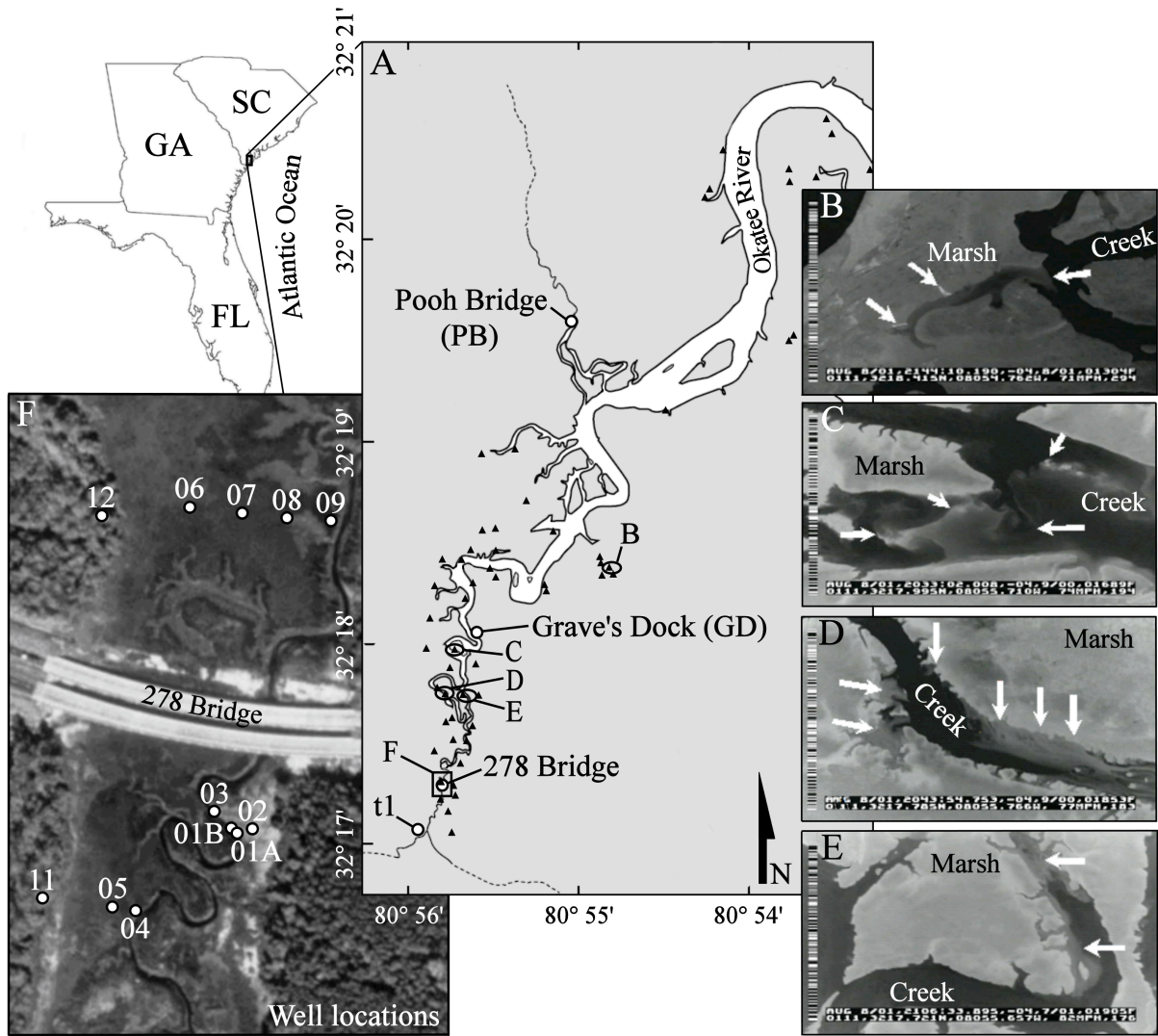


Figure 4.2A-C.

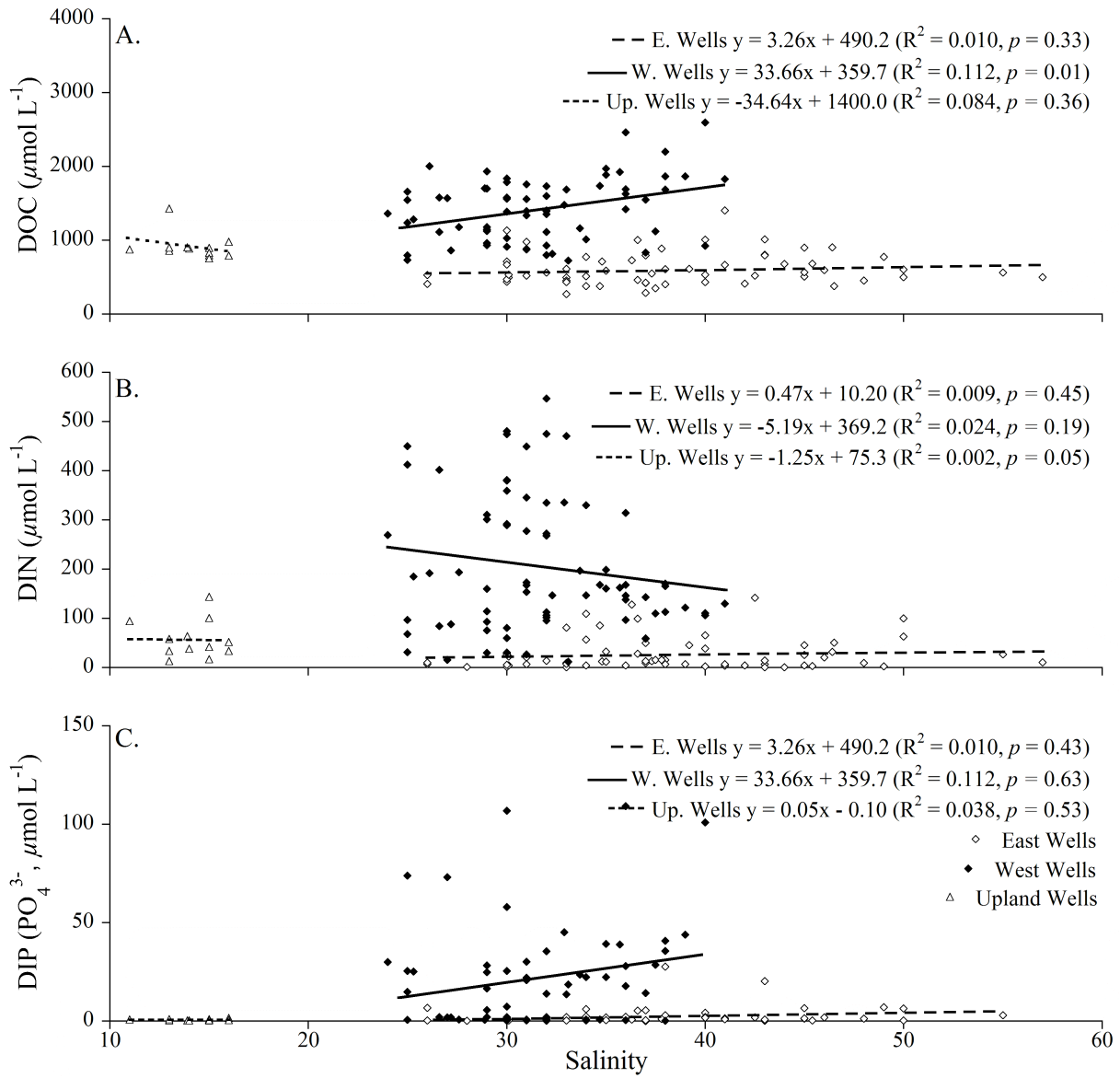


Figure 4.3A-B.

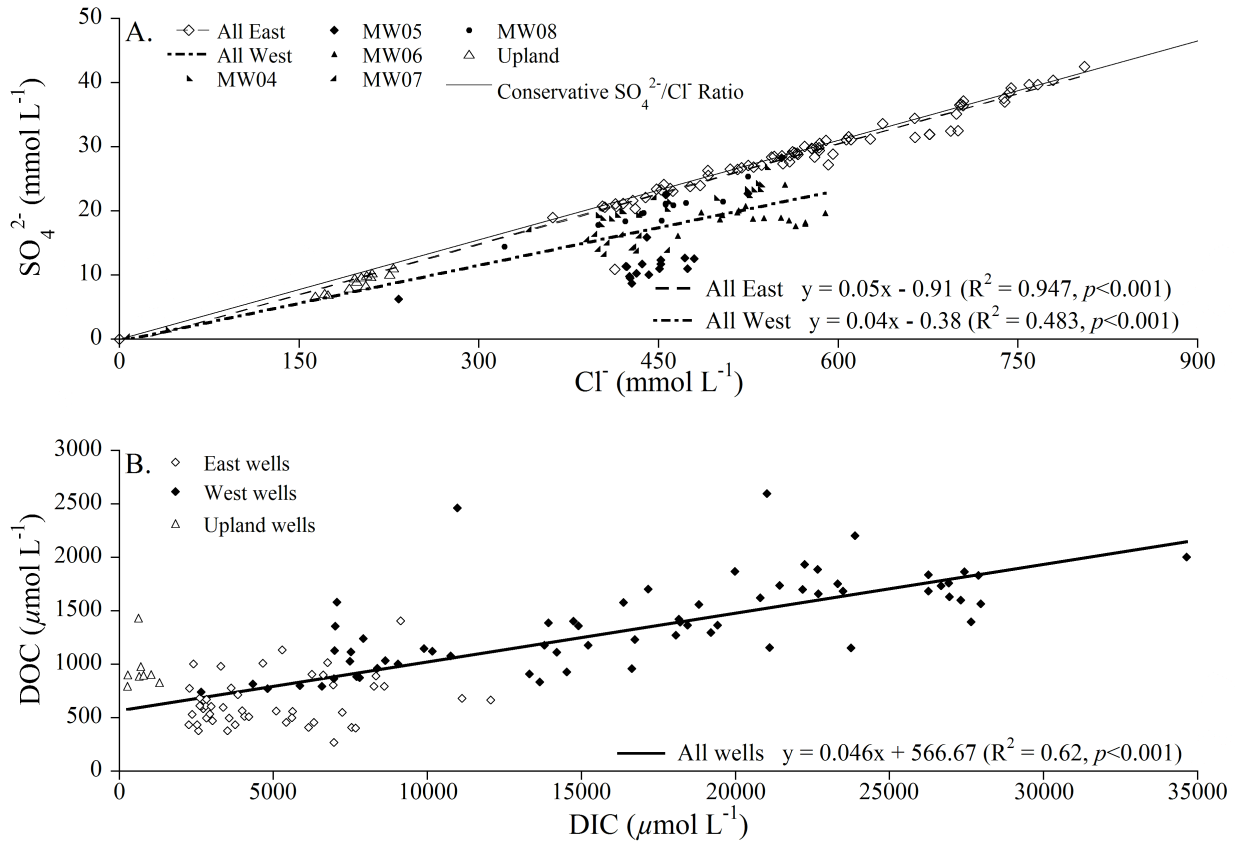


Figure 4.4A-F.

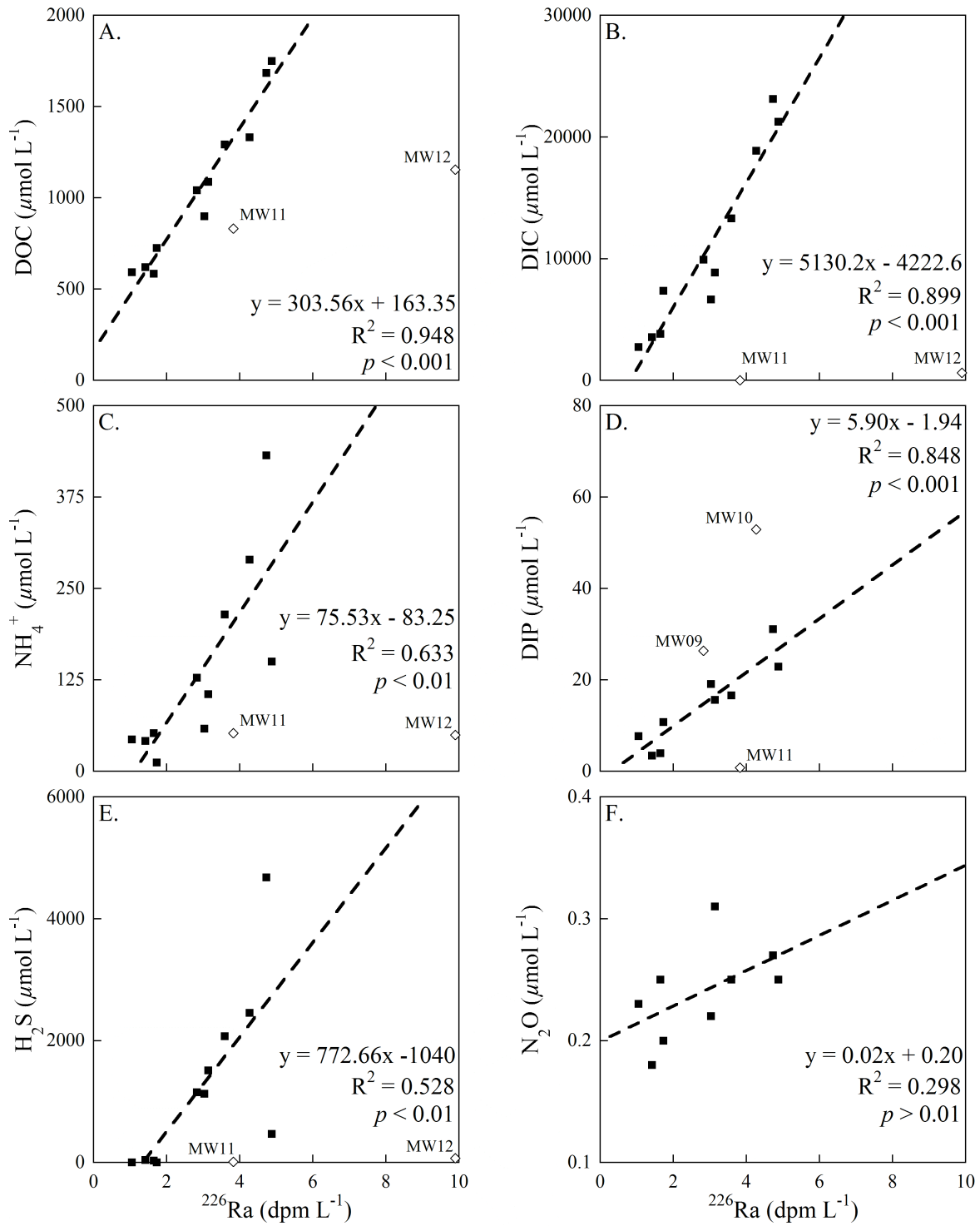
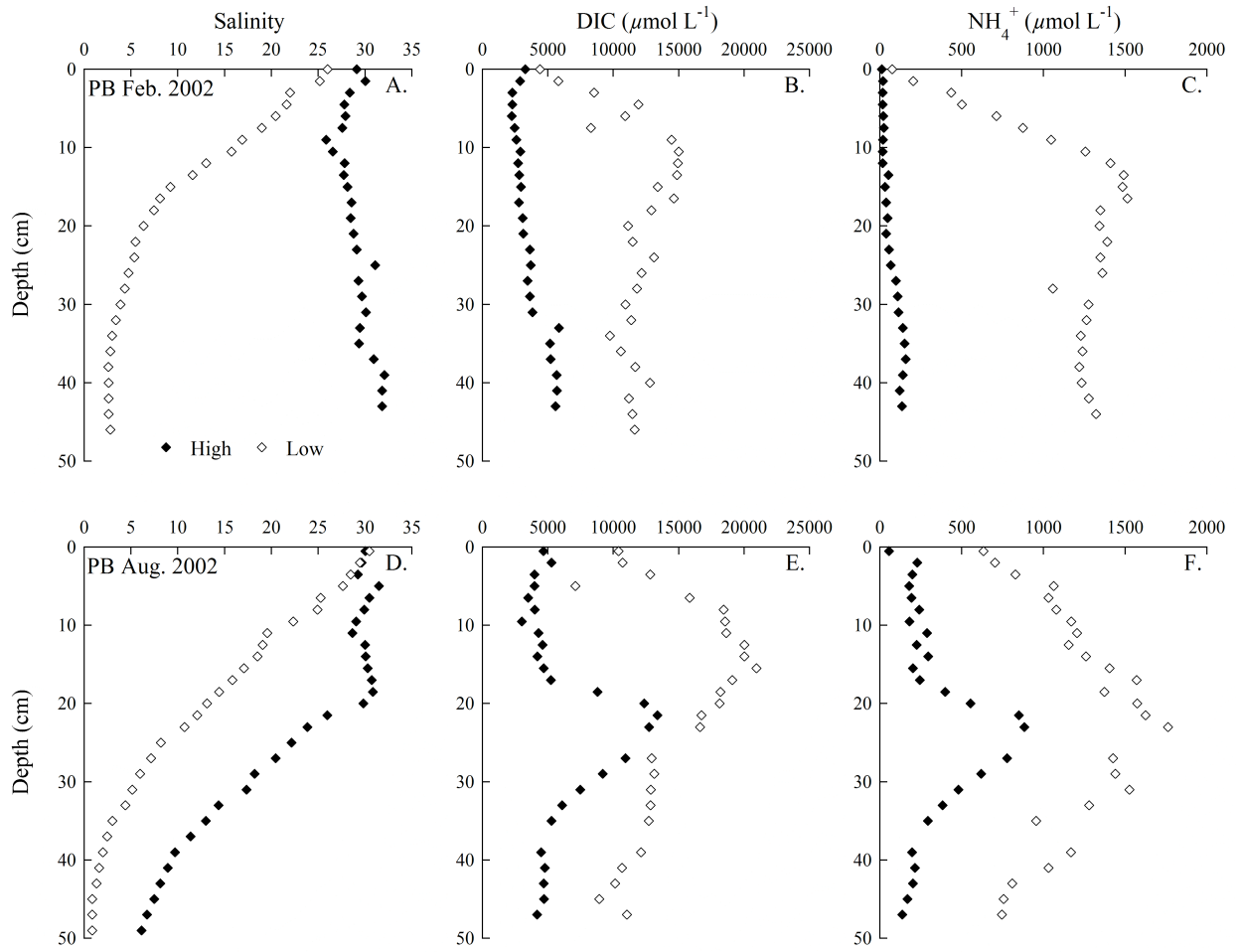


Figure 4.5A-F.



CHAPTER 5

HAMMOCK GROUNDWATER FLOW AND BIOGEOCHEMISTRY: FIELD MEASUREMENTS, LABORATORY ASSAYS, AND PREDICTIVE MODELING¹

¹Porubsky, W., S. Joye, W. Moore, K. Tuncay, and C. Meile. Submitted to *Limnology and Oceanography*, 09/08/2008.

ABSTRACT

A combination of field measurements, laboratory experiments and model simulations were used to characterize the groundwater biogeochemical dynamics along a shallow monitoring well transect on a coastal hammock. A switch in the redox status of the dissolved inorganic nitrogen (DIN) pool in the well at the upland/saltmarsh interface occurred during the spring-neap tidal transition: the DIN pool was dominated by NO_x ($\text{NO}_2^- + \text{NO}_3^-$) during spring tide and by ammonium (NH_4^+) during neap tide. A density-dependent reaction-transport model was used to investigate the relative importance of individual processes to the observed N redox-switch. With transport driven by measured pressure heads and using process parameterizations derived from the literature, targeted laboratory experiments and constrained by field observations, the observed N redox-switch was evaluated with regard to the relative roles of nitrification, denitrification (DNF), dissimilatory nitrate reduction to ammonium (DNRA), ammonium adsorption, and variations in inflowing water geochemistry between spring and neap tides. The latter was found to most significantly affect the observed pattern in DIN dynamics. Mimicking increased anthropogenic pressure in upland areas adjacent to marshes, the fate of dissolved organic matter and DIN originating from a septic system was studied. Simulation results indicated that while DNF increased ~15 fold, higher N removal rates could not keep pace with the increase in DIN loading, resulting in higher export of DIN to coastal waters.

INTRODUCTION

Quantification and characterization of nutrient delivery to the coastal ocean are critical for understanding anthropogenic impacts on ecosystem dynamics and global biogeochemical

cycles. This understanding requires an analysis of both riverine nutrient inputs (e.g., Cotrim da Cunha et al. 2007; Nixon et al. 1996), and an assessment of the contribution of groundwater derived nutrient inputs. Globally, volumetric groundwater discharge is only a fraction of riverine discharge (Burnett et al. 2003); however, in the upper Atlantic Ocean groundwater discharge of terrestrial freshwater and re-circulated seawater may amount to 80-160% of freshwater river discharge (Moore 1996; Moore et al. 2008). Because groundwater typically contains higher concentrations of nutrients than surface water, it can contribute significantly to nutrient budgets in estuarine systems (Valiela et al. 1990; Burnett et al. 2003; Kroeger and Charette 2008).

Nitrogen is generally the limiting nutrient to primary production in marine systems. As a consequence, the magnitude and bioavailability of nitrogen inputs are important for understanding ecosystem function (Nixon et al. 1996). Numerous anthropogenic point and non-point sources of nitrogen, in particular wastewater discharge and agricultural runoff (Nixon and Pilson 1983), have been identified as the primary causes of eutrophication (Valiela et al. 1997, Paerl et al 1998, Pinckney et al. 2001). An increasing number of occurrences of estuarine hypoxia/anoxia have been linked to higher nitrogen and organic matter delivery from developed watersheds (de Jonge et al. 1994, Paerl et al. 1998, Persky 1986). Hence, with coastal ecosystems under increasing pressure due to development and rising populations (Vitousek et al. 1997), insight into nutrient source, reactivity, and the processes responsible for their transformations has become increasingly important.

The two main forms of dissolved inorganic nitrogen (DIN) in groundwater are nitrate (NO_3^-) and ammonium (NH_4^+). Groundwater flow exposes DIN to different physico-chemical environments that impact the chemical composition of the fluid. In particular, the transition from fresh to saline groundwater constitutes a favorable setting for chemical and microbially-mediated

processes that alter the form, bioavailability, and concentration of nutrients (e.g. Moore 1999). Ammonium can be converted to NO_3^- under oxic conditions (nitrification), combined with NO_2^- to produce N_2 (anaerobic ammonium oxidation, anammox) or taken up or released in the creation/breakdown of organic matter; NH_4^+ is also subject to cation exchange. In addition to being biologically assimilated, NO_3^- can serve as a terminal electron acceptor leading to N_2 (denitrification (DNF) or anammox via NO_2^-) or NH_4^+ (dissimilatory nitrate reduction to ammonium, DNRA). Thus, the speciation of the groundwater-associated inorganic nitrogen both impacts and results from the microbial processes occurring along the transport route. Because DNF and anammox constitute nitrogen sinks by converting bioavailable N into dinitrogen gas, these processes can mitigate inputs of NO_3^- and reduce eutrophication of receiving waters.

Rates and controls of microbially mediated nitrogen transformation in coastal environments have been examined previously. The influence of sulfide inhibition on nitrification in estuarine and marsh sediments has been demonstrated both in the laboratory and the field (Joye and Hollibaugh 1995; Tobias et al. 2001). Several studies have employed both field and laboratory methods to examine the controls on DNF (Rysgaard et al. 1999; An and Joye 2001; Tobias et al. 2001), including temperature, substrate availability, and sulfide or oxygen concentration (Tiedje et al. 1982; Kelly-Gerreyn et al. 2001; An and Gardner 2002). The rates of DNRA have been the focus of several field studies investigating the fate of DIN in coastal sediments (Tobias et al. 2001; Gardner et al. 2006; Kartal et al. 2007). The abundance of electron donors and acceptors are critical factors determining the relative importance of DNRA vs. DNF. The potential importance of anammox (Thamdrup and Dalsgaard 2002; Risgaard-Petersen et al. 2003) in coastal areas at present is unclear. Additionally, sorption of NH_4^+ via ion exchange, a process sensitive to variations in salinity, can remove a significant portion of NH_4^+ from solution

and thereby affect transport and speciation of nitrogen (Seitzinger et al. 1991; Morse and Morin 2005; Böhlke et al. 2006).

Here we present an assessment of the fate of DIN in the groundwater discharge area of a coastal marsh-upland environment at Moses Hammock, located on Sapelo Island, Georgia, United States of America. Field observations in winter, spring and summer demonstrated a recurring change in the $\text{NO}_x/\text{NH}_4^+$ ratio of groundwater near the upland-marsh transition zone over spring-neap tidal cycles. Motivated by these field observations, targeted laboratory experiments were performed to quantify key processes in the nitrogen cycle. Field and laboratory findings were integrated into a variable density reactive transport model representing a vertical 2D cross section of the upland. Model simulations were carried out for both spring and neap tide conditions to identify the processes responsible for the observed variation in DIN speciation. Finally, building on the calibrated model and expanding beyond the relatively pristine conditions of Moses Hammock, simulations were performed to assess the potential impact of discharge from a septic tank on groundwater biogeochemistry and to quantify the N removal potential in the aquifer.

METHODS

Study site

Moses Hammock (MH) is a small (approximately 0.08 km²), sandy coastal hammock located on the western side of Sapelo Island, Georgia (Fig. 5.1). Moses Hammock is bordered to the west by the Duplin River whose 11 km² watershed is dominated (~80%) by *Spartina alterniflora* saltmarsh and unvegetated mudflats (Pomeroy and Wiegert 1981). The Duplin has a

tidal amplitude of approximately 3.4 m for spring tide (Chalmers 1997), with a salinity, averaged over all sampling periods, of 25.7.

Aside from seasonal use as a hunting camp, Moses Hammock is subjected to little anthropogenic DIN and DOM loading. The upland area of MH is forested and is separated from the upland of Sapelo Island by extensive saltmarsh areas. The freshwater lens on MH is isolated from the saline aquifer underlying the island (Schultz and Ruppel 2002). A 80 m long transect of partially screened, groundwater monitoring wells (< 5 m sampling depth) runs perpendicular to the Duplin River from the saltmarsh to the approximate center of Moses Hammock (Schultz and Ruppel 2002; Snyder et al. 2004; Fig. 5.1).

Field and laboratory methods

Well sampling

The MH well transect was sampled during low tide on consecutive spring and neap tides in August of 2003 and June 2004. Additional spring tide samplings occurred in April 2002, and January 2004; and additional neap tide samplings occurred in April 2003 and 2004, December 2004, and July 2006. Groundwater (GW) was collected for geochemical analysis using a peristaltic pump and rigid (acid-cleaned) polyethylene tubing. An Orion[®] galvanic dissolved oxygen probe (model no. 084260) was placed in the plastic receptacle and the groundwater was allowed to overflow the bottle ensuring minimum atmospheric contamination of the sample. The groundwater was pumped until the temperature and dissolved oxygen measurements stabilized and then a sample was collected into a gas tight bottle. Sub-samples were later dispensed for various analyses in the laboratory.

A small volume of water (~1.5 mL) was collected via a plastic syringe and passed through a flow-through cell containing a Sensorex[®] 450C flat surface combination pH/reference electrode. Sulfide concentration was determined via colorimetry on a 2 mL sub-sample that was fixed in the field with zinc acetate (Cline 1969). Dissolved inorganic carbon (DIC) was determined on a 2 mL aliquot that was introduced into a He-purged, crimp-sealed 14 mL headspace vial (2 mL was removed from the vial prior to sample addition), which was then acidified with 0.1 mL of concentrated phosphoric acid. Carbon dioxide concentrations were determined by injecting 1 mL of the headspace gas into a Shimadzu[®] GC-14A gas chromatograph fitted with a Carbosphere[®] column (Alltech Associates, Inc.) to separate CO₂ and CH₄, a methanizer to convert CO₂ to CH₄, and a flame ionization detector to detect CH₄ signals. Concentrations of CO₂ were determined by comparison of sample areas to the area obtained from a certified mix (10.04% CO₂ in Helium, Scott Specialty Gases[®], and 10.0% CH₄ in Helium, National Welders Supply Co.[®]), and linearity of the detector signal was confirmed over a range of diluted standards.

Approximately 30 mL of sample was filtered (National Scientific[®], Target 0.2 μm pore size) and stored at 4 °C for subsequent determination of nutrient species (nitrite, and nitrate + nitrite (NO_x)). A 5 mL aliquot of the filtered sample was transferred immediately to a 7 mL glass vial and fixed with 0.2 mL of phenol solution (9.6% phenol by volume) for determination of NH₄⁺ concentration using colorimetry (Solorzano 1969). Nitrite and NO_x concentrations were determined by vanadium reduction and NO detection using an Antek[®] 745 NO₃⁻/NO₂⁻ reduction assembly and 7050 NO analyzer. Nitrate concentration was calculated as the difference between NO_x and NO₂⁻.

For determination of reduced iron (Fe^{2+}), sulfate (SO_4^{2-}), chloride (Cl^-), and dissolved organic carbon (DOC) concentrations, 20 mL of sample was filtered into a glass vial and acidified with 100 μL of concentrated nitric acid. Reduced iron was measured using standard colorimetric methods (Stookey 1970). Sulfate and Cl^- concentrations were determined by ion chromatography on a Dionex[®] DX 500. Dissolved organic carbon was measured using a Shimadzu[®] total organic carbon analyzer (TOC-5000). Acidified samples were sparged with CO_2 free air for 15 minutes prior to DOC measurement to remove inorganic carbon. Salinity (S) was calculated from Cl^- concentrations, $S = (35.453 \cdot 10^3 \cdot [\text{Cl}^-]) / (1 + 1.80655 \cdot 35.453 \cdot 10^3 \cdot [\text{Cl}^-])$ where $[\text{Cl}^-]$ is in mmol L^{-1} (Mantyla 1987). Concentrations of geochemical species were compared between spring and neap tides by single factor analysis of variance (ANOVA).

Pressure head data collection

In December 2005 and April 2006, monitoring wells 0217, 0201, and 0214 (Fig. 5.1) were instrumented with pressure data loggers (Onset[®] HOBO Water Level Logger, model U20-001-001) that remained submerged for the duration of the data collection (~ 2 months). In addition, well 0201 was instrumented with a second pressure logger suspended in the well housing above the water level to correct for changes in barometric pressure. All pressure data was corrected to a common depth and data from wells 0201 and 0214 was used to constrain the imposed pressure gradient across the model domain.

Radium sampling

GW samples were collected in August 2004 for the determination of the activities of ^{228}Ra and ^{226}Ra . Approximately 5 L of GW was collected following the initial geochemical

sampling at multiple times during a 4-day period. The GW sample was passed through a column of MnO₂-coated acrylic fiber at a rate of < 1 L min⁻¹ to quantitatively collect the radium (Moore 1976). The fiber was collected in a plastic bag and the long-lived radium isotope activities were determined in a gamma ray spectrometer (Moore 1984). Twenty liter samples were collected from the Duplin River and processed in the same manner.

Ammonium adsorption

Ammonium adsorption coefficients were determined for sediments collected from three depths (0.9 – 1.0 m, 1.2 – 1.3 m, and 2.0 – 2.1 m) within the saturated zone of the MH upland within 1.5 m of well 0201. For all three depths, incubations were carried out at five salinities ranging from 1 to 28. Incubations were performed in duplicate on 1.2 g of wet sediment in 15 ml centrifuge tubes amended with 10 mL of artificial seawater at the appropriate salinity and a final NH₄⁺ concentration of 100, 500, or 1000 μmol NH₄⁺ L⁻¹. Concentrations of dissolved and exchangeable NH₄⁺ were quantified after a 24 hr incubation; the exchangeable NH₄⁺ was determined by adding 10 mL of 2 N KCl to the sediment (after collection of the supernatant) (Seitzinger et al. 1991; Morse and Morin 2005).

Modeling methods

The MH well transect was represented by a 60 x 4.5 m saturated model domain (dashed line in Fig. 5.1, encompassing wells 0201 to 0214 and containing the entire salt-freshwater transition), in which the distribution of 23 chemical species was computed for spring and neap tide conditions, subject to transport and reaction. The concentrations of biogeochemical constituents were calculated subject to advective and diffusive/dispersive transport and reactions:

$$\frac{\partial \xi C_i}{\partial t} = \nabla \cdot (D^* \nabla C_i - \mathbf{u} C_i) + \xi R_i \quad (5.1)$$

where ξ is porosity for solutes and $1 - \text{porosity}$ for solids, D^* is the dispersion tensor. \mathbf{u} is the Darcy velocity, derived from the computed pressure distribution taking into account density variations as a function of salinity. For solids, the transport terms were set to 0. A detailed description of the governing equations is given in Appendix 5.1. Porosity was set to the average value measured in multiple upland cores for depths within the model domain, and the intrinsic permeability was set to the average of all hydraulic conductivities reported for MH (Schultz and Ruppel 2002), including the values derived from larger scale estimates which account for any heterogeneity in the aquifer. The longitudinal dispersivity (0.3 m) for the 60 m long model domain was set to an average value for sandy sediments reported in Moltyaner et al. (1993). Transverse dispersivity (α_T) was set to 10% of the longitudinal dispersivity. Model parameters, including those for the reactions (see below) are assumed spatially constant, and do not reflect potential but unknown variations in subsurface characteristics (for a list of parameters see Appendix 5.3).

Model setting

At the upland model boundary, concentrations and pressure were imposed based on field measurements averaged over multiple sampling dates (*upland*; Table 5.1). Top and bottom boundaries of the model domain are closed, reflecting the low direct impact of rain over long time periods ($\sim 130 \text{ cm yr}^{-1}$; SINERR/GCE/UGAMI weather station at Marsh Landing, Sapelo Island, Georgia). On the saltwater side, pressure was imposed based on the field data, and chemical constituents were subject to either in- or out- flow. Outflowing solute fluxes were derived from computed concentrations inside the model domain, while the composition of the

inflowing water is a mixture of Duplin water and well 0217, whose screening depth reflects deep marsh pore water (Table 5.1). The relative contribution of these two water bodies was determined based on measured salinities, so that they match the salinity for well 0201, located next to the domain boundary. The contribution of 0217 water varied between spring (35%) and neap (78%) tides with the remaining water attributed to the Duplin.

In the simulation investigating the potential impact of increased anthropogenic forcing in hammock environments, elevated NH_4^+ , NO_3^- and DOM concentrations were imposed in a 1 m depth segment (-2 to -3 m) at the upland boundary. The septic plume composition was based on DeSimone et al. (1996; Table 5.1).

Reaction network

The reaction network encompasses primary reactions involving the reduction of organic matter, secondary reactions involving the re-oxidation of reduced metabolites, mineral precipitation and dissolution, sorption-desorption and acid-base equilibria (see Appendix 5.2), and was parameterized using literature and experimentally determined values (Appendix 5.3). The degradation of organic matter was assumed to be first order with respect to the available reactive organic matter, which includes all DOM in the model. The contribution of different pathways to the total rate of organic matter degradation (“primary reactions”) was implemented using Monod expressions (Eq. 5.2). If the concentration of the oxidant for any given primary reaction is sufficiently high the reaction proceeds essentially unhindered; however, at low concentrations of the electron acceptor, its availability becomes limiting, allowing other metabolic pathways to occur. The breakdown of organic matter was formulated as a progression of primary reactions, from aerobic respiration, to dissimilatory nitrate reduction, manganese

oxide reduction, iron oxyhydroxide reduction, sulfate reduction and methanogenesis, reflecting differences in energy yield (e.g. Froelich et al. 1979; Hunter et al. 1998; Appendix 5.2):

$$pr_j = \left(k_{\text{DOM}} \cdot [\text{DOM}] - \sum_{n=1}^{j-1} pr_n \right) \cdot \frac{[C]_j}{[C]_j + Km_j} \quad (5.2)$$

where pr_j refers to the rate for primary reaction j , k_{DOM} is the first order rate constant, $[\text{DOM}]$ is the dissolved organic matter concentration, Km and $[C]$ are the half saturation constant and the concentration of the respective terminal electron acceptor (O_2 , NO_3^- , MnO_2 , $\text{Fe}(\text{OH})_3$, and SO_4^{2-}) in reaction j , respectively.

Special consideration was given to the partitioning of NO_3^- between the two dissimilatory nitrate reduction pathways implemented in the model, as the resulting N-products differ in their bioavailability. The relative importance of DNF and DNRA has been linked to two factors that were deemed pertinent to this groundwater system: 1) the concentration of sulfide (TS), and 2) the ratio of dissolved organic matter to nitrate (DOM/NO_3^-). At relatively low sulfide concentrations ($< 20 \mu\text{mol L}^{-1}$) a strong inhibitory effect of sulfide on DNF – but not DNRA – was observed in laboratory incubations of intertidal sediment from a site on the Satilla River, GA (W. Porubsky submitted, Chapter 2). This observed inhibition of DNF by sulfide was expressed via the fraction of the DNF rate that occurs at a given sulfide concentration:

$f_S = \left(\max \left(TS_{\text{DNF}}^{\text{MIN}}, [TS] \right) / TS_{\text{DNF}}^{\text{MIN}} \right)^{0.675}$, where $TS_{\text{DNF}}^{\text{MIN}}$ is a minimum total sulfide concentration of $1.5 \mu\text{mol L}^{-1}$ that causes inhibition.

The ratio of the electron donor to electron acceptor (reflected by the DOM/NO_3^- ratio) has been proposed as a control on the balance of DNF and DNRA (Tiedje et al. 1982). A linear relationship between the DOM/NO_3^- and the DNRA/DNF from intertidal sediments was applied, with higher DOM/NO_3^- ratios correlating with increased DNRA activity relative to DNF (W.

Porubsky submitted, Chapter 2): $(DNRA/DNF) = 0.0629 \cdot (DOM/NO_3^-) - 0.4481$; where $DNRA/DNF$ represents the ratio of the rates of DNRA and DNF. Combined, the ratio of DNRA/DNF and the inhibition of DNF by sulfide yield the fraction of the total NO_3^- reduction rate available to DNF ($pr_{2,DNF}$) and DNRA ($pr_{2,DNRA}$), respectively:

$$pr_{2,DNF} = pr_2 \cdot f_S \cdot f_R \quad (5.3a)$$

$$pr_{2,DNRA} = pr_2 - pr_{2,DNF} = pr_2 (1 - f_S \cdot f_R) \quad (5.3b)$$

where f_R is the ratio of DNF to the total nitrate reduction rate,

$$f_R = (DNF / (DNF + DNRA)) = (1 + (DNRA/DNF))^{-1}.$$

The seven primary reactions lead to the production of reduced inorganic species which can then be re-oxidized by both chemical and microbially-mediated reactions (Appendix 5.2).

These secondary reactions were described by bimolecular rate laws (Hunter et al. 1998):

$$sr_j = sk_j \cdot [RED] \cdot [OX] \quad (5.4)$$

where sr_j is the j^{th} secondary reaction rate, sk_j is the j^{th} apparent rate constant, and [RED] and [OX] represent the concentration of the reductant and the oxidant respectively. In addition, sulfide inhibition of nitrification (sr_4 ; Appendix 5.2) was taken into account through an inhibition factor (f_{NITR}), which was used as a multiplier in Eq. 5.4. It was obtained from fitting the data in Joye and Hollibaugh (1995): $f_{NITR} = \max(0, 1 - 41.7 \cdot [TS] - 5.8 \cdot [TS]^2)$ where the concentration of total sulfide ([TS]) is in mmol L^{-1} .

Mineral precipitation-dissolution reactions (Appendix 5.2) were considered reversible and dependent on the saturation state Ω_j of each mineral, determined from the activities of the species involved in the precipitation-dissolution reaction and the equilibrium constant (Appendix 5.3). The general forms of the precipitation and dissolution reactions, respectively, are:

$$\begin{aligned} mr_j^{\text{PREC}} &= mk_j^{\text{PREC}} \cdot (\Omega_j - 1) \quad \text{for } \Omega_j \geq 1 \\ mr_j^{\text{DISS}} &= mk_j^{\text{DISS}} \cdot [C_j] \cdot (1 - \Omega_j) \quad \text{for } \Omega_j < 1 \end{aligned} \quad (5.5)$$

where mr_j^{PREC} and mr_j^{DISS} are the precipitation and dissolution rates for the j^{th} mineral, mk_j^{PREC} and mk_j^{DISS} are the corresponding apparent rate constants, and C_j is the concentration of mineral j . Concentrations of chemical species subject to rapid acid-base equilibration were determined from the modeled components DIC ($= \text{H}_2\text{CO}_3 + \text{HCO}_3^- + \text{CO}_3^{2-}$) and TS ($= \text{H}_2\text{S} + \text{HS}^- + \text{S}^{2-}$), assuming local equilibrium, taking into account the ionic strength (derived from salinity) and the pH of the groundwater. The latter was obtained by identifying the pH at which the modeled alkalinity ($= 2 \text{CO}_3^{2-} + \text{HCO}_3^- + \text{OH}^- + 2\text{S}^{2-} + \text{HS}^- - \text{H}^+$) was consistent with DIC and TS concentrations. In an iterative approach (Luff et al. 2001), at each computational node and timestep, activity coefficients were expressed as a function of ionic strength, and $[\text{H}^+]$ was computed using a Newton-Raphson root finding algorithm.

Reflecting the rapid and reversible exchange between dissolved and adsorbed NH_4^+ (Rosenfeld 1979), ammonium sorption was also part of the equilibration module (Appendix 5.2) in which total ammonium was distributed between the sorbed and dissolved phase, using the experimentally determined value of the apparent adsorption coefficient K_n as a function of salinity.

RESULTS

Field and laboratory data

Groundwater biogeochemistry

The well transect at the Moses Hammock site was sampled at low tide during four spring tides and six neap tides. There were only small differences in the median salinity value for each

well (Fig. 5.2A) in spring versus neap tides; the highest salinities were observed near the saltmarsh-upland boundary and salinity decreased toward the upland. The range of salinity was greatest in well 0214 which was in the saltwater/freshwater transition zone (Fig. 5.2A), and the observed salinity range in well 0204 was greater during spring than during neap tides.

Dissolved organic carbon (DOC) concentrations were lowest in well 0212 located furthest upland (Fig. 5.2B). Dissolved organic carbon concentrations were higher in the other wells, and were generally higher and more variable during neap than spring tide (Fig. 5.2B). Even the substantially higher median DOC concentrations in wells 0217 and 0201 did not constitute a significant difference between spring and neap tide ($p > 0.5$ for well 0201 and $p > 0.2$ for well 0217, Fig. 5.2B). Concentrations of DOC in the Duplin were similar to those in wells 0217 and 0201 during spring tides (Fig. 5.2B).

Median concentrations of oxidized nitrogen species ($\text{NO}_x = \text{NO}_2^- + \text{NO}_3^-$) were below $10 \mu\text{mol L}^{-1}$ in all wells during neap tides (Fig. 5.2C). During spring tides, however, the two wells closest to the Duplin (0217 and 0201) exhibited median concentrations of approximately $20 \mu\text{mol NO}_x \text{ L}^{-1}$. Spring tide NO_x concentrations in well 0201 were significantly higher than neap tide concentrations ($p < 0.05$). NO_x concentrations in well 0212, the furthest upland, were approximately $1 \mu\text{mol L}^{-1}$ during both spring and neap tides and below that in the Duplin (Fig. 5.2C).

The median NH_4^+ concentration in well 0212 was approximately $2 \mu\text{mol L}^{-1}$ during both spring and neap tides (Fig. 5.2D). During spring tides, NH_4^+ concentrations were $\leq 10 \mu\text{mol L}^{-1}$ in wells 0217, 0201, and 0202 (Fig. 5.2D). Ammonium concentrations reached approximately $20 \mu\text{mol L}^{-1}$ in wells 0204 and 0214 for both spring and neap tides. Wells 0217, 0201, and 0202 had

significantly ($p < 0.05$) higher NH_4^+ concentrations (by 4 times) during neap tides compared to spring tides (Fig. 5.2D).

Groundwater transport

Data retrieved from the pressure loggers showed larger diurnal pressure fluctuations during spring tides compared to neap tides but a rather constant diurnally averaged pressure gradient. Diurnal variations in pressure were highest in well 0217 and decreased toward the upland as the tidal influence was attenuated. Precipitation events were evident in the observed freshwater heads, but showed little effect on the pressure gradient across the domain (see Appendix 5.4).

The Duplin River was significantly enriched in ^{226}Ra and ^{228}Ra relative to surface seawater and exhibited a high $^{228}\text{Ra}/^{226}\text{Ra}$ activity ratio. The $^{228}\text{Ra}/^{226}\text{Ra}$ activity ratio of well 0201 qualitatively matches that measured in the Duplin (Fig. 5.3). Well 0201 had the highest $^{228}\text{Ra}/^{226}\text{Ra}$ activity ratio and while well 0217 was nearest to the river, it had a lower $^{228}\text{Ra}/^{226}\text{Ra}$ activity ratio and higher ^{226}Ra concentration than the river or wells 0201 and 0202. Well 0212 did not experience elevated salinity levels, thus rates of Ra desorption were low as reflected in the low Ra concentrations (Fig. 5.3).

Ammonium adsorption

Ammonium adsorption coefficients (K_n) were determined experimentally at three depths in the Moses Hammock upland within 1.5 m of well 0201 (see Appendix 5.5). K_n values were lowest in the 0.9 – 1.0 m depth and highest in the 1.2 – 1.3 m depth. The K_n values for the deepest depth (2.0 – 2.1m), located in the model domain and hence used in the simulations, fell

between those from the shallow and mid-depth samples. The K_n - salinity relationship from the deepest depth was used in the model because it fell between the other two values. Experimental results showed a decrease of K_n with increasing salinity, with a K_n value of approximately 1.4 at a salinity of 28 and a K_n value of 3.5 at 1.

Modeling results

To assess the dominant causes for the observed spring-neap variation in the Moses Hammock subsurface biogeochemistry, model simulations were run to steady state for the two endmember settings. Due to the absence of a significant difference in the tidally averaged pressure gradient between spring and neap tides, simulations were run with the same tidally averaged freshwater head (Appendix 5.3), which resulted in saline water infiltrating approximately 50 m into the upland (Fig. 5.4). The model results match the salinity values determined in the field, with wells 0204 and 0214 being located in the fresh-saltwater transition zone (Figs. 5.2A and 5.4).

The mixing of two water bodies of distinct redox chemistry and the breakdown of DOM are the main drivers for biogeochemical reactions in groundwater. Both factors differ between neap tide and spring tide, with the inflowing spring tide water lower in DOM and NH_4^+ but higher in O_2 and NO_3^- (Table 5.1). Because total DOM measurements may provide a poor approximation of the reactive substrate concentrations, and due to the large range of DOM degradation rates reported in the literature (Hunter et al. 1998 and references therein), the DIC concentrations measured in the field were used to constrain the DOM degradation rate, $R = k_{\text{DOM}} \cdot [\text{DOM}]$. The DOM concentration at the upland boundary, located between wells 0214 and 0212, was set to the average value determined in these wells (Fig. 5.2B, Table 5.1). The

inflowing DOM concentration at the seaward side was determined from the mixing of Duplin and well 0217 water for spring and neap tides respectively (Fig. 5.2B, Table 5.1). Iteratively adjusting the value of k_{DOM} , appropriate DIC concentrations were obtained for k_{DOM} on the order of 10^{-11} s^{-1} (Appendix 5.3), well within the range reported in Hunter et al. (1998).

Modeled NO_3^- values reached a maximum of approximately $25 \mu\text{mol NO}_3^- \text{ L}^{-1}$ at the saltmarsh-upland boundary (Fig. 5.5A) in spring tide simulations. Nitrate concentrations of approximately $5 \mu\text{mol L}^{-1}$ persist to approximately 6.5 m into the domain. Nitrate concentrations in the neap tide simulation matched the values measured in the field (Figs. 5.2C, 5.5B), and were much lower than in the spring tide simulation.

Simulated dissolved ammonium ($\text{NH}_4^+_{\text{DISS}}$) concentrations were approximately $10 \mu\text{mol L}^{-1}$ within 10 m of the saltmarsh-upland boundary (Fig. 5.5C) and increased to approximately $40 \mu\text{mol L}^{-1}$ at 20 m under spring tide conditions. Dissolved NH_4^+ concentrations in neap tide simulations were approximately 3.5 times higher than the corresponding spring tide values (Figs. 5.5C and D). Modeled $\text{NH}_4^+_{\text{DISS}}$ concentrations between 10 and 20 m showed a similar pattern for both spring and neap tide simulations and were slightly higher than the concentrations determined in the field (Figs. 5.2D, 5.5C and D).

Adsorbed ammonium ($\text{NH}_4^+_{\text{ADS}}$) presented a similar pattern as $\text{NH}_4^+_{\text{DISS}}$ at the saltmarsh-upland boundary, where the concentration was approximately $20 \mu\text{mol dm}^{-3}$ (Fig. 5.5E) under spring tide conditions. Further into the domain where salinity was lower, the ratio of $\text{NH}_4^+_{\text{ADS}}$ to $\text{NH}_4^+_{\text{DISS}}$ increased. Adsorbed NH_4^+ concentrations were elevated at the saltmarsh-upland boundary in neap tide simulations, due to higher $\text{NH}_4^+_{\text{DISS}}$ concentrations (Fig. 5.5F).

Modeled peak nitrification rates were highest ($2.8 \mu\text{mol N m}^{-3} \text{ h}^{-1}$) in the spring simulation and were confined within 1 m of the saltmarsh-upland boundary. Nitrification rates

declined rapidly with increasing distance from the marsh and were O₂ limited (data not shown). Nitrification showed a similar distribution in the neap tide simulation with peak rates approximately 50% lower than spring rates. Modeled peak DNF rates in the spring tide simulation were also highest near the saltmarsh-upland boundary ($0.2 \mu\text{mol N m}^{-3} \text{ h}^{-1}$) where NO₃⁻ concentrations were highest (Fig. 5.5A). Rates quickly decreased with distance into the upland and were limited by NO₃⁻ availability. Peak DNF rates were 3 times lower in the neap tide simulation than in the spring tide simulation. Lower DNF rates in the neap tide simulation correlated with both lower NO₃⁻ concentrations (Fig. 5.5B) and higher DOM concentrations (data not shown). The resulting higher DOM/NO₃⁻ ratio favored dissimilatory nitrate reduction to ammonium (DNRA), which exhibited its peak rates ($0.2 \mu\text{mol N m}^{-3} \text{ h}^{-1}$) near the saltmarsh-upland boundary under neap tide conditions. As with DNF, the maximum DNRA rate corresponded to zones with the highest NO₃⁻ values. Under neap tide conditions peak DNRA rates were approximately 3 times higher than the corresponding peak DNF rates, while at spring tide, the peak DNRA rates were approximately 20% lower than the corresponding DNF rates.

Septic Inputs

The septic effluent resulted in a DOM and DIN rich plume traveling towards the marsh (dark colors, Figs. 5.6A and B) with the plume being pushed upward due to the presence of the fresh-saltwater interface. Compared to the pristine conditions, the septic plume increased the DOM and DIN loading 1.5 and 50 fold, respectively, but only led to a ~15% increase in the integrated DOM pool, and a 5 fold increase in the integrated DIN pool. Rates of DNF were highest and dominated the dissimilatory reduction of NO₃⁻ within 10 m of the plume discharge area. Dissimilatory nitrate reduction to ammonium dominated NO₃⁻ reduction further

downstream. DNF was capable of removing ~35% of the NO_3^- originating from the septic tank while DNRA removed ~40% of the plume NO_3^- .

DISCUSSION

Microbial processes

The concentration and speciation of dissolved inorganic nitrogen (DIN) can be altered by a number of microbially mediated processes including nitrification, denitrification, dissimilatory nitrate reduction to ammonium, and anammox. While the anammox process is potentially capable of removing N from the subsurface, it occurs at only low rates in nearby coastal marsh sediments (~6% of the total N_2 production; W. Porubsky submitted, Chapter 2), and has not yet been documented in groundwater, so it was not considered in the current model.

Nitrification could potentially impact the redox switch observed in well 0201 by oxidizing the higher NH_4^+ pool around well 0201 during neap tide. However, simulations indicate that nitrification was of minor importance within the model domain. While modeled peak nitrification rates are on the low end of nitrification rates reported in the literature (Böhlke et al. 2004; Vervaet et al. 2004; Smith et al. 2006) simple mass balance considerations support this general finding. If all O_2 in the 0-10 m zone near well 0201 was used to fuel nitrification, this would change NO_3^- by <1%. Similarly, with low O_2 concentrations in the inflowing water, compared to NO_3^- during both spring and neap tides, complete use by nitrification would maximally increase the NO_3^- flux by ~40%, which is insufficient to explain the observed variation in well 0201. Therefore, while nitrification was occurring in the domain, O_2 limitation restricts its importance in the upland aquifer.

Since DNF and DNRA impact concentration, speciation and bioavailability of the DIN pool in different ways, it is important to understand the factors regulating the balance of the two processes. Potential factors that can control the balance of DNF and DNRA include temperature (Kelly-Gerreyn et al. 2001), O₂ content (Fazzolari et al 1998; Silver et al 2001), sulfide concentration (An and Gardner 2002), and the DOM/NO₃⁻ ratio (Tiedje et al. 1982). Neither temperature nor O₂ are likely causes for any potential switch between the DNF and DNRA at MH due to the small range of temperatures encountered over a spring-neap tidal cycle (average 1°C difference in well 0201 between spring and neap tides, with an approximately 3°C seasonal range) and the limited change in the O₂ content (5 - 15 μmol L⁻¹) observed over both spring-neap tidal cycles and throughout the year. Similarly, measured sulfide concentrations in the wells near the upland-marsh boundary were typically zero, and model simulations do not indicate significant sulfide levels near the upland-marsh boundary, so sulfide could not be responsible for a switch between DNF and DNRA. Sulfide inhibition of both DNF and nitrification at [H₂S] ≤ 20 μmol L⁻¹ (Gould and McCready 1982; Jensen and Cox 1992; Joye and Hollibaugh 1995) are unlikely to impact the balance of the two processes in the area surrounding well 0201. However, differences in the DOM content of the inflowing saline water during spring tide (0.4 mmol C L⁻¹) and neap tide (0.6 mmol C L⁻¹) alters the DOM/NO₃⁻ ratio in the area around well 0201 (Table 5.1). The changes in DOM concentration shift the balance of DNF and DNRA toward DNRA under neap tide conditions (Eq. 10), which promotes higher NH₄⁺ concentrations in the area around well 0201 (Fig. 5.5D).

To assess whether the differences in DNF and DNRA rates were large enough to cause the observed switch in the composition of DIN between spring and neap tides, the rates of DNF and DNRA were integrated over the 10 m nearest the marsh-upland boundary over which

variations in DIN pools were observed (i.e. well 0201, Fig. 5.5) for both spring tide and neap tide endmember conditions. Under spring tide conditions, $\sim 32 \mu\text{mol NO}_3^- \text{ d}^{-1}$ was reduced by DNF, about 11 times more than under neap tide conditions. However, DNRA rates exceeded DNF rates by a factor of 2-12 for spring and neap tides, respectively. A higher rate of DNRA under spring tide conditions ($\sim 57 \mu\text{mol N d}^{-1}$) than under neap tide conditions ($\sim 33 \mu\text{mol N d}^{-1}$) contradicts the observed lower NH_4^+ concentrations in well 0201 at spring tide and thus is not capable of causing the observed redox switch.

Higher NH_4^+ concentrations under neap conditions could result from increased NH_4^+ production via organic matter degradation of a larger DOM pool. However, the integrated net rate of NH_4^+ production, resulting from production by the degradation of DOM via primary reactions, DNRA, and losses from nitrification, was similar under spring and neap tide conditions ($\sim 94 \pm 11 \mu\text{mol N d}^{-1}$). Although DNF rates showed a stark difference between spring and neap tides, the rates were much lower than DNRA rates and total NH_4^+ production rates, both of which showed much lower spring-neap variation (22-42%) than DNF. The lack of variability in net NH_4^+ production between spring and neap tide conditions can therefore not account for the observed change in NH_4^+ concentration in well 0201.

Ion exchange processes

Laboratory assays showed a strong dependency of ammonium sorption on pore water salinity, such that as the salinity increases, NH_4^+ desorbs (Appendix 5.5; Seitzinger et al. 1991). The sorbed pool is particularly sensitive to changes in salinity at the fresh endmember, e.g. associated with an inland migration of the saltwater wedge. In the field, salinity varied over a range of 5 to 20 in well 0214. To assess the potential impact that such a shift would have on the dissolved and adsorbed NH_4^+ pools, we compared the sorbed NH_4^+ pool for two salinity

distributions consistent with the observational data – one as shown in Fig. 5.4, the other with a saltwedge extending further inland but retaining the discharge face. After re-equilibrating the total ammonium pool, the adsorbed NH_4^+ pool in the entire domain was lower by $\sim 2\%$ in the setting with the saltwater intruding further inland. Averaged over the entire domain, the difference of 0.6 moles of NH_4^+ corresponds to an increase of $\sim 3.3 \mu\text{mol L}^{-1}$ in dissolved ammonium, which exceeds the impact of microbial processes or inflow over the spring-neap tidal cycle. However, there is no indication for any significant salinity fluctuation near well 0201, and the time of travel for the liberated NH_4^+ at the saltwater-freshwater transition zone would preclude it from impacting the NH_4^+ concentration in well 0201 over a spring-neap tidal cycle, and thus influencing the observed switch in N speciation in the well. Thus, sorption-desorption mainly changes bioavailability of NH_4^+ locally, and only a prolonged change in the freshwater flow (i.e. drought conditions) could result in long term shifting of the salt wedge and lead to impacts on the DIN speciation downstream.

Transport

The two radium isotopes, ^{226}Ra and ^{228}Ra , have half-lives of 1600 and 5.7 yrs, respectively, and are continually produced from their long-lived parents, ^{232}Th and ^{230}Th . As a consequence of its shorter half life, ^{228}Ra activity is replenished more quickly after removal of pore fluid (Moore 2003). The substantial Ra activities and high $^{228}\text{Ra}/^{226}\text{Ra}$ activity ratio measured in the Duplin River are consistent with a source of groundwater similar to that sampled at well 0201. The radium data indicates that the area surrounding well 0201 is frequently flushed and that flushing decreases inland (Fig. 5.3). The impact of the transport of the infiltrating water with different chemical make-ups is twofold: 1) it leads to a direct change in concentrations in

the domain, and 2) it impacts the physico-chemical and microbial processes occurring within the domain.

At the marsh/upland boundary, flow out of the domain is confined to the upper meter while below that flow is directed into the domain, adding both NO_3^- and NH_4^+ to the area around well 0201 thus directly impacting the N speciation. The mass of NH_4^+ that enters the area around well 0201 under neap tide conditions is ~3 times greater than the production of NH_4^+ from DNRA and approximately 1.5 times greater than the integrated net NH_4^+ production within 10 m of the marsh/upland boundary and thus dominates the pore water composition. Because of temporal variations in source water composition (Table 5.1) approximately 4 times more NO_3^- enters the domain under spring tide conditions than under neap tide, while conversely, under neap tide conditions, approximately 4 times more NH_4^+ is transported into the domain. Differences in NO_3^- and NH_4^+ concentrations in the saline inflowing water between spring and neap tides is the dominant factor influencing the switch between N species in the area surrounding well 0201.

At Moses Hammock, the observed changes in nitrate and ammonium concentrations in well 0201 are predominantly driven by changes in the inflowing saline water. The factors that influence the N-speciation of the marsh porewater entering the upland model domain over spring-neap tide cycles remain an area for further examination. The DIN speciation and concentrations of the Duplin River did not vary over spring/neap tidal cycles (Figs. 5.2C and D). Since the changes in the inflowing DIN can not be linked to variations in the NO_3^- concentration of the Duplin, the variations must occur in the marsh porewater. Nitrification rates reported for surficial saltmarsh sediments ($0.4\text{-}6 \text{ mmol N m}^{-2} \text{ h}^{-1}$) are typically higher than those reported for groundwater (Anderson et al. 1997; Tobias et al. 2001; Smith et al. 2006). The increase in NO_3^-

in well 0217, and hence the infiltrating water at spring tide, may reflect a spring-neap tide variation in marsh nitrification, possibly the result of more oxygenated conditions. We further hypothesize that at Moses Hammock, decreased flushing of the upper marsh during neap tide leads to the accumulation of reduced compounds via organic matter degradation, consistent with observations in the Parker River, where variations in the NH_4^+ concentrations over spring-neap tidal cycles were driven by biogeochemical processes and flushing of the marsh, with neap NH_4^+ concentrations ~3.5 times higher than spring concentrations (Vörösmarty and Loder 1994). Under spring conditions, when the upper marsh is inundated during high tides, the upper marsh is flushed with oxygenated water that stimulates nitrification, causing the low ammonium/nitrate rich water observed in well 0217 that infiltrates with the inflowing saline water, while under neap tide the upper marsh does not flood.

Potential Anthropogenic Impact

The increase in DOM and NO_3^- concentrations promoted higher rates of DNF and DNRA in the septic plume, leading to a lower dispersal of NO_3^- relative to DOM (Figs. 5.6A and B). The spatial distribution of DNF and DNRA can be attributed to the distribution of NO_3^- , DOM, and H_2S in the domain. NO_3^- concentrations were highest in the septic inflow, resulting in the lowest DOM/ NO_3^- ratio, promoting DNF relative to DNRA. Further from the effluent source, where migration of the DOM plume and lower NO_3^- concentrations (due to removal via DNF) led to higher DOM/ NO_3^- ratios, DNRA became the dominant process. Increased DOM concentrations also migrated into the saltwater zone which, in the presence of SO_4^{2-} , stimulated sulfate reduction, leading to increased sulfide concentrations and inhibition of DNF (not shown).

CONCLUSIONS

By using a combination of field observations, laboratory assays, and modeling, we were able to examine the biogeochemical dynamics in a coastal hammock groundwater system. Model results indicate that microbial processes can impact the speciation of DIN, but the magnitude of the impact is not large enough to account for the observed switch in DIN speciation over spring-neap tidal cycles. Ion exchange constants determined from field samples indicated that ammonium sorption can lead to retardation of NH_4^+ transport and remove a significant fraction of NH_4^+ from the dissolved pool. While variations in pore water salinity can lead to desorption of significant amounts of NH_4^+ , this also does not explain the observed switch in DIN speciation because the small variations in salt concentrations observed at well 0201 together with low flow velocities prevent an efficient removal of desorbed ammonium over daily or even biweekly timescales. Instead, variations in the chemical composition of the inflowing water over spring-neap tidal cycles - driven by a variation in composition of marsh porewater, likely due to flushing and nitrification, and mixing with creek water - are predominantly responsible for the observed spring-neap redox oscillation in the upland groundwater well adjacent to the marsh.

When assessing the effect of increased anthropogenic pressure in the form of septic effluents, total model-predicted DNF increased ~15 times in response to increased DOM and DIN concentrations. While denitrification removes a significant fraction of the N loading, it is limited by the onset of sulfidic conditions and in settings with an abundance of electron donor relative to electron acceptor concentrations. Our results suggest that the conversion of nitrate to ammonium restricts the removal of the bioavailable N loading via denitrification, limiting its mitigating effect on marsh eutrophication.

ACKNOWLEDGMENTS

We thank C. Ruppel for installation of the well transect at Moses Hammock, and M. Erickson and N. Weston for assistance in the field and in the laboratory. This publication was supported by the Georgia Sea Grant Program of the National Sea Grant College, NOAA; under NOAA Grant NA04OAR4170033 (to CM), NA06RG0029-R/WQ11 and R/WQ12A (to SBJ) and by the NSF funded Georgia Coastal Ecosystems Long Term Ecological Research (LTER) program (OCE 99-82133 and OCE 06-20959).

LITERATURE CITED

- An, S., and W. Gardner. 2002. Dissimilatory nitrate reduction to ammonium (DNRA) as a nitrogen link, versus denitrification as a sink in a shallow estuary (Laguna Madre/Baffin Bay, Texas). *Marine Ecology Progress Series* 237: 41-50.
- An, S., and S. Joye. 2001. Enhancement of coupled-denitrification by benthic photosynthesis in shallow estuarine sediments. *Limnology and Oceanography* 46: 62-74.
- Anderson, I., C. Tobias, B. Neikirk, and R. Wetzel. 1997. Development of a process-based nitrogen mass balance for a Virginia (USA) *Spartina alterniflora* salt marsh: Implications for net DIN flux. *Marine Ecology Progress Series* 159: 13-27.
- Böhlke, J., J. Harvey, and M. Voytek. 2004. Reach-scale isotope tracer experiment to quantify denitrification and related processes in a nitrate-rich stream, midcontinent United States. *Limnology and Oceanography*. 49: 821-838.
- Böhlke, J., R. Smith, and D. Miller. 2006. Ammonium transport and reaction in contaminated groundwater: Application of isotope tracers and isotope fractionation studies. *Water Resources Research* 42, W05411, doi:10.1029/2005WR004349, 2006.

- Burnett, W., H. Bokuniewicz, M. Huettel, W. Moore, and M. Taniguchi. 2003. Groundwater and pore water inputs to the coastal zone. *Biogeochemistry* 66: 3-33.
- Chalmers, A. 1997. The ecology of Sapelo Island National Estuarine Research Reserve. NOAA Report NA470R0414, 138 pages.
- Cline, J. 1969. Spectrophotometric determination of hydrogen sulfide in natural waters. *Limnology and Oceanography* 14: 454-458.
- Cotrim da Cunha, L., E. Buitenhuis, C. Le Quéré, X. Giraud, and W. Ludwig. 2007. Potential impact of changes in river nutrient supply on global ocean biogeochemistry. *Global Biogeochemical Cycles* 21, doi:10.1029/2006GB002718.
- de Jonge, V., W. Boynton, C. D'Elia, R. Elmgren, and B. Welsh. 1994. Responses to developments in eutrophication in four different North Atlantic estuarine systems, pp. 179-196. In K. Dyer and R. Orth [eds.] *Changes in fluxes in estuaries: Implications from science to management*. Olsen & Olsen.
- DeSimone, L., P. Barlow, and B. Howes. 1996. A nitrogen-rich septage-effluent plume in a glacial aquifer, Cape Cod, Massachusetts, February 1990 through December 1992. USGS Water-Supply Paper 2456.
- Fazzolari, E., B. Nicolardot, and J. Germon. 1998. Simultaneous effects of increasing levels of glucose and oxygen partial pressures on denitrification and dissimilatory nitrate reduction to ammonium in repacked soil cores. *European Journal of Soil Biology* 34: 47-52.
- Froelich, P., G. Klinkhammer, M. Bender, N. Luedtke, G. Heath, D. Cullen, and P. Dauphin. 1979. Early oxidation of organic matter in pelagic sediments of the eastern equatorial Atlantic: Suboxic diagenesis. *Geochimica et Cosmochimica Acta* 43: 1075-1090.

- Gardner, W., M. McCarthy, S. An, D. Sobolev, K. Sell, and D. Brock. 2006. Nitrogen fixation and dissimilatory nitrate reduction to ammonium (DNRA) support nitrogen dynamics in Texas estuaries. *Limnology and Oceanography* 51(1, part 2): 558-568.
- Gould, W., and G. McCready. 1982. Denitrification in several soils: Inhibition by sulfur anions. *Canadian Journal of Microbiology* 28: 334-340.
- Hunter, K., Y. Wang, and P. Van Cappellen. 1998. Kinetic modeling of microbially-driven redox chemistry of subsurface environments: Coupling transport, microbial metabolism, and geochemistry. *Journal of Hydrology* 209: 53-80.
- Jensen, K., and R. Cox. 1992. Effects of sulfide and low redox potential on the inhibition of nitrous oxide reduction by acetylene in *Pseudomonas nautical*. *FEMS Microbiology Letters* 96: 13-18.
- Joye, S., and J. Hollibaugh. 1995. Sulfide inhibition of nitrification influences nitrogen regeneration in sediments. *Science* 270: 623-625.
- Kartal, B., M. Kuypers, G. Lavik, J. Schalk, H. Op den Camp, M. Jetten, and M. Strous. 2007. Anammox bacteria disguised as denitrifiers: Nitrate reduction to dinitrogen gas via nitrite and ammonium. *Environmental Microbiology* 9: 635-642.
- Kelly-Gerreyn, B., M. Trimmer, and D. Hydes. 2001. A diagenetic model discriminating denitrification and dissimilatory nitrate reduction to ammonium in a temperate estuarine sediment. *Marine Ecology Progress Series* 220: 33-46.
- Kroeger, K., and M. Charette. 2008. Nitrogen biogeochemistry of submarine groundwater discharge. *Limnology and Oceanography* 53: 1025-1039.

- Luff, R., M. Haeckel, and K. Wallmann. 2001. Robust and fast FORTRAN and MATLAB[®] libraries to calculate pH distributions in marine systems. *Computational Geosciences* 27: 157-169.
- Mantyla, A. 1987. Standard seawater comparisons updated. *Journal of Physical Oceanography* 17: 543-548.
- Meile, C., and K. Tuncay. 2006. Scale dependence of reaction rates in porous media. *Advances in Water Resources* 29: 62-71.
- Moltyaner, G., M. Klukas, C. Willis, and R. Killey. 1993. Numerical simulations of Twin Lake natural gradient tracer tests: a comparison of methods. *Water Resources Research* 29: 3433-3452.
- Moore, W. 1976. Sampling ²²⁸Ra in the deep ocean. *Deep-Sea Research* 23: 647-651.
- Moore, W. 1984. Radium isotope measurements using germanium detectors. *Nuclear Instruments and Methods* 223: 407-411.
- Moore, W. 1996. Large groundwater inputs to coastal waters revealed by ²²⁶Ra enrichments. *Nature* 380: 612-614.
- Moore, W. 1999. The subterranean estuary: A reaction zone of ground water and sea water. *Marine Chemistry* 65: 111-125.
- Moore, W. 2003. Sources and fluxes of submarine groundwater discharge delineated by radium isotopes. *Biogeochemistry* 66: 75-93.
- Moore, W., J. Sarmiento, and R. Key. 2008. Submarine groundwater discharge revealed by ²²⁸Ra distribution in the upper Atlantic Ocean. *Nature Geoscience* doi:10.1038/ngeo183.
- Morse, J., and J. Morin. 2005. Ammonium interaction with coastal marine sediments: influence of redox conditions on K^* . *Marine Chemistry* 95: 107-112.

- Nixon, S. and M. Pilson. 1983. Nitrogen in estuarine and coastal marine ecosystems, pp. 565-648. *In* E. Carpenter D. Capone [eds.] Nitrogen in the Marine Environment. Academic Press.
- Nixon, S., J. Ammerman, L. Atkinson, V. Berounsky, G. Billen, W. Boicourt, W. Boynton, T. Church, D. Ditoro, R. Elmgren, J. Garber, A. Giblin, R. Jahnke, N. Owens, M. Pilson, and S. Seitzinger. 1996. The fate of nitrogen and phosphorus at the land sea margin of the North Atlantic Ocean. *Biogeochemistry* 35: 141-180.
- Paerl, H., J. Pinckney, J. Fear, and B. Peierls. 1998. Ecosystem responses to internal and watershed organic matter loading: consequences for hypoxia in the eutrophying Neuse River Estuary, North Carolina, USA. *Marine Ecology Progress Series* 166: 17-25.
- Persky, J. 1986. The relations of ground-water quality to housing density, Cape Cod, Massachusetts. USGS Water-Resources Investigations Report 86-4093.
- Pinckney, J., H. Paerl, P. Tester, and T. Richardson. 2001. The role of nutrient loading and eutrophication in estuarine ecology. *Environmental Health Perspectives* 109: 699-706.
- Pomeroy, L., and R. Wiegert. [eds] 1981. The Ecology of a Salt Marsh. Springer-Verlag, pp. 1-271.
- Risgaard-Petersen, N., L. Nielsen, S. Rysgaard, T. Dalsgaard, and R. Meyer. 2003. Application of the isotope pairing technique in sediments where anammox and denitrification coexist. *Limnology and Oceanography-Methods* 1: 63-73.
- Rosenfeld, J. 1979. Ammonium adsorption in nearshore anoxic sediments. *Limnology and Oceanography* 24: 356-364.
- Rysgaard, S., P. Thastum, T. Dalsgaard, P. Christensen, and N. Sloth. 1999. Effects of salinity on NH_4^+ adsorption capacity, nitrification, and denitrification in Danish estuarine sediments. *Estuaries* 22: 21-30.

- Schultz, G., and C. Ruppel. 2002. Constraints on hydraulic parameters and implications for groundwater flux across the upland-estuary interface. *Journal of Hydrology* 260: 255-269.
- Seitzinger, S., W. Gardner, and A. Spratt. 1991. The effect of salinity on ammonium sorption in aquatic sediments: implications for benthic nutrient recycling. *Estuaries* 14: 167-174.
- Silver, W., D. Herman, and M. Firestone. 2001. Dissimilatory nitrate reduction to ammonium in upland tropical forest soils. *Ecology* 82: 2410-2416.
- Smith, R., L. Baumgartner, D. Miller, D. Repert, and J. Böhlke. 2006. Assessment of nitrification potential in groundwater using short term, single-well injection experiments. *Microbial Ecology* 51: 22-35.
- Snyder, M., M. Taillefert, and C. Ruppel. 2004. Redox zonation at the saline-influenced boundaries of a permeable surficial aquifer: Effects of physical forcing on the biogeochemical cycling of iron and manganese. *Journal of Hydrology* 296: 164-178.
- Solorzano, L. 1969. Determination of ammonia in natural waters by the phenylhypochlorite method. *Limnology and Oceanography* 14: 799-801.
- Stookey, L. 1970. Ferrozine – a new spectrophotometric reagent for iron. *Analytical Chemistry* 42: 779-781.
- Thamdrup, B., and T. Dalsgaard. 2002. Production of N₂ through anaerobic ammonium oxidation coupled to nitrate reduction in marine sediments. *Applied and Environmental Microbiology* 68: 1312-1328.
- Tiedje, J., A. Sexton, D. Myrold, and J. Robinson. 1982. Denitrification: Ecological niches, competition, and survival. *Antonie van Leeuwenhoek Journal of Microbiology* 48: 569-583.
- Tobias, C., I. Anderson, E. Canuel, and S. Macko. 2001. Nitrogen cycling through a fringing marsh-aquifer ecotone. *Marine Ecology Progress Series* 210: 25-39.

- Valiela, I., J. Costa, K. Foreman, J. Teal, B. Howes, and D. Aubrey. 1990. Transport of groundwater-borne nutrients from watersheds and their effects on coastal waters. *Biogeochemistry* 10: 177-197.
- Valiela, I., G. Collins, J. Kremer, K. Lajtha, M. Geist, M. Seely, J. Brawley, and C. Sham. 1997. Nitrogen loading from coastal watersheds to receiving estuaries: New method and application. *Ecological Applications* 7: 358-380.
- Vervaet, H., P. Boeckx, A. Boko, O. Van Cleemput, and G. Hofman. 2004. The role of gross and net N transformation processes and NH_4^+ and NO_3^- immobilization in controlling the mineral N pool of a temperate mixed deciduous forest soil. *Plant and Soil* 264: 349-357.
- Vitousek, P., H. Mooney, J. Lubchenco, and J. Melillo. 1997. Human domination of Earth's ecosystems. *Science* 277, doi:10.1126/science.277.5325.494.
- Vörösmarty, C. and T. Loder III. 1994. Spring-neap tidal contrasts and nutrient dynamics in a marsh-dominated estuary. *Estuaries* 17: 537-551.

Table 5.1. Initial and boundary conditions

species	upland boundary		marsh boundary		
	upland	plume	spring	neap	septic
salt	1	1	25	25.33	25.165
[DOM]	0.585	1.17	0.401	0.599	0.5
[O ₂]	0.007	0.007	0.016	0.006	0.011
[DIC]	4.63	4.63	4.52	6.56	5.54
[NO ₃ ⁻]	0.005	0.67	0.021	0.007	0.014
[NH ₄ ⁺] _{DISS}	0.01	1.93	0.008	0.032	0.02
[Mn ²⁺]	0	0	0	0	0
[Fe ²⁺]	0.001	0.001	0.004	0.004	0.004
[SO ₄ ²⁻]	0.82	0.82	19.94	18.72	19.33
[TS]	0	0	0	0	0
[CH ₄]	0	0	0	0	0
[MnO ₂]	0	0	0	0	0
[Fe(OH) ₃](s)	0	0	0	0	0
[MnCO ₃](s)	0	0	0	0	0
[FeCO ₃](s)	0	0	0	0	0
[FeS](s)	0	0	0	0	0
[CaCO ₃](s)	0	0	0	0	0
[CaSO ₄](s)	0	0	0	0	0
[S ⁰](s)	0	0	0	0	0
[NH ₄ ⁺] _{ADS} (s)	0.045	6.8	0	0	0
[ALK]	1.687	1.687	3.985	5.116	4.55
pH	6.11	6.11	7.22	6.9	7.03

upland refers to the concentrations set at the right hand upstream boundary.

These values are fixed and set to average concentrations determined from well 0212 and 0214.

plume denotes the composition of the septic plume, entering between 2 and 3 m depth at the right hand boundary.

spring and *neap* refer to inflowing concentrations and were determined from the Duplin and well 0217 for spring and neap tides respectively (see Methods for details).

septic indicates the average of spring and neap inflow used in the septic plume simulation.

Concentrations are in moles m⁻³_f for solutes and moles m⁻³_s for solids. Brackets denote concentrations, subscripts _f and _s denote fluid and solid volume, respectively. The initial alkalinity is calculated from the initial DIC and TS concentration and the initial pH.

FIGURE LEGENDS

Figure 5.1. Site map indicating the location of Moses Hammock (MH) on the western side of Sapelo Island, Georgia. The bottom panel illustrates an approximation of the well transect at MH with individual wells identified. Dashed box delineates the model domain.

Figure 5.2A-D. Boxplot of groundwater data for spring tides (white bars) and neap tides (dark bars). Wells are identified in the bottom panel, and boxes appear relative to the spatial distribution of the wells (x-axis). (A) Salinity, (B) DOC, (C) NO_x and (D) NH_4^+ data for the MH well transect. Boxplots illustrate the lowest non-outlier observation, the lower quartile, the median, the upper quartile, and the highest non-outlier observation.

Figure 5.3. Radium data collected from the MH well transect in August 2004. Like symbols are replicates from the same well collected at different tide stages over 5 days. Numbers identify each well and the Duplin River.

Figure 5.4. Modeled and field measured salt distributions. Small inset boxes represent the screened interval for each well, with the grayscale illustrating the median measured (spring tide) salinities for each well.

Figure 5.5A-F. Modeled nitrogen species distributions. Each panel illustrates the first 20 m of the domain for either the spring tide (left panels) or neap tide (right panels) simulations. (A) and (B) depict the modeled NO_3^- distribution, (C) and (D) depict the modeled $\text{NH}_4^+_{\text{DISS}}$ distribution, and panels (E) and (F) depict the modeled $\text{NH}_4^+_{\text{ADS}}$ distribution. Small inset boxes (A-D) represent

the screened interval for the depicted well, with the grayscale illustrating the median measured concentrations for each well.

Figure 5.6A-B. Modeled (A) DOM and (B) DIN distributions for septic plume simulation in $10^2 \mu\text{mol L}^{-1}$. Contour lines denote the salinity distribution.

Figure 5.1.

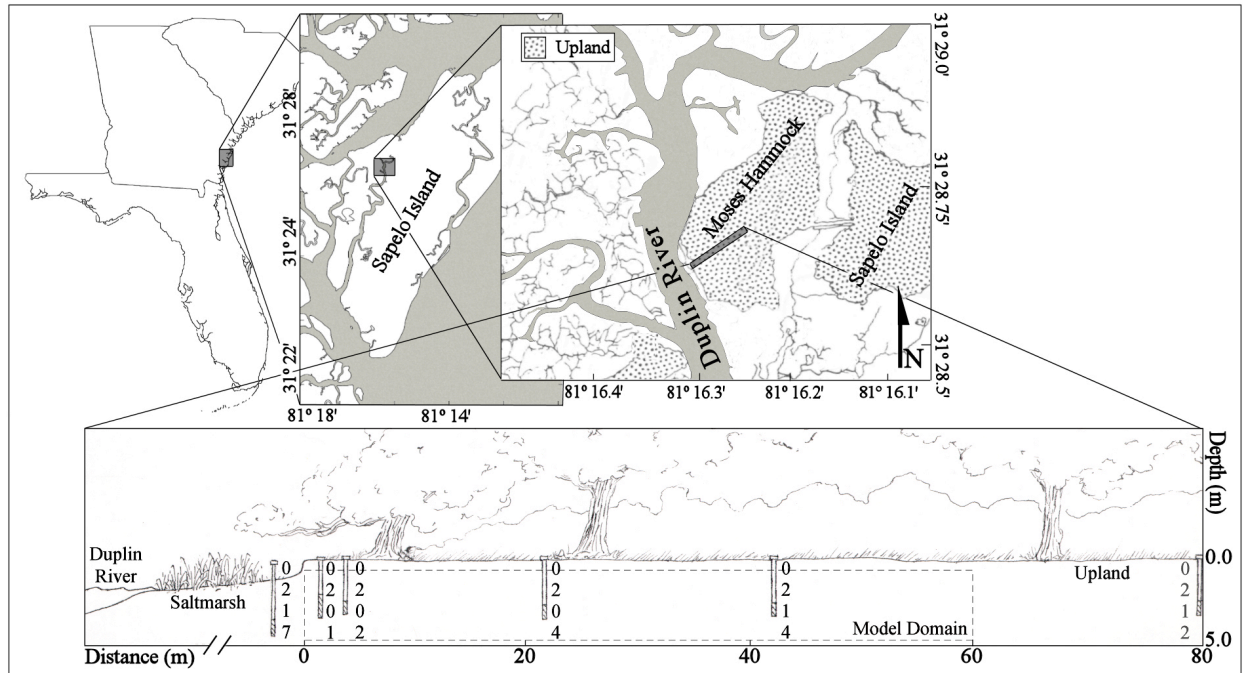


Figure 5.2A-D.

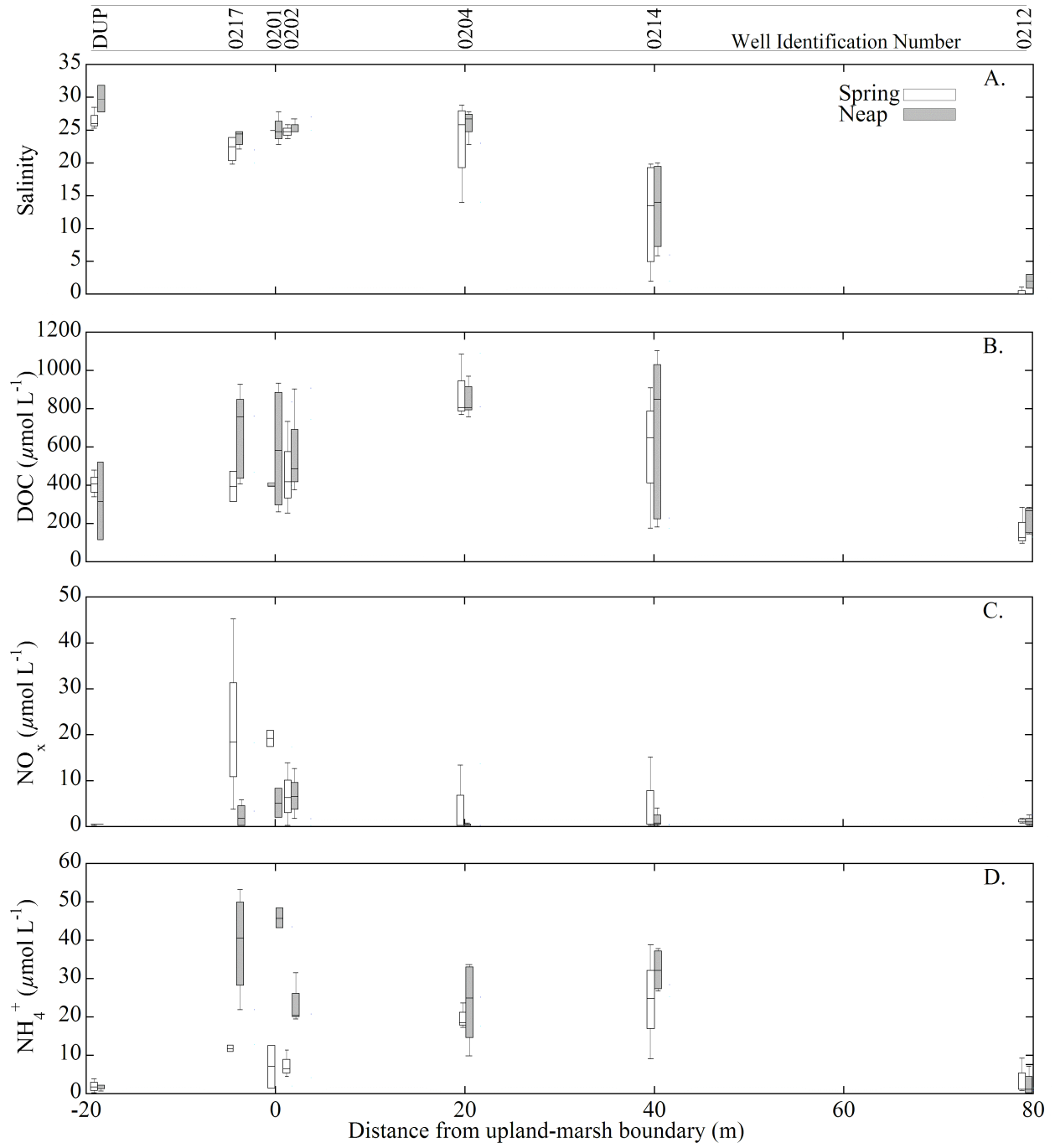


Figure 5.3.

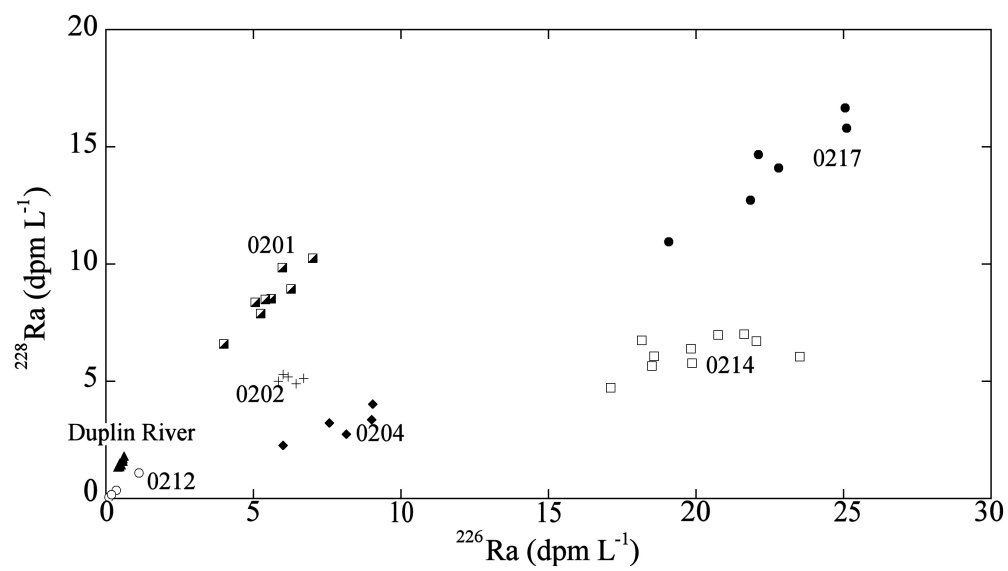


Figure 5.4.

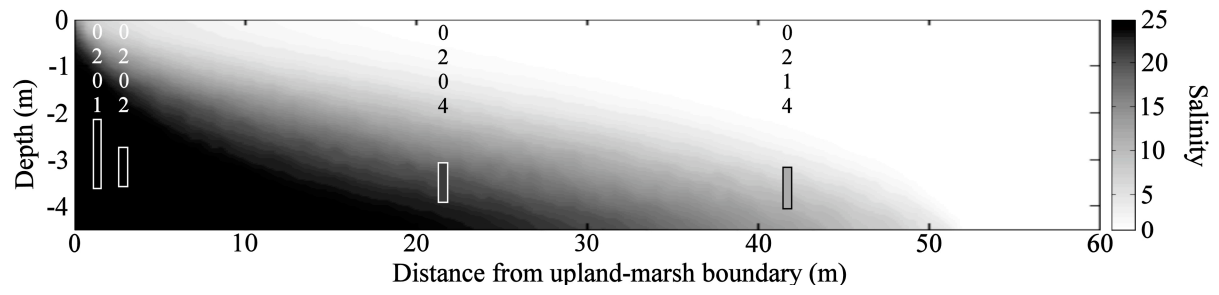


Figure 5.5A-F.

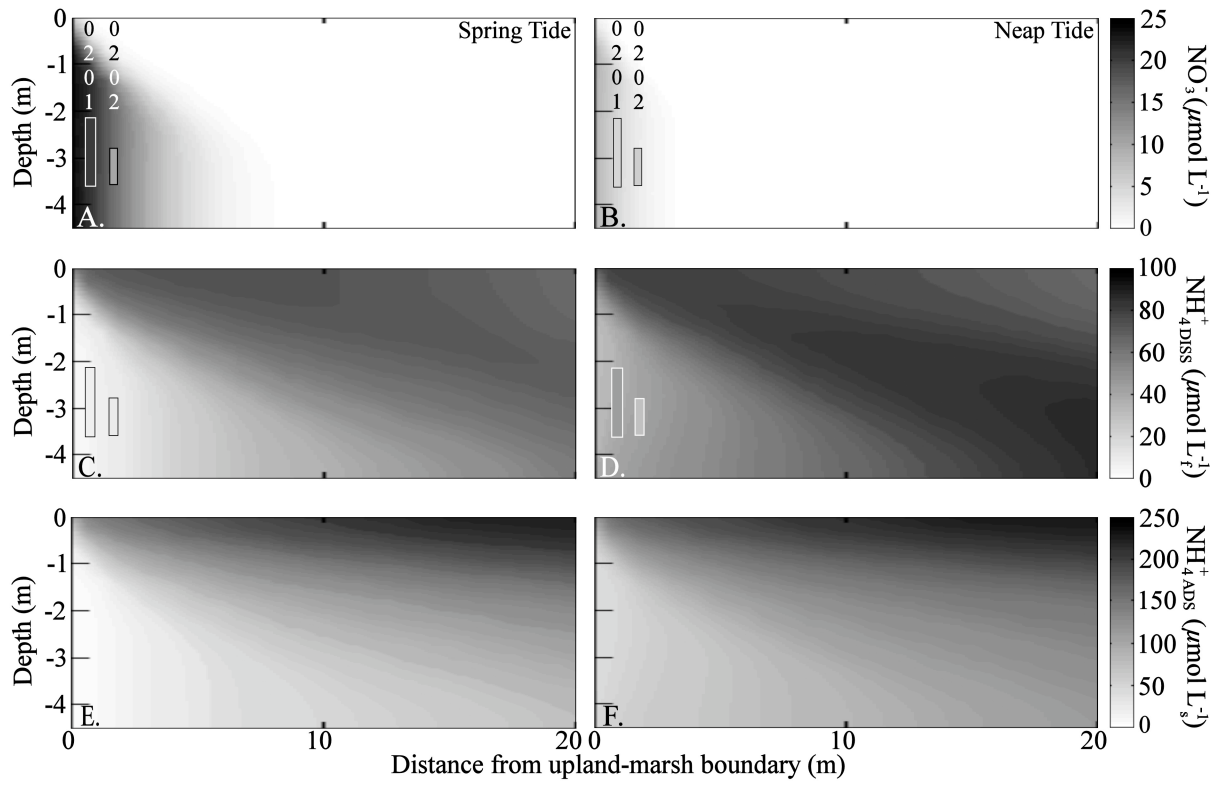
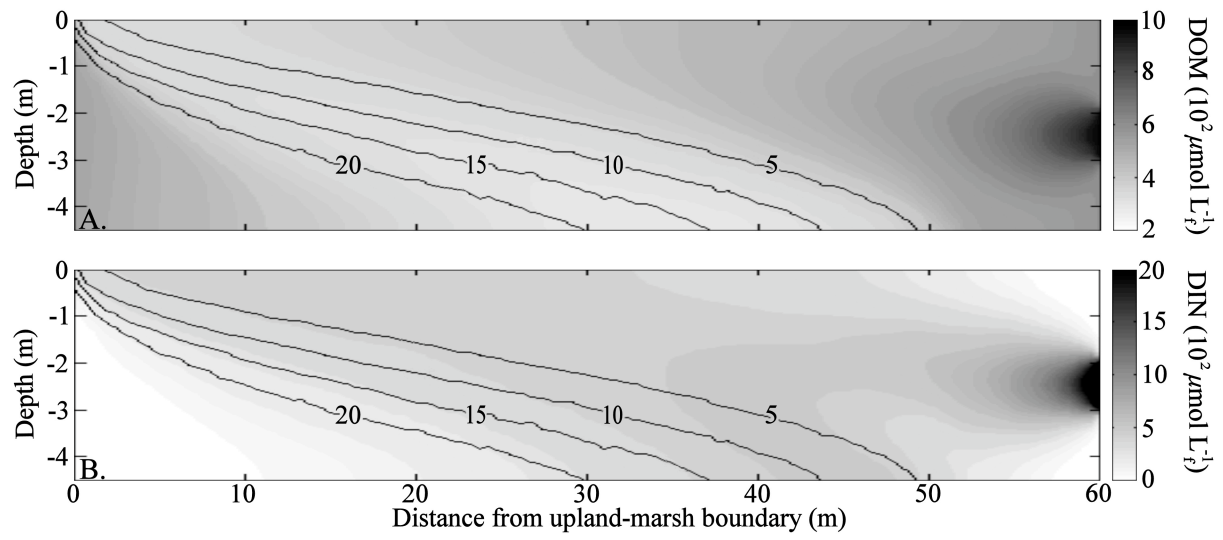


Figure 5.6A-B.



Appendix 5.1. Governing equations and implementation.

Governing equations

The governing equation is based on conservation of fluid mass, expressed as:

$$\frac{\partial(\rho\phi)}{\partial t} = -\nabla \cdot (\rho\phi v) \quad (5.1.1)$$

where ϕ is porosity [-], t is time, v is fluid velocity, ∇ is the gradient operator, and ρ is fluid density [M L⁻³], dependent on temperature (T), salinity (S) and pressure (p). Here, ρ is expressed as a linear function of salinity at a given temperature T^* [°C]:

$$\rho(S) = 1000.0821 - 0.0324(T^* - 4) - 0.0052(T^* - 4)^2 + (0.7925 - 0.0021(T^* - 4))S \quad (5.1.2)$$

which is based on a polynomial fit to the UNESCO equation of state ρ (S,T,p), with an error < 0.3 kg m⁻³ for 0 < S < 35, 4 < T < 35 °C at p = 1 bar. Assuming constant temperature and

porosity, the left hand side of Eq. 5.1.1 is approximated by $\gamma\phi \frac{\partial S}{\partial t} + \beta\phi \frac{\partial p}{\partial t}$, where the salinity and

pressure coefficients $\gamma = \left. \frac{\partial \rho}{\partial S} \right|_{p^*, T^*}$, $\beta = \left. \frac{\partial \rho}{\partial p} \right|_{S^*, T^*}$ are set to 0.7665 kg m⁻³ ppt⁻¹ and 4.55*10⁻⁷ kg m⁻³

Pa⁻¹, respectively. Using Darcy's law to describe the flow (e.g. Bear 1972), the fluid velocity v can be expressed as a function of material properties and the pressure field:

$$\phi v = -\frac{\kappa}{\mu} (\nabla p - \rho \vec{g}) \quad (5.1.3)$$

where κ is permeability (m²), μ is dynamic viscosity, set to 0.001 kg m⁻¹ s⁻¹, and g is gravitational acceleration. Combining Eqs. 5.1.1 and 5.1.3, the governing equation for the evolution of the pressure field becomes:

$$\phi\beta \frac{\partial p}{\partial t} = \nabla \cdot \left(\frac{\kappa\rho}{\mu} (\nabla p - \rho \vec{g}) \right) - \phi\gamma \frac{\partial S}{\partial t} \quad (5.1.4)$$

Solid phase chemical constituents are considered immobile, and mass conservation is expressed as:

$$\frac{d(1-\phi)C_i}{dt} = (1-\phi)R_i \quad (5.1.5)$$

where C_i is the solid mass of species i per volume solid phase and R_i the net rate of production or consumption per volume solid phase. For solutes, one can write:

$$\frac{\partial \phi C_i}{\partial t} = \nabla \cdot (D^* \nabla C_i) - \nabla \cdot (\phi v C_i) + \phi R_i \quad (5.1.6)$$

where C_i is the solute concentration of species i in the fluid and the reaction rate R is expressed per volume pore fluid. The diffusion-dispersion tensor, D^* [$L^2 T^{-1}$] is defined as (Scheidegger 1961):

$$D_{ij}^* = \phi D^m \delta_{ij} + (\alpha_L - \alpha_T) \frac{v_i v_j}{|v|} + \alpha_T |v| \delta_{ij} \quad (5.1.7)$$

where D^m is the tortuosity corrected in situ molecular diffusion coefficient, δ_{ij} is the Kronecker symbol, and α_L (m) and α_T (m) are longitudinal and transverse dispersivities, respectively.

Implementation

In each timestep, the pressure field is solved from which the velocity field is calculated. Subsequently, the evolution of the chemical species is computed. For solutes, this is accomplished using sequential non-iterative operator splitting (Steefel and MacQuarrie 1996). In this approach, concentrations of all species are first calculated subject to advective and dispersive transport only, so that the temporal evolution is uncoupled and hence can be solved for each chemical compound individually. The governing equations are discretized using a Galerkin finite element formulation and forward Euler time stepping. The resulting algebraic set of equations is

solved using a diagonally preconditioned conjugate gradient solver (Reddy 1993; Meile and Tuncay 2006). The impact of the reactions is then computed by solving a set of coupled, typically stiff, ordinary differential equations for each node, using the public domain solver VODE (Brown et al. 1989) with backward differentiation and the generation of full Jacobian matrix settings. Equilibrium reactions are implemented via operator splitting through mass conserving distribution functions at the end of each time step.

The implementation of the reaction network solver has been tested by comparison to simulations with explicit rate formulations and implementations using a fully implicit Newton-Raphson approach (Regnier et al. 1997; Meile 2003). Simulations are performed at grid Peclet numbers < 4 , and the time step is adapted depending on Courant numbers (< 1), and adjusted to resolve large temporal changes in concentrations. The finite element mesh has been produced using the open source software *emc2* (Saltel and Hecht 1995), and postprocessing is done with the open-source software *OpenDX* and within the proprietary *MATLAB* environment.

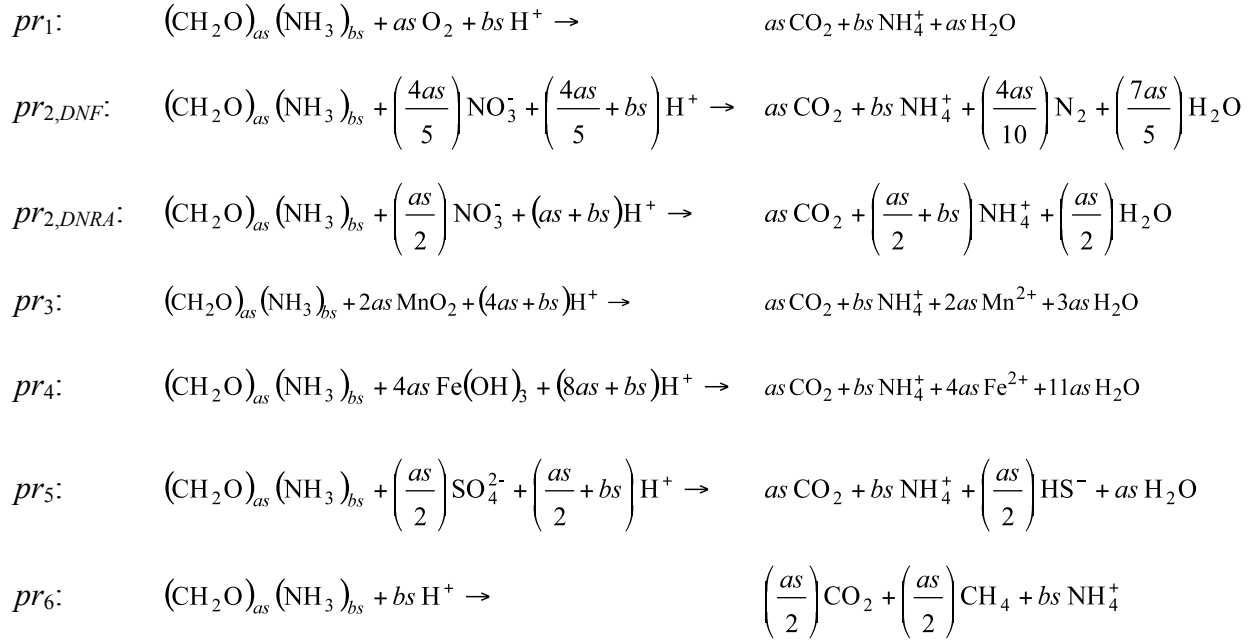
LITERATURE CITED FOR APPENDIX 5.1

- Bear, J. 1972. Dynamics of Fluids in Porous Media. American Elsevier Publishing Company, Inc. pp. 764.
- Brown, P., G. Byrne, and A. Hindmarsh. 1989. VODE: A variable-coefficient ODE solver. *SIAM Journal of Scientific and Statistical Computing* 10: 1038-1051.
- Meile, C. 2003. Heterogeneity, uncertainty and process identification in early diagenesis: New model developments with applications to biological mixing. Ph.D. thesis. Utrecht Univ.
- Meile, C., and K. Tuncay. 2006. Scale dependence of reaction rates in porous media. *Advances in Water Resources* 29: 62-71.

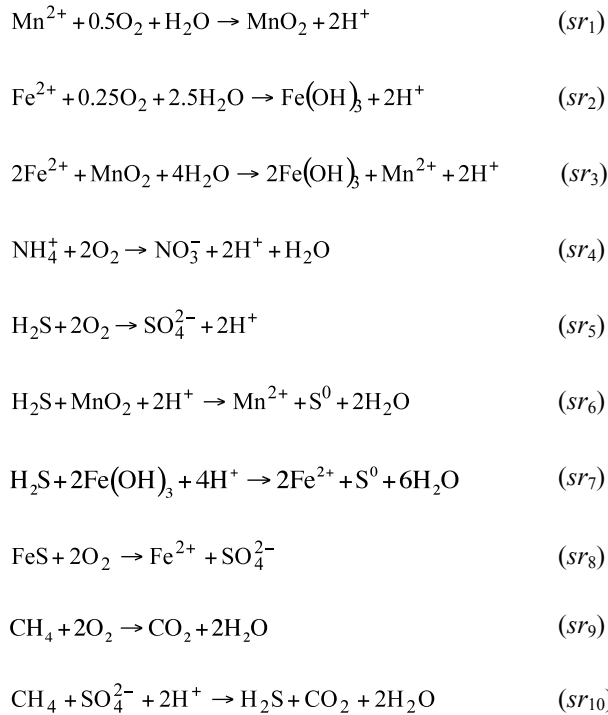
- Reddy, J. 1993. An introduction to the finite element method. 2nd ed. New York: McGraw Hill, Inc.
- Regnier, P., R. Wollast, and C. Steefel. 1997. Long-term fluxes of reactive species in macrotidal estuaries: Estimates from a fully transient, multicomponent reaction-transport model. *Marine Chemistry* 58: 127-145.
- Saltel, E., and F. Hecht. 1995. EMC2 Wysiwyg 2D finite elements mesh generator. RT n°188 INRIA. pp. 1-67.
- Scheidegger, A. 1961. General theory of dispersion in porous media. *Journal of Geophysical Research* 66: 3273-3278.
- Steefel, C., and K. MacQuarrie. 1996. Approaches to modeling of reactive transport in porous media, pp. 83-130. *In* P. Lichtner, C. Steefel, and E Oelkers [eds.] Reactive transport in porous media, Vol. 34. Mineralogical Society of America.

Appendix 5.2. Reaction network.

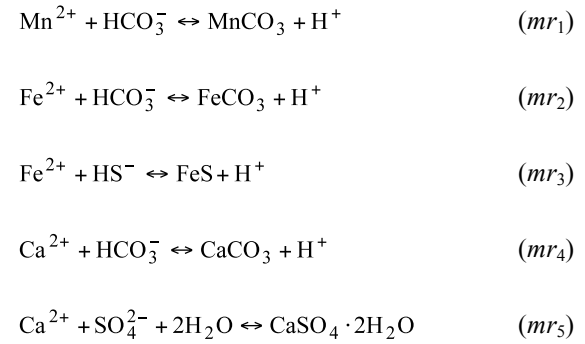
Primary reactions:



Secondary reactions:



Mineral precipitation-dissolution reactions:



Adsorption reactions:



Appendix 5.3. Model parameters.

Parameter	Value	Units	Source
<u>Organic matter composition and reactivity</u>			
<i>as</i> (Redfield carbon)	106	-	1
<i>bs</i> (Redfield nitrogen)	16	-	1
k_{DOM}	9.51×10^{-12}	s^{-1}	2, modified ^a
<u>Half saturation constants</u>			
K_{mO_2}	0.02	$\text{moles m}^{-3}_{\text{f}}$	2, 3
K_{mNO_3}	0.005	$\text{moles m}^{-3}_{\text{f}}$	2, 3
K_{mMnO_2}	0.0875	$\text{moles m}^{-3}_{\text{s}}$	2
K_{mFeOH_3}	0.0875	$\text{moles m}^{-3}_{\text{s}}$	2
K_{mSO_4}	0.03	$\text{moles m}^{-3}_{\text{f}}$	2
<u>Sorption</u>			
K_n	Dependent on salinity	$\text{moles m}^{-3}_{\text{s}} / \text{moles m}^{-3}_{\text{f}}$	this study ^b
<u>Secondary reaction rate constants</u>			
$sk1$	3.17×10^{-4}	$(\text{moles m}^{-3}_{\text{f}})^{-1} \text{s}^{-1}$	2
$sk2$	3.17×10^{-4}	$(\text{moles m}^{-3}_{\text{f}})^{-1} \text{s}^{-1}$	2
$sk3$	3.17×10^{-8}	$(\text{moles m}^{-3}_{\text{f}})^{-1} \text{s}^{-1}$	2
$sk4$	1.59×10^{-4}	$(\text{moles m}^{-3}_{\text{f}})^{-1} \text{s}^{-1}$	2
$sk5$	5.07×10^{-5}	$(\text{moles m}^{-3}_{\text{f}})^{-1} \text{s}^{-1}$	2
$sk6$	6.34×10^{-7}	$(\text{moles m}^{-3}_{\text{f}})^{-1} \text{s}^{-1}$	2
$sk7$	2.54×10^{-7}	$(\text{moles m}^{-3}_{\text{f}})^{-1} \text{s}^{-1}$	2
$sk8$	9.51×10^{-6}	$(\text{moles m}^{-3}_{\text{f}})^{-1} \text{s}^{-1}$	2
$sk9$	3.17×10^{-1}	$(\text{moles m}^{-3}_{\text{f}})^{-1} \text{s}^{-1}$	2
$sk10$	3.17×10^{-7}	$(\text{moles m}^{-3}_{\text{f}})^{-1} \text{s}^{-1}$	2
<u>Mineral precipitation (<i>mkp</i>) and dissolution (<i>mkd</i>) rate constants</u>			
$mk1p$	3.17×10^{-9}	$\text{moles m}^{-3}_{\text{t}} \text{s}^{-1}$	2
$mk1d$	3.17×10^{-12}	s^{-1}	2
$mk2p$	1.59×10^{-9}	$\text{moles m}^{-3}_{\text{t}} \text{s}^{-1}$	2
$mk2d$	1.59×10^{-12}	s^{-1}	2
$mk3p$	1.90×10^{-9}	$\text{moles m}^{-3}_{\text{t}} \text{s}^{-1}$	2
$mk3d$	3.17×10^{-12}	s^{-1}	2
$mk4p$	1.90×10^{-9}	$\text{moles m}^{-3}_{\text{t}} \text{s}^{-1}$	2
$mk4d$	1.59×10^{-11}	s^{-1}	2
$mk5p$	1.90×10^{-9}	$\text{moles m}^{-3}_{\text{t}} \text{s}^{-1}$	2
$mk5d$	1.59×10^{-11}	s^{-1}	2
<u>Solubility constants ^c</u>			
K_1	$10^{-10.41}$	-	4
K_2	$10^{-10.55}$	-	4
K_3	$10^{-2.95}$	-	5
K_4	$10^{-8.48}$	-	4

K_5	$10^{-4.58}$	-	4
<u>Physical characteristics</u> ^d			
ϕ	0.4	$\text{m}_f^3 \text{m}_t^{-3}$	Field data
κ	3.5×10^{-12}	m^2	6
α_L	0.3	m	7
α_T	0.03	m	10% of α_L
Δh	0.001	m/m	Field data

Subscripts _f, _s, and _t denote fluid, solid, and total respectively. ϕ is porosity, κ is permeability, and α_L and α_T are longitudinal and transverse dispersivity respectively. 1. Redfield 1934; 2. Hunter et al. 1998; 3. Van Cappellen and Wang 1996; 4. Stumm and Morgan 1996; 5. Morse et al. 1987; 6. Schultz and Ruppel 2002; 7. Molyaner et al. 1993.

^a See 'Modeling results' section.

^b The ammonium coefficient from the 2-2.1 m depth-range was used as it corresponds to the model domain.

^c The solubility constants define the saturation states for MnCO_3 , FeCO_3 , FeS , CaCO_3 and CaSO_4 , respectively, as:

$$\Omega_1 = \frac{a_{\text{Mn}^{2+}} \cdot a_{\text{HCO}_3^-}}{a_{\text{H}^+} \cdot K_1}, \quad \Omega_2 = \frac{a_{\text{Fe}^{2+}} \cdot a_{\text{HCO}_3^-}}{a_{\text{H}^+} \cdot K_2}, \quad \Omega_3 = \frac{a_{\text{Fe}^{2+}} \cdot a_{\text{HS}^-}}{a_{\text{H}^+} \cdot K_3}, \quad \Omega_4 = \frac{a_{\text{Ca}^{2+}} \cdot a_{\text{HCO}_3^-}}{a_{\text{H}^+} \cdot K_4}, \quad \Omega_5 = \frac{a_{\text{Ca}^{2+}} \cdot a_{\text{SO}_4^{2-}}}{K_5}, \text{ where}$$

a denote activities.

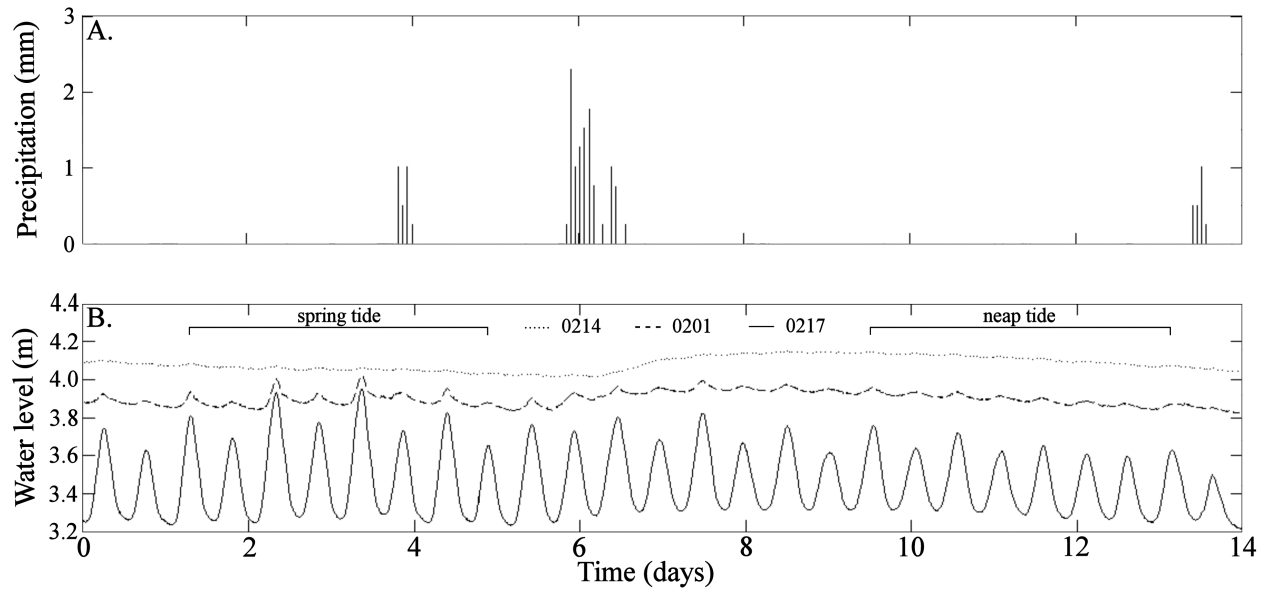
^d Porosity is an average of the measured values (0.2-0.5). The imposed head difference is at the low end of the observed pressure gradient from well 0201 and 0214, selected based on the comparison of model results to measured salinities.

LITERATURE CITED FOR APPENDIX 5.3

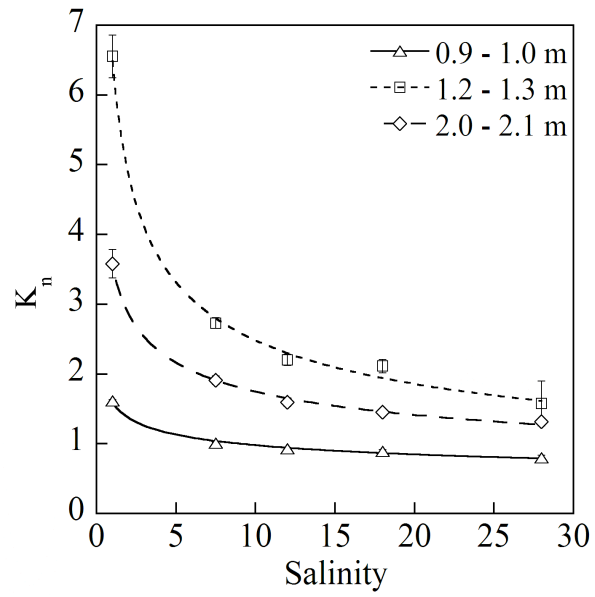
- Hunter, K., Y. Wang, and P. Van Cappellen. 1998. Kinetic modeling of microbially-driven redox chemistry of subsurface environments: Coupling transport, microbial metabolism, and geochemistry. *Journal of Hydrology* 209: 53-80.
- Molyaner, G., M. Klukas, C. Willis, and R. Killey. 1993. Numerical simulations of Twin Lake natural gradient tracer tests: A comparison of methods. *Water Resources Research* 29: 3433-3452.
- Morse, J., F. Millero, J. Cornwell, and D. Rickard. 1987. The chemistry of the hydrogen sulfide and iron sulfide systems in natural waters. *Earth-Science Reviews* 24: 1-42.

- Redfield, A. 1934. On the proportions of organic derivations in seawater and their relation to the composition of plankton, pp. 177-192. *In* R. Daniel [ed] James Johnson Memorial Volume. University Press of Liverpool.
- Schultz, G., and C. Ruppel. 2002. Constraints on hydraulic parameters and implications for groundwater flux across the upland-estuary interface. *Journal of Hydrology* 260: 255-269.
- Stumm, W. and J. Morgan. 1996. *Aquatic Chemistry: Chemical Equilibria and Rates in Natural Waters*. Wiley, New York.
- Van Cappellen, P., and Y. Wang. 1996. Cycling of iron and manganese in surface sediments: A general theory for the coupled transport and reaction of carbon, oxygen, nitrogen, sulfur, iron, and manganese. *American Journal of Science* 296: 197-243.

Appendix 5.4. Precipitation data (A) from the SINERR/GCE/UGAMI weather station at Marsh Landing, Sapelo Island, Georgia from December 12-24, 2005, and corresponding well water levels (B) corrected to a common depth.



Appendix 5.5. Field measured ammonium adsorption coefficients ($K_n = [\text{mol}/\text{m}^3_{\text{solid}} / \text{mol}/\text{m}^3_{\text{fluid}}]$
 $= \text{NH}^+_{4,\text{ADS}} / \text{NH}^+_{4,\text{DISS}}$) vs. salinity.



CHAPTER 6

CONCLUSIONS

Shallow coastal aquifers and intertidal sediments are key locations for biogeochemical processing of nutrients and organics where a combination of microbial and hydrological processes impact the delivery of materials to the coastal ocean. As anthropogenic pressure continues to mount in the coastal counties of Georgia and South Carolina, understanding the interacting roles played by various microbially mediated processes, benthic microalgae, and local hydrology will be important for assessing the system response to such pressures. The work presented here examined several key steps in the delivery of nutrients and organics to coastal waters.

Fluxes between the sediment and water column play an important role in estuarine nutrient cycles. The work presented in **CHAPTERS 2 and 3** expands our knowledge of how both dissimilatory and assimilatory processes can impact the amount and form of nutrients and organics available for diffusive transport to the water column. Under light replete conditions, autotrophic metabolism dominated and BMA formed an effective cap at the sediment water interface regulating the flux of nutrients across the interface (**CHAPTERS 2 and 3**). The addition of nitrogen relieved BMA from primary nutrient limitation and indicated that BMA were sequentially limited by nitrogen and then silicate (**CHAPTER 3**). The BMA inhabited sediments served as a sink for water column nitrogen, however, the N addition led to a decoupling of DOC production and heterotrophic consumption and sediments became a source

of organics to the water column. The observed decoupling of BMA production and bacterial consumption of DOC illustrates a potentially important aspect of ecosystem response to increased nutrient loads.

Under dark conditions, heterotrophic metabolism led to release of nutrients from the sediment to the water column and dissimilatory processes dominated the nitrogen cycle (**CHAPTERS 2 and 3**). DNF, DNRA, and anammox competed for substrate with DNF being the dominant dissimilatory process. From this work it is apparent that a suite of factors, including the concentration of H_2S and the ratio of $\text{DOC}:\text{NO}_3^-$, influenced these dissimilatory processes. While DNF was the dominant dissimilatory sink for NO_3^- , anoxic conditions resulted in greater sediment-water column exchange of nitrogen than light-replete conditions (**CHAPTER 2**).

While both BMA and dissimilatory nitrate reducers significantly impact diffusive fluxes at the sediment-water column interface; large scale groundwater inputs can be dominated by advective fluxes in some systems (**CHAPTERS 4 and 5**). The work presented in Chapter 4 documented the significant contributions of groundwater to the Okatee River estuary. Variations in hydrology, likely combined with organic matter supply, can impact the microbial activity and geochemistry of shallow coastal aquifers. Less flushing and more organic matter in the groundwater on the western side of the Okatee led to higher sulfate reduction rates and concentration of reduced metabolites (**CHAPTER 4**). Loading rates derived from radium isotope data indicated that even though the eastern side of the Okatee may be more frequently flushed, the significantly higher concentration of organics, DIC and nutrients observed in the western groundwater represent the majority of the advective groundwater input to the Okatee (**CHAPTER 4**).

The link between hydrology and microbial processes also impacted the speciation of DIN in the upland at Moses Hammock. In **CHAPTER 5** we found that microbial processes in the upland aquifer of Moses Hammock were not capable of generating the observed redox switch in the DIN pool. In fact the transport of high NO_3^- low NH_4^+ water on spring tide was the likely source of the switch and it appears that nitrification occurring in the upper marsh and the hydrological connection between the marsh and the upland may have led to the switch.

The role of salt marsh sediments as a site of significant processing of groundwater transported materials can also be seen in the nitrogen cycling from the Okatee marshes. The large amount of ‘missing’ DIN in the upper reaches of the Okatee suggested a significant N sink within the marsh. While pDNF rates from the Okatee could account for a large fraction of the DIN supply, in situ rates were much lower and could not be responsible for the missing DIN (**CHAPTER 4**). Given that DNF can potentially mitigate subsurface DIN loads prior to export to coastal waters, the effectiveness of DNF as an N sink is an important topic for further examination. In **CHAPTER 5** we found that an increase in DIN and DOM load through a simulated septic effluent plume resulted in increased DNF, but complex interaction of negative controls (H_2S) and competing processes (DNRA) limited the N mitigation potential of the process. Given the role of groundwater as a significant source of nutrients to the coastal ocean it is imperative that we understand the processes at work within the aquifers and intertidal sediments that act as the conduit for the delivery of these materials.